MEDICAL UNIVERSITY OF VIENNA

Immune-Metabolic Crosstalk During Infection Associated Cachexia

Doctoral thesis at the Medical University of Vienna
for obtaining the academic degree

Doctor of Philosophy

Submitted by

MSc, Hatoon Baazim

Supervisor:
Priv.-Doz.Dr. Andreas Bergthaler

CeMM Research Center for Molecular Medicine of the
Austrian Academy of Sciences

Lazarettgasse 14, AKH BT25.3, 1090 Vienna Austria

Vienna, (September/2019)

Declaration:

The current thesis has been written in a cumulative format. It includes one publication where I am the first author, published in Nature Immunology on the 20th of May 2019 DOI: 10.1038/s41590-019-0397-y. The work showcased in this thesis has been conceptualized by myself and my PhD supervisor Dr. Andreas Bergthaler, who is the corresponding author on this publication. I have designed and performed in vivo experiments and the subsequent sample processing and data analysis in both CeMM Research Center for Molecular Medicine of the Austrian Academy of Sciences and at the Department for Biomedical research of the Medical University of Vienna.

My specific contributions to the publication on which this thesis is based are as follows:

I have designed, performed and analyzed the data of the experiments shown in (Figure 1a, f and g, Figure 2e-i, Figure 3d, Figure 4a, b and i, Figure 5, Supplementary figure 1b-j, Supplementary figure 2a, f, g and h, Supplementary figure 3b, h, I and j, Supplementary figure 4a-c). For the experiment shown in (Figure 1b-d, Figure 2a and Supplementary figure 1a) I performed the infection of the mice. The data acquisition was performed by our collaborators. For (Figure 2b, Figure 5a and Supplementary figure 2b-c) I performed the infection, and collected the tissue samples then analyzed the acquired data from H/E and IF staining. I designed, performed and analyzed the monoclonal antibody depletion experiments shown in (Fig 3b). For the RNAseq data, I performed the infection, sample collection and processing shown in (Figure 4c-g and Supplementary figure 4d). I also took part in the RNAseq data analysis shown in (Supplementary figure 4d).

I have also designed and, with the assistance of my supervisor Dr. Andreas Bergthaler, coordinated the experiments performed by our collaborators.

The contributions of the co-authors of the study is as described below:

Martina Schweiger, Thomas Scherer, Bojan Vilagos, Alan Aderem and Rudolf Zechner made significant contributions to the experimental design, shared reagents and/or genetically modified animals and/or contributed to the interpretation of the data. Michael Moschinger, Haifeng Xu, Kseniya Khamina, Lindsey Kosack, Mark Smyth, Alex Lercher and Philipp A. Lang designed, performed experiments and/or provided some technical support. Alexandra Popa performed the bioinformatic data analysis of the RNA-seq data. Suchira Gallage, Adnan Ali, and Mathias Heikenwälder performed mouse calorimetry analysis using metabolic cages. Joachim Friske, and Thomas H. Helbich performed MRI analysis. Doron Merkler provided histologic (H/E) immunohistochemical staining.

The graphic design of all the figures included in this thesis and in the publication was done by me (Hatoon Baazim).

Table of contents:

List of figures:

Abstract (English):

Cachexia remains an enigmatic syndrome that manifest alongside a variety of chronic inflammatory diseases, infections and malignancies, with very limited treatment options. Infection-associated cachexia is particularly underdiagnosed and understudied form of the syndrome. In this study, we implement an integrative approach to investigate the physiological, cellular and molecular changes during infection-associated cachexia in a murine model of chronic viral infection. We found that the onset of cachexia was couple to short-term anorexia, lethargy and triggered a depletion of both fat and muscle mass. We further characterized global changes in the adipose tissue architecture and metabolic program. In addition, we use a number of pharmachological and genetic perturbation to identify the inflammatory and immune triggers upstream of peripheral tissue wasting. Surprisingly, the classical cytokines associated with cancer cachexia did not contribute to wasting in this model. Instead, cachexia was triggered by $CD8^+$T cells at a timepoint preceding the peak of T cell response and required T cell–intrinsic type I interferon signaling and antigen-specific priming. Our results link systemic antiviral immune responses to adipose-tissue remodeling and reveal an underappreciated role of $CD8^+$T cells in infection-associated cachexia.

Abstract (German):

Kachexie bleibt ein rätselhaftes Syndrom, welches sich im Laufe von verschiedenen Entzündungs-, Infektions- und Krebserkrankungen manifestiert, mit sehr limitierten Behandlungsoptionen. Die Infektions-assoziierte Kachexie ist eine besonders unterdiagnostizierte und wenig studierte Unterform dieses Syndroms. In dieser Studie implementieren wir eine integrative Herangehensweise, um die physiologischen, zellulären und molekularen Veränderungen während Infektions-assoziierter Kachexie in einem Mausmodell für chronische virale Erkrankungen zu studieren. Wir fanden heraus, dass die Anfangsphase der Kachexie mit kurzzeitiger Anorexie und Lethargie verknüpft ist, was einen Schwund von Fett- und Muskelmasse zur Folge hat. Wir haben darüber hinaus die globalen Veränderungen im Aufbau und Metabolismus des Fettgewebes charakterisiert. Zusätzlich verwenden wir eine Vielzahl an pharmakologischen und genetischen Pertubationen, um die entzündlichen und immunologischen Auslöser, die für den peripheren Gewebeschwund verantwortlich sind, zu identifizieren. Überraschenderweise tragen die klassischen Zytokine, welche mit Krebs assoziierter Kachexie in Verbindung gebracht werden, in diesem Modell nicht zum Gewebeschwund bei. Stattdessen wird die Kachexie von CD8+ T-Zellen zu einem Zeitpunkt, der vor dem Maximum der T-Zell Antwort stattfindet, hervorgerufen. Dieser Prozess ist abhängig von T-Zell intrinsischen Interferon Typ 1 Signalen, sowie Antigen-spezifischem Priming. Unsere Erkenntnisse verbinden systemische antivirale Immunantworten mit Veränderungen im Fettgewebe und enthüllen eine unterschätzte Rolle von CD8+ T-Zellen in Infektions-assoziierter Kachexie.

Publications rising from this thesis:

Hatoon Baazim*, Martina Schweiger, Michael Moschinger, Haifeng Xu, Thomas Scherer, Alexandra Popa, Suchira Gallage, Adnan Ali, Kseniya Khamina, Lindsay Kosack, Bojan Vilagos, Mark Smyth, Alexander Lercher, Joachim Friske, Doron Merkler, Alan Aderem, Thomas H. Helbich, Mathias Heikenwälder, Philipp A. Lang, Rudolf Zechner & Andreas Bergthaler**. **CD8 T cells induce cachexia in chronic viral infection.** *Nature Immunology, 20: 701-710, June 2019,* https://doi.org/10.1038/s41590-019-0397-y

* First Author

**Senior Author

Abbreviations:

LPS: lipopolysaccharide

L. monocytogenes: Listeria monocytogenes

E. coli: Escherichia coli

S. Typhimurium: Salmonella Typhimurium

ROS: reactive oxygen species

IL1β: interleukin 1 beta

HIV: human immunodeficiency virus

TB: tuberculosis

BMI: body mass index.

CT: computed tomography

MRI: magnetic resonance imagining

HALS: HIV-1-associated lipodystrophy syndrome

NEFA: none-esterified fatty acids

TG: triacylglyceride

ATGL: Adipose triglycerides lipase

HSL: hormone sensitive lipase

vLDL: very low density lipoproteins

LPL: lipoprotein lipase

FA CoA: fatty acyl-CoA

MG: monoacylglycerol

DG: diacylglycerol

DGAT: acyl-CoA:diacylglycerol acyltransferase

TSHR: thyroid-stimulated hormones receptor

β-AR: beta adrenergic receptor

NPR-A: Natriuretic peptides receptor A

fT4: free thyroxine

fT3: free triiodothyronine

AC: adenyl cyclase

GNAS: guanine nucleotide-binding protein, Alpha stimulating activity polypeptide 1

cAMP: cyclic adenyl monophosphate

PKA: protein kinase A

cGMP: cyclic guanine monophosphate

PKG: protein kinase G

CGI-58: Gene Identification-58

MGL: monoacylglyceride lipase

FAO: fatty acid oxidation

TNF: necrosis factor

IL6: interleukin 6

IFNγ: interferon gamma

WAT: white adipose tissue

BAT: brown adipose tissue

UCP1: uncoupling protein 1

Pnpla2: patatin-like phospholipase domain containing 2

Lipe: lipase, hormone sensitive

Plin1: perilipin1

AMPK: monophosphate-activated protein kinase

PI3K: phosphoinositide 3-kinase

AKT: serine/threonine-specific protein kinase

mTOR: member of the phosphatidylinositol 3-kinase related kinase family

FOXO: fokhead box protein O

Murf1: muscle-specific RING-finger1

MyoD1: myoblast determination protein 1

NF-κB: nuclear factor kappa light chain enhancer or activated B cells

P38 MAPK: p38 mitogen-activated protein kinase

APP: acute phase proteins

JAK: Janus kinases

STAT: signal transducer and activator of transcription proteins

MEK: mitogen-activated protein kinase kinase

ERK: extracellular signal-related kinase

PDE3B: phosphodiesterase 3

MBH: mediobasal hypothalamus

CNS: central nervous system

AgRP: agouti-related peptide

NPY: neuropeptide Y

POMC: pro-opiomelanocortin

PYY: peptide YY, peptide tyrosine tyrosine

HPA: hypothalamic-pituitary adrenal axis

GC: glucocorticoids

GR: glucocorticoid receptor

GHS-R: growth hormone secretagogue receptor

COPD: chronic obstructive pulmonary disease

LLC: Lewis lung carcinoma

Apc: adenomatous polyposis coli

HCC: hepatocellular carcinoma

LCMV: Lymphocytic choriomeningitis virus

NP: nucleoprotein

GP: glycoprotein

i.c : intracranial

i.v : intravenous

i.p : intraperitoneal

LCMV-Arm: LCMV strain Armstrong

LCMV-WE: LCMV strain WE

LCMV-Cl13: LCMV strain clone 13

LCMV-docile: LCMV strain docile

FFU: focus forming unitls

DC: dendritic cells

PAMPs: pathogen-associated molecular patterns

PRR: Pattern-recognition receptors

TLR: Toll-like receptor

RIG-I: retinoic acid-inducible gene I

MDA5: melanoma differentiation-associated protein 5

IRF: interferon regulatory factor

IFNAR: interferon receptor

ISGF3: IFN-stimulated gene factors 3

ISG: IFN-stimulated genes

pDC: plasmacytoid DCs

TCR: T cell receptor

MHC: histocompatibility complex

GrmB: granzyme B

PFN: perforin

PD-L1: programmed death receptor ligand 1

PDAC: Pancreatic ductal adenocarcinoma

Acknowledgements:

I want to direct my deepest and most sincere appreciation to my PhD supervisor Dr. Andreas Bergthaler for giving me the opportunity to join his lab. Dr. Bergthaler has invested a lot of efforts into cultivating a welcoming, friendly and stimulating lab environment, and has been a valuable mentor and an inspiring figure over the years. He has placed a lot of trust in me and helped me gain independence and grow into the scientist that I am today. I also thank everyone in the Bergthaler lab for being a constant source of support, ideas, and wonderful companionship. I could not have asked for a better PhD experience.

To Prof. Giulio Superty-Furga, the Scientific Director of CeMM, Research Center for Molecular Medicine, I thank you very much for all you do and did to make this incredible institute a reality. It has been truly a pleasure to be part of your vision, and a unique and valuable experience that I will always treasure. I'm very grateful for the support and inspiration I've received from all the CeMM faculty, and that of my dear colleagues, and friends.

Many special thanks go to my very dear friends and PhD companions André Rendeiro, Rico Ardy and Tamara Casteels who've been there for me in the best times and the worst. I am blessed for your presence in my life.

To my family, I would like to express how grateful I am for your encouragement and understanding, and for helping me to chase my dreams and seize the opportunities that come. A special gratitude goes out to my mother Awatif Batarfi, for believing in me, and blessing my wings as I took flight. And finally, I'd like to dedicate this thesis to the memory of my father, Abobakr Baazim, may he rest in peace. *The candle that burnt to light the way for us.*

Introduction:

When an organism is faced with a prolonged exposure to a critical conditions, be it external, such as predation or famine, or internal such as infections or malignancies, it needs to develop specialized strategies to maximize its chances of survival (Wang *et al*, 2019; Hotamisligil, 2017; Hayward *et al*, 2013). In the case of infections, innate surveillance machineries are able to identify the threat, and acquire the essential information to initiate critical decision making processes during the first hours following infection (Shin *et al*, 2016; Moseman & McGavern, 2013). The biological nature of the pathogen, initial inoculum and replicating rate as well as its pathogenicity and tropism, are all factors that influence whether the immune system will launch a defensive response or activate tolerogenic responses (Ayres & Schneider, 2012; Medzhitov *et al*, 2012). This is because immunological responses aimed at combating pathogens are energetically very expensive, and can cause immunopathology and tissue damage that then may require tissue repair. Meanwhile, the energy reserves available for the host are limited. Moreover, the basal energy requirements designated to support growth, reproduction and maintenance programs, the so-called life history traits, must be taken into consideration (Stearns 1992).

Many efforts have been made towards a better understanding of the major regulatory pathways coordinating organismal energy distribution. Even within homeostatic conditions this remains a very challenging endeavor that involves complex and overlapping signaling pathways across multiple organs (Lempradl *et al*, 2015; Krauss *et al*, 2012). Moreover, these pathways are often influenced by circadian regulation, nutritional state as well as other developmental and environmental changes across the organism's life cycle (Sahar & Sassone-Corsi, 2012; Di Francesco *et al*, 2018). Over the past few years, a number of studies described a variety of mechanisms by which metabolism influences immune responses and vice versa, launching a new field of research in immunometabolism (Buck *et al*, 2017; Mathis, 2019; O'Neill *et al*, 2016).

The first landmark studies in immunometabolism mostly focused on exploring the metabolic regulation within innate and adaptive immune cells *in vitro* using metabolic flux analysis and pharmacological manipulations (Krawczyk *et al*, 2010; Michalek *et al*, 2011; Shi *et al*, 2011; Haschemi *et al*, 2012). As the field matured, more *in vivo* studies emerged and focused on the consequences of the metabolic reprogramming during infection (Geltink *et al*, 2018; Norata *et al*, 2015). A number of these studies described multiple mechanisms by which trade-offs are made between life history traits and the immune response. Many of these strategies can manifest as pathophysiological and behavioral changes termed "sickness-behavior" (Shattuck & Muehlenbein, 2015; Harden *et al*, 2015). This includes thermal-regulation (hyperthermia in humans, and hypothermia in some murine infections), anorexia, lethargy, and/or social isolation (Filiano *et al*, 2016). It's important to note that all such manifestations of disease are

neither always beneficial nor always detrimental, but are highly context dependent. Studies of different infection models described a specialized role for anorexia, rendering it as both adaptive and maladaptive (Wang *et al*, 2016; Rao *et al*, 2017). In this context, anorexia is defined as a reduction in food intake, commonly due to inflammation-induced hypothalamic regulation, which results in a significant body weight loss. This is to be distinguished from anorexia nervosa, a mental illness in which the fear of weight gain, and the desire to be thin causes individuals to restrict their dietary intake to a degree that renders them critically malnourished (Attia, 2010). Additionally, parallel trade-off strategies can be coordinated independently within the same organism to address different aspect affecting host survival. For instance, during lipopolysaccharide (LPS) injection, or *Listeria monocytogenes (L. monocytogenes)* infection, an adaptive role has been shown to both homeothermic regulation and anorexia (Wang *et al*, 2016; Ganeshan *et al*, 2019). Hypometabolic hypothermic response was shown to promote disease tolerance and survival, independently of anorexia and lethargy (Ganeshan *et al*, 2019), while anorexia-induced ketogenesis proved essential in mitigating reactive oxygen species (ROS)-induced neuronal damage and thus promoting host survival. Reversing *L. monocytogenes*-associated anorexia through nutritional supplement, in particular, glucose supplement, resulted in lethality (Wang *et al*, 2016). On the other hand, supplementing glucose to anorexic mice during influenza infection increased their survival, suggesting a detrimental mode of anorexia (Wang *et al*, 2016). During *Salmonella typhimurium (S. typhimurium)* infection, the pathogen itself actively inhibits anorexia in the host by blocking the interleukin 1-beta (IL1β)-mediated gut-brain signaling axis. By doing so *S. typhimurium* promoted host survival, and maintained the host's food consumption, which subsequently facilitates prolonged pathogen transmission through fecal shedding (Rao *et al*, 2017).

The work of this thesis investigates the pathophysiology of a more enigmatic nature called "Cachexia". It is a complex syndrome which engages multiple inflammatory, metabolic and behavioral programs across different organs and results in a severe depletion of muscle and fat mass (Fearon *et al*, 2011). Cachexia occurs alongside numerous chronic inflammatory illnesses and is often associated with advanced stages of disease. This includes many aggressive cancer types, chronic infections with human immunodeficiency virus (HIV) or tuberculosis (TB), and other chronic illnesses such as multiple sclerosis, chronic kidney failure, or chronic heart failure (Baracos *et al*, 2018; Keithley & Swanson, 2013; Cheung *et al*, 2010). The manifestation of cachexia has a severe impact on the patient's prognosis and survival. It also affects their mental health and that of their care-givers due to the severe visual effect of such an extreme weight loss, as well as the inability of the patients to care for some of their basic daily needs (Lok, 2015). During cancer-associated cachexia, patients with a very advanced stage of cachexia (so called refractory cachexia) reach a state of weakness in which

therapeutic interventions become inappropriate (Fearon 2011). Moreover, the depleted muscle mass and strength could result in cardiac arrhythmias, respiratory weakness or other complications that may result in mortality (Baracos *et al*, 2018).

1.1 Cachexia: clinical diagnosis, and human data.

In 2011, the results of an international Delphi consensus process was published in the Lancet Oncology led by Fearon et al.(Fearon *et al*, 2011). This process brought together a diverse group of medical and surgical oncologists, palliative care physicians and nutritionists to formalize a definition for cancer-associated cachexia. The consensus reached described cachexia as a multifactorial syndrome, during which skeletal muscle mass is depleted either with or without the depletion of fat mass, and a result of a negative energy balance, and reduced food intake. Importantly, conventional nutritional supplementation is insufficient in reversing cachexia.

In practical terms cachexia in human patients is diagnosed by an involuntary weight loss of over 5% over the course of 6 months (Fearon *et al*, 2011; Baracos *et al*, 2018; Tisdale, 2002). However there are two factors that call for making exceptions to this criteria. The first concerns individuals with a low body mass index (BMI), here cachexia could be defined by the loss of over 2% of body weight with a BMI lower than 20kg/m^2 and/or sarcopenia (Fearon *et al*, 2011). The second concerns individuals with obesity, a very prevalent demographic in modern western societies, and one that is on the rise in many developing countres. In this case weight loss could easily go undetected, especially if muscle loss occurs without a significant loss of fat mass (Martin *et al*, 2013). These variations in the patient's baseline bodyweight makes diagnosis solely on the basis of weight insufficient, especially considering that amongst individuals with the same underlying illness, weight loss occurs at variable stages of disease and progresses at different rates (Baracos *et al*, 2018). This creates a need to set and standardize more sophisticated diagnostic criteria, which incorporate weight loss with computed tomography (CT) or magnetic resonance imagining (MRI) measurement, evaluation of food intake and metabolic alterations (Martin, 2016; Fearon *et al*, 2011). To comprehensively evaluate the loss of muscle and fat mass, most clinical studies used axial lumbar CT scans, which are anchored at the 3rd lumbar vertebra. At this position, a good correlation has been established with the whole body volume of the respective tissue (Baracos *et al*, 2018; Martin, 2016). Cachectic patients are also evaluated for the cause of their reduced food intake, as it is important to establish whether it is due to damage to their digestive track or caused by alterations in their appetite (Baracos *et al*, 2018). Other measurements of serum inflammatory cytokines and signaling hormones have been used to diagnose cachexia, however, these criteria show high variability amongst patients (Martin, 2016). In the case of patients suffering from infection-associated cachexia, there is little data available mostly due

to the low rate of diagnosis. During HIV infection, it is often difficult to distinguish HIV-associated cachexia from HIV-1-associated lipodystrophy syndrome (HALS) (Kotler, 2004; Wanke, 2004). As opposed to cachexia, lipodystrophy is characterized by abnormal lipid redistribution, and its ectopic deposition in other organs, such as liver and muscles. Moreover, lipodystrophy occurs in association with infections such as HIV and tuberculosis (TB), or can result from genetic defects that give rise to either partial or complete lipodystrophy (Vegiopoulos *et al*, 2017).

1.1.1 Adipose tissue wasting.

Adipose tissue wasting is a prominent feature of both cancer- and infection-associated cachexia. In general terms, the proinflammatory state that follows an infection or malignancy, triggers global changes that effect lipid metabolism and adipose tissue homeostasis (Hotamisligil, 2017; Mathis, 2019). The exact inflammatory and/or hormonal mediators of adipose tissue wasting are not entirely defined, and tend to vary across diseases. Adipose tissue lipogenesis and lipid uptake becomes restricted and the rate of lipolysis is increases, which results in a severe depletion of the adipose lipid droplets, and excessive release of none-esterified fatty acids (NEFA) and glycerol into the circulation. This excess of circulating lipids leads to lipotoxicity, increased reactive lipid species and aggravates metabolic dysfunction (Vegiopoulos *et al*, 2017; Sassoon, 2016; Fukawa *et al*, 2016).

When examining adipocyte morphology, it becomes clear that lipid droplets occupy most of the cell volume. Lipid droplets contain mainly neutral lipids in the form of triacylglyceride (TGs) coated by a layer of phospholipids and lipid-associated proteins, such perilipin. During the postprandial state, perilipin act as a protective coat that shields the lipid droplet from the hydrolytic activity of adipose lipases. Meanwhile, adipose triglycerides lipase (ATGL) and hormone sensitive lipase (HSL) are suspended in the cytosol. Ingested dietary lipids are packaged into chylomicrons and very low density lipoproteins (vLDL) in the liver, and then released into the circulation. When they reach the adipose tissue, vascular lipases, mainly lipoprotein lipase (LPL) are secreted into the capillary lumen to hydrolyze the chylomicrons and vLDL TG content. This is an essential step that allows lipid uptake into the cells (Whitehead, 1909), either passively through cellular diffusion, or actively through membrane proteins such as the lipid scavenger receptor CD36 (Balaban *et al*, 2015). Within adipocytes, NEFAs are converted into fatty acyl-CoA (FA CoA) to serve as an acyl-donor for TG synthesis, either through the glycerol phosphate pathway, or through the monoacylglycerol (MG) pathway (Coleman *et al*, 2002). Both pathways converge upon the synthesis of diacylglycerols (DG), which are then further esterified into TGs and packaged into a membrane bilayer through acyl-CoA:diacylglycerol acyltransferase (DGAT) family enzymes DGAT1 and DGAT2,

the rate-limiting enzyme being DGAT2, due to its higher enzymatic activity at lower substrate levels (Liang *et al*, 2008).

When fasting, or undergoing stressful conditions, lipolysis is activated in response to a number of stimuli that either bind and activate cell surface receptors or diffuse through the cell membrane. On the cell surface, thyroid stimulated hormone receptors (TSHRs), beta-adrenergic receptors (β-ARs) and natriuretic peptide receptor A (NPR-A) activate lipolysis in response to signals from free thyroxine (fT4) and free triiodothyronine (fT3), catecholamines, or natriuretic peptides respectively (Duncan *et al*, 2007; Nielsen *et al*, 2014). The binding of TSHRs or β-ARs to their ligands leads to the activation of adenyl cyclase (AC) through guanine nucleotide-binding protein (GNAS), and the release of cyclic adenyl monophosphate (cAMP), which in turn phosphorylates protein kinase A (PKA). In humans the activation of NPR-A leads to the release of cyclic guanine monophosphate (cGMP), which in turn phosphorylates protein kinase G (PKG) (Nielsen *et al*, 2014). PKA and/or PKG subsequently phosphorylate both perilipin and HSL (Ser660). Phosphorylated HSL (pHSL) translocated towards the surface of the lipid droplet, whereas phosphorylated perilipin undergoes conformational changes that lead to increased access to the lipid droplet, allowing pHSL and ATGL to bind to their lipid substrate (Zechner *et al*, 2012). Moreover, when perilipin is phosphorylated it releases the Comparative Gene Identification-58 (CGI-58) which is otherwise bound to it. CGI-58 then binds to ATGL, which is an essential step for ATGL to reach its full hydrolytic capacity (Lass *et al*, 2006; Lu *et al*, 2010). ATGL also interacts with G0G1 switch protein 2 (G0S2), however the full nature of their interaction is still not fully understood (Lu *et al*, 2010). HSL/pHSL and ATGL activity mediates about 90% of lipolysis in the adipocytes (Schweiger *et al*, 2006). HSL mediates stimulated lipolysis and is capable of hydrolyzing TGs and DGs, though it has a higher affinity for the latter. ATGL mediates basal lipolysis, and mainly acts on TGs. The remaining MG are broken down by MG lipase (MGL) and the resulting NEFAs are released into the circulation. NEFAs are taken up by other tissue as substrates for fatty acid oxidation (FAO), ketoneogenesis or other synthetic or signaling pathways (Rambold *et al*, 2015; Nielsen *et al*, 2014; Calder, 2012). Glycerol is transported into the liver, where it is used in gluconeogenesis (Jelen *et al*, 2011) (Figure 1).

It is worth noting that lipogenesis and lipolysis are not mutually exclusive processes, but they are constantly held in balance to mediate a cycle of hydrolysis and re-esterification. This creates a buffering system to prevent the accumulation of reactive lipid species, provides intermediary molecules and allows for the replenishment of the adipose lipid pool (Zechner *et al*, 2012; Arner & Langin, 2014). Within the lifespan of an adipocyte, which is approximately 10 years, its lipid content is renewed over 6 times, a rate which inversely correlates with adipose tissue inflammation, highlighting an important role for the hydrolysis-re-esterification cycle in maintaining tissue homeostasis (Arner *et al*, 2011; Rydén *et al*, 2013).

During cancer-associated cachexia, a number of proinflammatory cytokines including tumor necrosis factor (TNF), interleukin 6 (IL6) and interferon gamma (IFNγ) have been shown to mediate adipose tissue wasting by increasing energy expenditure, lipid mobilization or by increased catecholamine signaling (Arner & Langin, 2014). The increase in energy expenditure could be partially attributed to the increased rate of adipose tissue beiging/browning, which takes place in a subset of adipocytes called beige/bright adipocytes (Petruzzelli *et al*, 2014; Kir *et al*, 2014). This subset of cells has a distinct lineage from both white (WAT) and brown (BAT) adipocytes. In steady state, beige adipocytes accumulate large lipid droplets and behave as WAT. However, when non-shivering thermogenic demand is increased, these cells adopt a more BAT-like behavior, by increasing their mitochondrial content and performing uncoupling protein 1 (UCP1)-mediated thermogenesis (Wu *et al*, 2012; Petruzzelli *et al*, 2014). This process consumes a large amount of NEFAs which is thought to account for a portion of the energy loss during certain types of cancer-associated cachexia. The extent to which adipose tissue beiging contributes to cachexia in humans, however, is still controversial (Baracos *et al*, 2018). The cachexia-associated increase in lipolysis occurs through a variety of pathways associated with systemic inflammation. On a transcriptional level, increased ATGL (*Pnpla2*) and/or HSL (*Lipe*) mRNA expression can

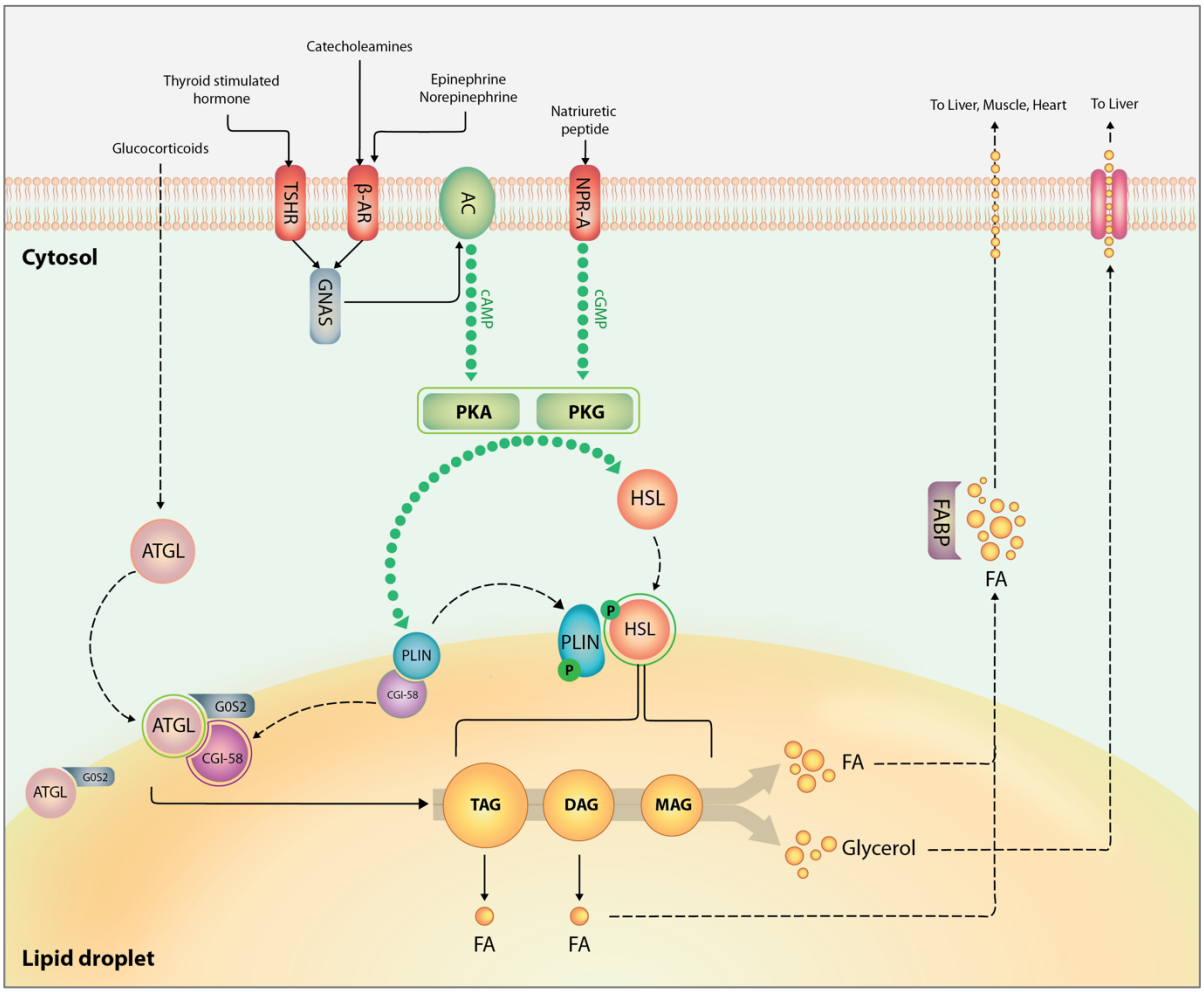

Figure 1: Adipose tissue lipolysis.
Activation of lipolysis during fasted state is mediated by a number of hormonal signals, including glucocorticoids (GCs), thyroid stimulated hormones (TSH), catecholamines, and natriuretic peptides (NP). GCs diffuse freely across the cellular membrane and mediate a variety of functions through the binding to their cytosolic GC-receptor (GR). The binding of TSHR, β-ARs or NPR-A to their respective ligands triggers the release of cAMP/cGMP, the phosphorylation of PKA/PKG, and their downstream targets, including HSL, ATGL and PLIN. This leads to the increased lipolysis and the breakdown of TGs, DGs, and MG into free fatty acids and glycerol which are then released into the circulation.

promote lipolysis. Although, the two do not always correlate, indicating that other regulatory approaches are more important in regulating ATGL and HSL activity (Zechner *et al*, 2012).
Increased adipose tissue lipolysis also occurs due to decreased perilipin (*Plin1*) mRNA expression, rendering lipid droplets more exposed to lipolysis (Silvério *et al*, 2017). Other factors can affect the PKA-mediated phosphorylation, either directly, or by blocking adenyl monophosphate-activated protein kinase (AMPK), a negative regulator of PKA phosphorylation (Djouder *et al*, 2010).

1.1.2 Muscle atrophy.

Muscle atrophy is perhaps the most studied aspect of cachexia, as it is thought to be the main factor leading to functional impairment and mortality (Cohen *et al*, 2014). The reduced muscle mass and strength limits the patient's ability to perform daily activities and to care for themselves, which could have a big impact on their psyche, and put them in a greater risk of harm (Lok, 2015). Moreover, muscle atrophy is not only limited to skeletal muscles but could also interfere with both cardiac and pulmonary function (Baracos *et al*, 2018; Argilés *et al*, 2018). In both humans and mice, the onset of cachexia results in a reduction of heart size (Olivan *et al*, 2012; Barkhudaryan *et al*, 2017), cardiac fibrosis, and alterations in myocardial ultrastructure and contractile protein complex composition (Belury *et al*, 2010), these and other factors could result in life threatening cardiac arrhythmias.
Muscle atrophy is attributed to three major factors: increased proteasomal activity (Sandri, 2016), increased autophagy (Von Haehling *et al*, 2017), and reduction of muscle regeneration (Bossola *et al*, 2016). These processes share common upstream signaling pathways, mainly the PI3K-AKT-mTOR signaling axis (Cohen *et al*, 2014). During normal muscle growth, the activation of this pathway leads to increased protein synthesis, and suppresses the transcription factor forkhead box protein O (FOXO) (Glass, 2005). However, when muscle atrophy is induced in conditions such as cachexia, PI3K-AKT-mTOR pathway signaling is

attenuated. As a result, the rate of protein synthesis drops, and the FOXO proteins are free to translocate into the nucleus. FOXO1 and FOXO3, then mediates the increased mRNA expression of muscle-specific RING-finger1 (*Murf1*) and *atrogin1*, both of which are proteasomal proteases, commonly used as markers for muscle atrophy due to their consistent increase across different models (Cohen *et al*, 2014). Moreover, FOXO1 and FOXO3 also mediate the increased expression of genes involved in autophagy, a process by which cells degrade unnecessary and dysfunctional organelles and cellular components (Von Haehling *et al*, 2017). Muscle regeneration is also affected during cachexia, as indicated by the decreased expression of myoblast determination protein 1 (Myod1). Myod1 is a master regulator of muscle regeneration and growth. During cachexia, its expression is suppressed through the activation of the NF-κB pathway, which prevents muscle stem cells from differentiating into mature myotubes (Guttridge *et al*, 2000).

Several lines of evidence suggest that adipose tissue wasting predisposes or aggravates muscles atrophy. This could be either through adipocyte secretion of proinflammatory factors and cytokines, which directly trigger muscle atrophy (Argilés *et al*, 2018), or through the increased release of NEFA in the circulation (Fukawa *et al*, 2016). The excessive rate of FAO in skeletal muscles during cachexia leads to high levels of oxidative stress and ROS generation. This in turn activates p38 mitogen-activated protein kinase (p38 MAPK) pathways, and leads to muscular defects (Fukawa *et al*, 2016).

1.1.3 Soluble signaling regulators of cachexia.

Amongst the clinical data available from cachectic patients during cancer, infection and chronic illness, circulating cytokine profiles and acute-phase proteins (APP) are abundant. However, these measurements are inconsistent and thus ill-suited as diagnostic criteria (Martin, 2016; Baracos *et al*, 2018). A plausible explanation for these inconsistences is the difference in the inflammatory context and/or genetic background of the patients.

TNF, IL6, IL1 and IFNγ are some of the most prominent cytokines associated with cachexia (Fearon *et al*, 2012; Argilés *et al*, 2009). In the periphery, these pro-inflammatory cytokines can induce wasting by modulating gene expression through their activation of master regulatory pathways, such as the Janus kinase family protein/signal transducer and activator of transcription protein (JAK/STAT) pathway or the NF-kB pathways (Fearon *et al*, 2012; Guttridge *et al*, 2000). For instance, in adipocyte cultures, TNF has been shown to inhibit adipocyte differentiation (Sethi & Hotamisligil, 1999), lipogenesis and lipid uptake (Price *et al*, 1986), and to promote ATGL-mediate lipolysis (Yang *et al*, 2011; Patel & Patel, 2016). TNF effects on lipolysis occur downstream of mitogen-activated protein kinase kinase and extracellular signal-related kinase (MEK/ERK) signaling axis. MEK/ERK TNF-mediated pathway activation leads to the inhibition of phosphodiesterase 3 (PDE3B) (Aoyagi *et al*,

2015). PDE3B is an enzyme downstream of insulin receptor signaling that limits PKA activity through the sequestration of cAMP, and its conversion into 5'AMP (Nielsen *et al*, 2014). TNF also mediates skeletal muscle wasting through its engagement with the NF-kB pathway (Patel & Patel, 2016).

Many of these cytokines can also mediate both behavioral and physiological changes through central regulation (Burfeind *et al*, 2016). The mediobasal hypothalamus (MBH) is part of the central nervous system (CNS) that is particularly sensitive to inflammation, and can regulate both feeding behavior and systemic metabolism (Cone *et al*, 2001). This modulation is likely to be through cytokines targeting orexigenic neurons such as agouti-related peptide (AgRP) or neuropeptide Y (NPY), or targeting anorexigenic neurons such as pro-opiomelanocortin (POMC) (Grossberg *et al*, 2010). Cachectic patients suffering from pulmonary TB infection showed elevated serum levels of peptide YY (PYY) (Chang *et al*, 2013), an appetite-regulating hormone, which is secreted in the intestine and mediated a feedback regulation by interacting with NPY in the hypothalamus (Vincent & le Roux, 2008).

Alternatively, cytokine signaling in the MBH, for example by IL1β, can lead to activation of the hypothalamic-pituitary adrenal axis (HPA) (Katsuura *et al*, 1988; Braun *et al*, 2011). This activation of HPA, results in increased glucocorticoid (GC) production, which are known to promote lipolysis in adipose tissue (Xu *et al*, 2009), and increased proteasomal degradation, while inhibiting protein synthesis in muscles (Wing & Goldberg, 1993; Braun *et al*, 2011). In the adipose tissue, GCs exhibit their effect on lipolysis through their engagement with the cytosolic GC-receptor (GR) and its translocation into the nucleus, which then triggers a wide range of transcriptional modulation (John *et al*, 2016). This includes the increased expression of β-ARs and decreased PDE3B expression, which promote PKA-mediated lipolysis (Nielsen *et al*, 2014). Additionally GCs increased ATGL and HSL expression while decreasing the expression of perilipin (Xu *et al*, 2009).

Adipose tissue inflammation, also leads to the increased production of leptin, an adipokine with a wide range of influence. It acts as a proinflammatory cytokine (Procaccini *et al*, 2013; Cava & Matarese, 2004), promotes adipose tissue lipolysis (Friedman & Halaas, 1998; Vegiopoulos *et al*, 2017) and modulates feeding behavior through its STAT3 mediated hypothalamic signaling (Morrison, 2009; Zeng *et al*, 2015).

1.2 Therapeutic approaches.

In the majority of cases, therapeutic strategies addressing cachexia focus on establishing supportive dietary and exercise regiments that meet the patient's capacity (Arends *et al*, 2017). Indeed, multiple trials showed a measurable improvement in muscle strength after aerobic and resistance exercise during the early stages of cachexia (Stene *et al*, 2013). Nutritional support occurs in different forms, depending on the disease stage of the patient

(Fearon *et al*, 2011). During the early stages of cachexia, patients received dietary supplements and/or follow dietary programs under the close observation of a nutritionist. However, at an advanced stage patients suffering severe functional impairment are forced to rely on enteral or parenteral feeding (Arends *et al*, 2017; Baracos *et al*, 2018).

In some cases, orexigenic treatments are also implemented to increase the patient's appetite and food intake. Such an example is Anamorelin, a ghrelin agonist which stimulates food intake by binding to the growth hormone secretagogue receptor (GHS-R) (Von Haehling & Anker, 2014; DeBoer, 2011). Patients suffering from cancer-associated cachexia (DeBoer, 2011), as well as chronic obstructive pulmonary disease (COPD)-associated cachexia (Miki *et al*, 2012) receiving Anamorelin treatment showed some improvement in body weight, fat and lean mass, however, no correlation was made to strength or survival (Argilés *et al*, 2017; Von Haehling & Anker, 2014).

Other pharmacological treatments target either specific cachexia-associated proinflammatory cytokines such as IL6 and TNF, aim to alter muscle atrophy (Zhou *et al*, 2010), or target lipid metabolism (Argilés *et al*, 2017). However, in most of these cases, the involvement of these factors vary according to the underlying illness, which speaks for the importance of personalized treatment plans to achieve the most improvement.

1.3 Experimental models of Cachexia.

The majority of the mechanistic information available regarding cachexia is acquired through murine models of cancer-associated cachexia. Many of these models rely on ectopic or orthotopic injection of cancer cells that have been cultivated in culture (DeBoer, 2009). Both approaches have their limitations (Penna *et al*, 2016), and the choice of administration route has to be made carefully as it results in phenotypic variations both in the tumor growth and the manifestation of cachexia. When using ectopic injection, tumors grow at very high rate, while cachexia takes time to manifest. This leaves a very narrow time window to study cachexia, before it becomes ethically necessary to sacrifice the mice (DeBoer, 2009; Penna *et al*, 2016). On the other hand, using orthotopic injection requires performing surgery, which introduces an additional factor of variability and is more invasive. Even when using ectopic administration, the outcome can highly vary between subcutaneous or intramuscular injections. For instance, when administering Lewis lung carcinoma (LLC) cells subcutaneously, it takes 28 days for cachexia to develop. With intramuscular administration, cachexia develops within 15 days only. Moreover, the rate of metastasis is much higher with subcutaneous injection (Penna *et al*, 2016). Another examples is the C26 colon cancer model, where anorexia is only seen during subcutaneous but not intraperitoneal injection. In both cases, the mice do exhibit other signs of cachexia, including both adipose tissue and muscle wasting (Matsuyama *et al*, 2015).

Tumors used as cancer cachexia models also differ in their genetic background, an important variable to consider when weighing the translational potential of a dataset. The LLC cells were obtained from C57BL/6 mice that spontaneously developed tumors (Margret Lewis 1951). In this case, one could consider this a naturally developed tumor, though the highly inbred nature of these mice could be a contributing factor. The C26 colon cancer model, is chemically induced and therefore carries an artificial developmental pathway. It was isolated from a mouse that was exposed to carcinogens (Corbett *et al*, 1975).

In order to mimic the slow and gradual progression of cachexia observed in humans, a number of genetic models were developed. $APC^{min/+}$ mice, contain a mutation in the tumor suppressor gene adenomatous polyposis coli (*Apc*). They develop tumors when they're approximately 4 weeks old, and cachexia 10 weeks after the tumor development. Around 16 days after tumor development, a 15% weight loss is observed (Puppa *et al*, 2011; Baltgalvis *et al*, 2010). Other models include the $Tsc2^{+/-}$Eμ-Myc model for B lymphomas, the MKN-45 stomach cancer model, and the ASV-B model for hepatocellular carcinoma (HCC). There are also genetic models available for metastatic tumor models such as the two breast cancer metastasis models MDA-MB-231 and 4T1 mammary carcinoma (Konishi *et al*, 2015).

Models of cachexia outside the cancer setting are very limited, especially when it comes to infection-associated cachexia. Experimental models of parasitic infections develop cachexia gradually over a longer timeframe before reaching their endpoint. Such models include infection with *Toxoplasma gondii*, an obligatory intracellular protozoan with multiple hosts to support different stages of its life cycle (Molloy *et al*, 2013). When Toxoplasma cysts are ingested, mice lose up to 20% of their initial body within the first 10 days after infection. The infected mice display anorexia and wasting of their fat and muscle mass, which is sustained for over 90 days after infection, independently of the parasite load (Hatter *et al*, 2018). This long-term onset of cachexia gives this model a big advantage, as it simulates the prolonged nature of cachexia in humans, and allow for long-term investigations into therapeutic opportunities. Infection-associated cachexia also occurs in mice infected with *Trypanosoma cruzi*, another protozoan parasite (Teixeira *et al*, 2002). Yet, in this model weight loss is only seen around day thirty after infection (Truyens *et al*, 1999).

To acquire sterile models of cachexia, independent of infection and malignancy, the implementation of surgical procedures become necessary. For example, to investigate cachexia during chronic cardiac disease, models of myocardial infarction and aortic banding are often used to induce heart failure (DeBoer, 2009). Another two-step surgical procedure leaves the mice or rats with $1/6^{th}$ of a functional kidney, which renders them uremic, and induces slower weight gain and loss of muscle mass within two weeks following the surgery (Deboer *et al*, 2008).

1.4. Lymphocytic choriomeningitis virus (LCMV).

Lymphocytic choriomeningitis virus (LCMV), is a single stranded negative sense RNA virus belonging to the Arenaviredae family (Bergthaler *et al*, 2010, 2007; Buchmeier *et al*, 2007). LCMV is is a virus with a relatively simple genome of ten kilobases divided between two RNA segments in an ambisense orientation (Flatz *et al*, 2006; Buchmeier *et al*, 2007). The long (L) segment encodes for the RNA-dependent RNA polymerase and the matrix protein Z, required for virus budding from the cells. The short (S) segment codes for the viral nucleoprotein (NP), which enclose the virus RNA, and the glycoprotein (GP), required for binding to cell surfaces and entry (Bergthaler *et al*, 2010; Lee *et al*, 2002). On each segment, the two genes are separated by an intergenic region, which enables the viral RNA to fold into a stable secondary structure, and is thought to play an important role in the viral life cycle (Pinschewer *et al*, 2005). This viral model has been extensively studied in the past few decades and has been instrumental in establishing fundamental concepts in adaptive immunity and antiviral immune response (Zhou *et al*, 2012; Zinkernagel & Doherty, 1979). This is because LCMV provides a versatile tool capable of generating different pathophysiological conditions depending on the route of infection, the dose, and the strain of LCMV used. For instance, intracranial injection (i.c.) of LCMV results in severe meningitis ending in mortality within 6 to 8 days after infection. On the other hand intravenous (i.v.) or intraperitoneal injections (i.p.) generates a systemic infection, from which mice are able to recover (Hotchin & Benson, 1963). Moreover, there are multiple stains of the LCMV leading either acute (LCMV-Arm and LCMV-WE) or chronic (LCMV-Cl13 or LCMV-docile) (Bergthaler *et al*, 2007).

LCMV is not a cytolytic virus, and thus, the virus itself does not inflict direct cytotoxicity to the infected cells. However, LCMV elicits a very strong antiviral immune response, which is initiated at the innate phase by type I IFN signaling (Teijaro *et al*, 2013) and followed in the adaptive phase by a robust cytotoxic $CD8^+$ T cell response (Zinkernagel *et al*, 1986; Wherry *et al*, 2003). Thus, the pathologies associated with LCMV infection are primarily $CD8^+$ T cell-mediated immunopathologies (Pfau *et al*, 1982; Zinkernagel *et al*, 1986).

1.4.1 LCMV antiviral immune response.

The majority of the work discussed in this thesis utilize a model in which C57BL/6J mice were infected intravenously (i.v.) with a high dose $2x10^6$ focus forming units (FFU) of LCMV clone 13 (LCMV-Cl13). This results in chronic infection in which the virus is able to persist for over 60 days after infection (Bergthaler *et al*, 2010). The immune response triggered against LCMV-Cl13 can be divided into four main phases: the initial innate phase, mainly driven by type I IFN and cytokine signaling. The adaptive immune response, driven by cytotoxic $CD8^+$ T cell response, with assistance from $CD4^+$ T cells, and B cells that produce LCMV-binding

non-neutralizing and, in a later phase of the infection, neutralizing antibodies (Richter & Oxenius, 2013; Cerny *et al*, 1988). The viral persistence phase is associated with T cell exhaustion (Wherry *et al*, 2003; Cornberg *et al*, 2013) until the virus is cleared (Figure 2).

1.4.2 Type I IFN response.

Viral recognition starts within the first hours after infection, mainly through innate antigen presenting cells such as dendritic cells (DCs) and macrophages. These cells are able to recognize pathogen-associated molecular patterns (PAMPs) through specialized detectors

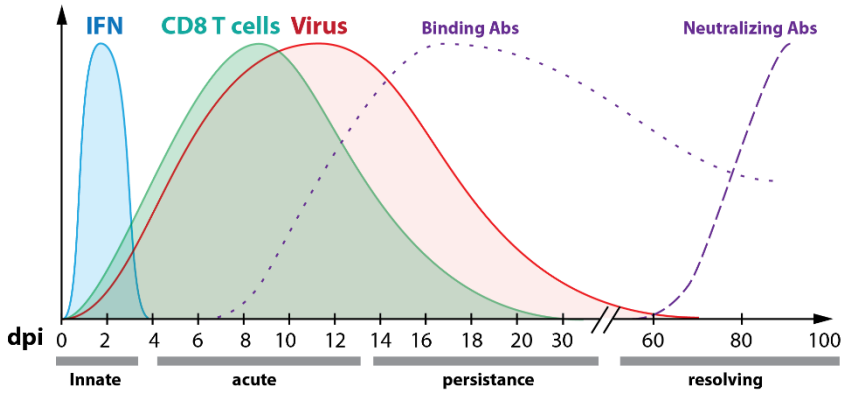

Figure 2: Antiviral response against chronic high dose LCMV Clone 13 infection.
Time kinetics depicting the different phases of the immune response following intravenous infection with high dose ($2x10^6$ FFU) LCMV-Cl13.

called the Pattern-recognition receptors (PRR). In the case of LCMV infection, the viral RNA acts as the PAMP and is recognized by a number of PRR (Sullivan *et al*, 2015), including endosomal Toll-like receptor 7 (TLR7) (Walsh *et al*, 2012; Bell, 2005), cytosolic retinoic acid-inducible gene I (RIG-I) and melanoma differentiation-associated protein 5 (MDA5) (Taylor & Mossman, 2013). In the cytosol, viral recognition via RIG-I and MDA5 triggers phosphorylation of interferon regulatory factor 3 (IRF3), its homodimerization and nuclear translocation, where it mediates increased IFN-β and IRF7 expression (Taylor & Mossman, 2013). This creates a self-propagating signal, as IRF7 protein forms heterodimers with nuclear IRF3 and further amplifies the type I IFN signal (Ning *et al*, 2011). On target cells, secreted IFNs bind to the IFN receptor (IFNAR), which initiates JAKs-mediated phosphorylation of STAT1 and STAT2. Phosphorylated STAT1 and STAT2 then bind to IRF9 forming a heterotrimeric complex called IFN-stimulated gene factor 3 (ISGF3). Finally, ISGF3 translocates into the nucleus and

induces the expression of a wide array of IFN-stimulated genes (ISGs) that participate in anti-viral responses (Pitha & Kunzi, 2007; Wu *et al*, 2016) (Figure 3). Early type I IFN production occurs in plasmacytoid DCs (pDC) (Swiecki & Colonna, 2015), which are preferential targets

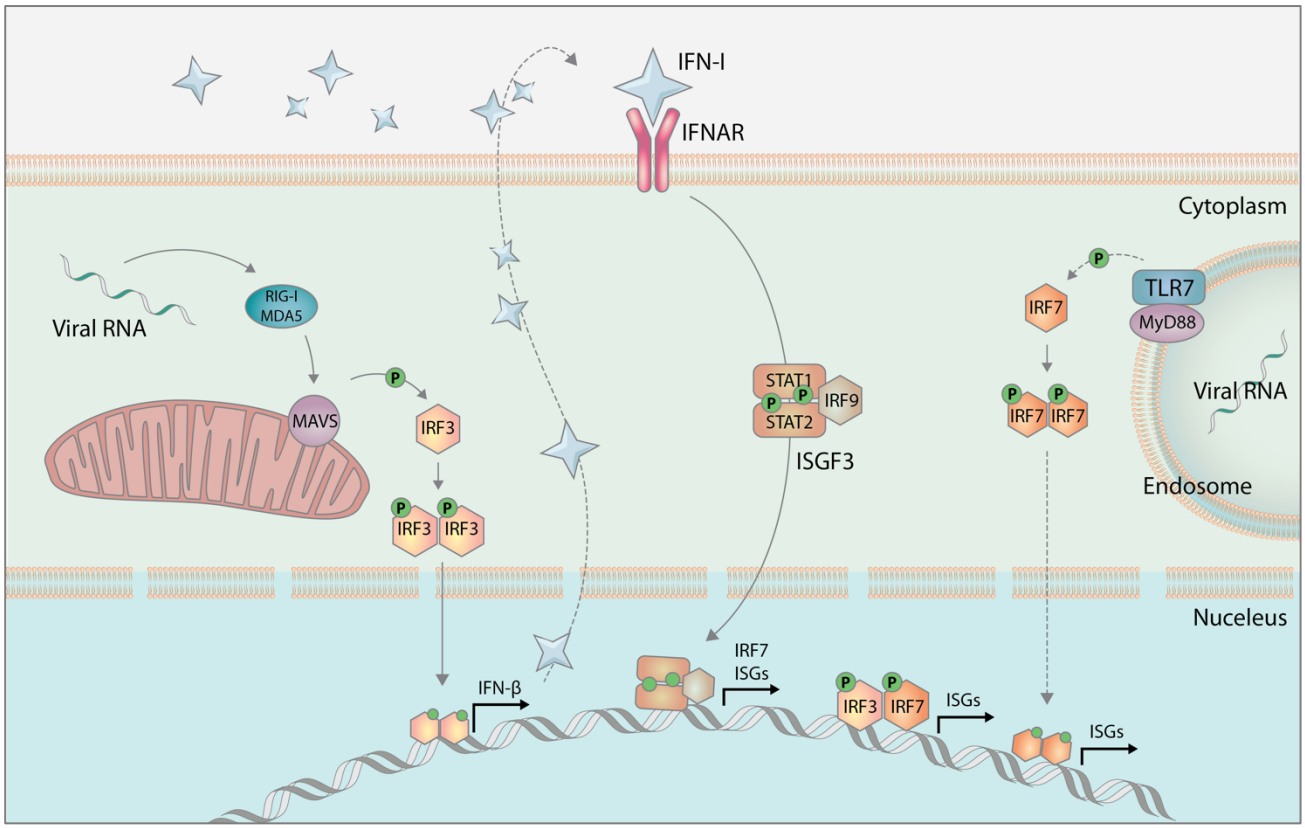

Figure 3: Type I IFN response.

Viral recognition in the cytosol, through RNA-specific PRRs such as RIG-I or MDA5 leads to MAVS-mediated phosphorylation of IRF3, its homodimerization and translocation to the nucleus which induces IFN-β expression. IFNs then propagate their signaling in an autocrine fashion through binding to type I IFN receptors, and the formation of ISGF3, which then translocate to the nucleus and induce the expression of IRF7 and other ISGs. Viral recognition can also occur in the endosomes, after viral internalization by phagocytes. This is mediates by the TLR7-MyD88 complex and the downstream dimerization of IRF7. IRF7 and IRF3 also form heterodimers further express ISGs.

of LCMV infection (Bergthaler *et al*, 2010; MacAl *et al*, 2012). The infection of the DCs allows the virus to resist their function, as it dampens their antigen presentation capacity (Sevilla *et al*, 2004), and type I IFN production. This also involves the binding of the viral NP to IRF3, which blocks IRF3-mediated IFNβ production (Martinez-Sobrido *et al*, 2006).

1.4.3 CD8$^+$ T cells response.

The adaptive immune response against LCMV is mainly driven by CD8$^+$ T cells. To initiate virus-specific CD8$^+$ T cell response, the cells needs to receive three distinct signals. The first is driven by T cell receptor (TCR) binding to the viral antigen presented by the major-histocompatibility complex (MHC) of APCs. Once this signal is received another co-stimulatory signal must follow through the binding of CD28 T cell receptor with its ligand B7 on the surface of APC, to insure the survival and maintenance of virus-specific CD8$^+$ T cell clones (Jenkins & Johnson, 1993). The third signal is mediated either by IL12 (Schmidt & Mescher, 1999) or type I IFN signaling (Curtsinger *et al*, 2005) (Figure 4). These Primed CD8$^+$ T cells can then mediate their effector function though cytokine secretion such as TNFα and IFNγ, or through the release of cytotoxic granules carrying granzyme B (GzmB) and perforin (PFN) (Zhou *et al*, 2002).

Variations in the inflammatory milieu, timing and intensity of the signals received by CD8$^+$ T cells during their priming trigger profoundly different response programs that distinguish acute from chronic infections (Virgin *et al*, 2009; Wherry, 2011). The IFN-I signal is critical for the increased expression of CD8$^+$ T cells inhibitory signals, such as IL10 and programmed death receptor ligand 1 (PD-L1) (Teijaro *et al*, 2013). Moreover, the viral replicative capacity is substantially higher in the LCMV-Cl13 model, which results in an increased pathogenic burden, and a prolonged TCR activation, which in turn activated the so called “exhaustion” transcriptional program (Bergthaler *et al*, 2010). Exhausted T cells exhibit dampened effector function and proliferation. This allows the virus to persist within its host for prolonged periods of time, yet keeps its replication in check, and minimize collateral tissue damage while T cells work slowly but steadily at clearing the infection (Wherry *et al*, 2003; Moskophidis *et al*, 1993; Virgin *et al*, 2009).

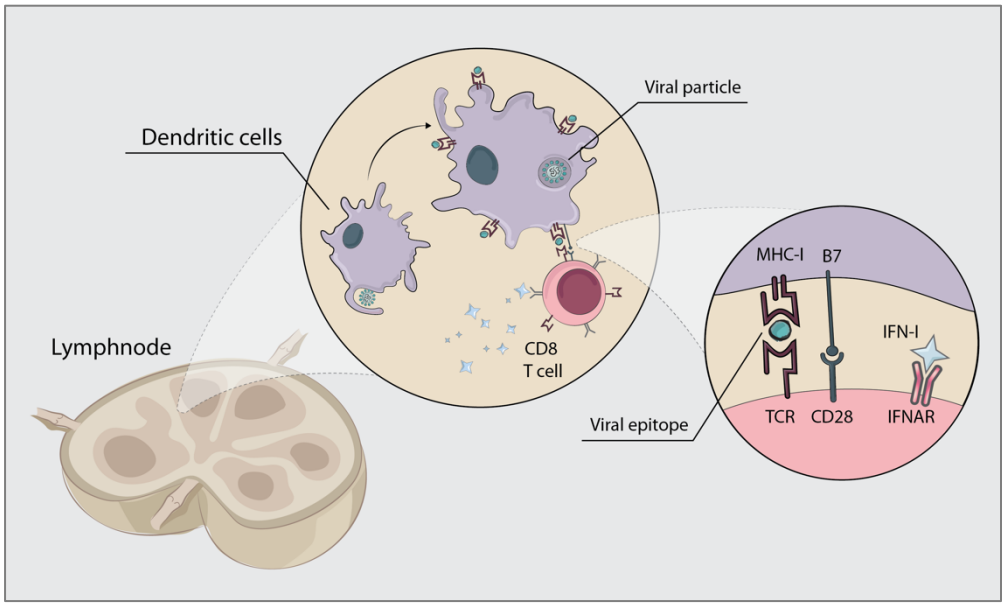

Figure 4: CD8$^+$ T cell priming.

Antigen recognition occurs in secondary lymphoid organs, such as the lymph nodes, where phagocytic cells, mainly DCs internalize viral particles, digest the viral peptides and then present them as epitopes on their surface MHC class I molecules. Virus-specific priming of CD8$^+$ T cells requires three critical signals: MHC-I-epitope binding to TCR, B7-CD28 binding, and a third signal from type I IFN or IL12.

2. Aims

The aim of this work was to achieve the following:

2.1 To establish that infection with chronic strain of LCMV is a valid model for studying infection-associated cachexia.

2.2 To characterize the similarities and differences between cancer-associated cachexia and infection-associated cachexia.

2.3 To identify the inflammatory and immune factors responsible for triggering cachexia during chronic viral infection.

3. Results.

3.1 Prologue.

Cachexia is a debilitating syndrome that effects the quality of life, morbidity and mortality of patients suffering a variety of chronic and terminal illnesses. It is a highly unmet medical need, where standards of care are lagging and treatment options are unavailable (Lok, 2015; Baracos *et al*, 2018). In this is study, we employed a benchmark model of chronic viral infection using lymphocytic choriomeningitis virus (LCMV) in order to delineate the mechanisms of immune-metabolic crosstalk during infection-associated cachexia (Figure 6). We characterized the common and unique properties of infection-associated cachexia in comparison to cancer-associated cachexia, with a focus on adipose tissue biology and the inflammatory triggers. During LCMV-induced infection-associated cachexia, the adipose tissue underwent severe morphological and metabolic reprogramming, similar to that seen during cancer associated cachexia. However, in this model adipose tissue beiging (browning) did not contribute to the tissue wasting. Moreover, we found that classical cachexia-associated cytokines such as TNFα, IFNγ, IL6 and IL1 are not involved in infection associated cachexia. Instead, the initiation of cachexia required $CD8^+$ T cell-intrinsic type I IFN signaling and antigen specific T cell priming. Our data identifies a novel signaling axis implicating antigen-specific $CD8^+$ T cells as previously unknown inducers of infection-associated cachexia (Baazim *et al*, 2019).

3.2 Scientific articles reporting on this study.

Not the usual suspect: type I interferon–responsive T cells drive infection-induced cachexia.
(Wang & Medzhitov, 2019)
Nature Immunology, News & Views, 2019
https://doi.org/10.1038/s41590-019-0374-5

Cachexia by T cells.
(Bird, 2019) *Nature Reviews Immunology, 2019*
http://www.nature.com/articles/s41577-019-0186-8

Cachexia Is Driven By Killer T Cells in a Mouse Model of Infection.
Katarina Zimmer, The Scientist.
https://www.the-scientist.com/news-opinion/cachexia-is-driven-by-killer-t-cells-in-a-mouse-model-of-infection-65922

Was den kranken Körper schwinden lässt
Wolfgang Dauble, Die Presse.
https://diepresse.com/home/premium/5634073/Was-den-kranken-Koerper-schwinden-laesst?from=suche.intern.portal

3.3 Graphical abstract.

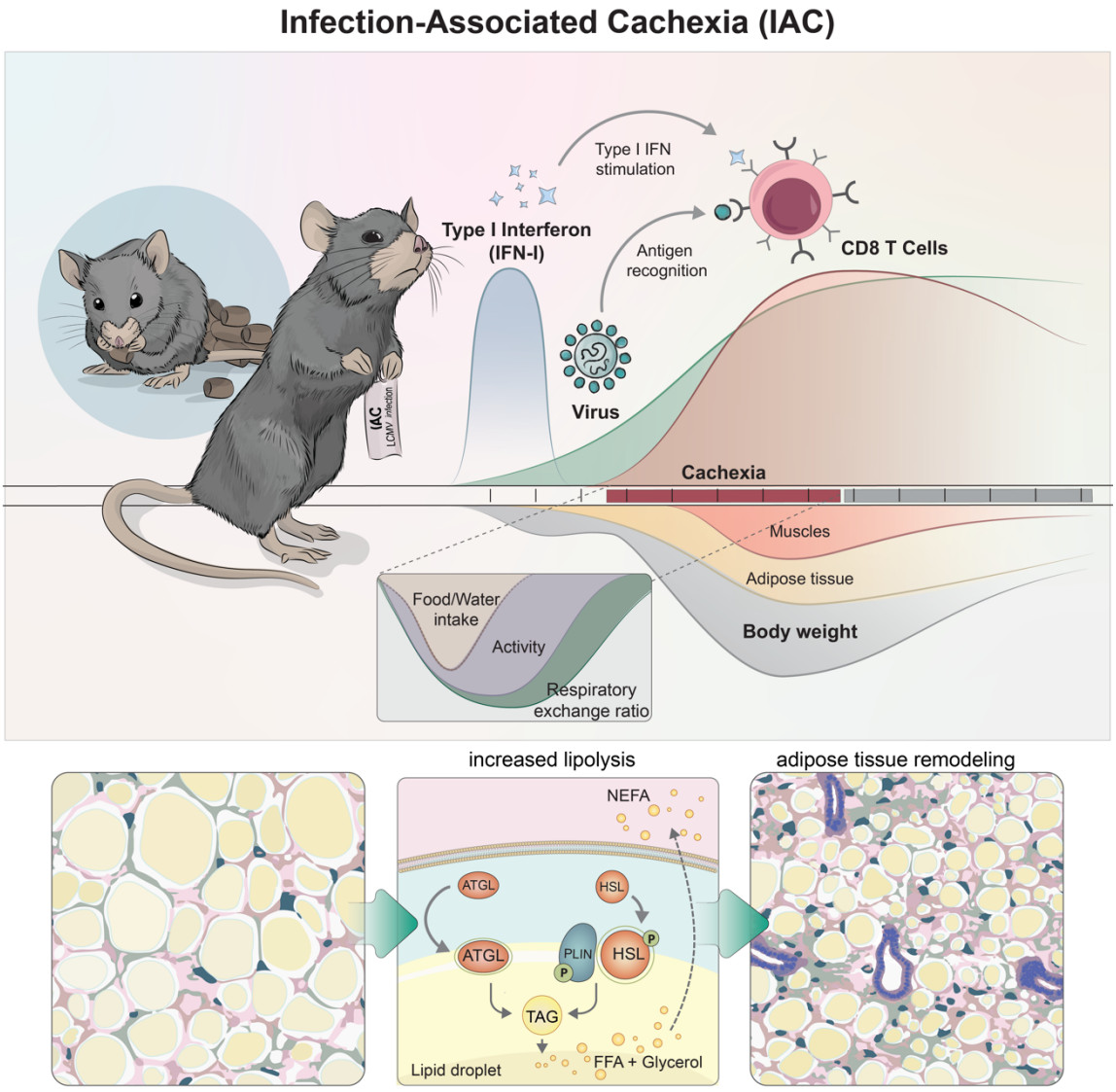

Figure 5: Infection-associated cachexia (IAC).

Following infection with a chronic virus, $CD8^+$ T cells are able to induce weight loss and cachexia. This requires virus-specific T cell activation as well as type I IFN signaling. The weight loss occurs as a result of depletion of both muscles and adipose tissue, and is associated with a reduction on food and water intake, reduced activity, and reduced respiratory exchange ratio (RER). During the development of cachexia, adipose tissue undergoes severe metabolic and structural reorganization.

3.4 Manuscript: CD8$^+$ T cells induce cachexia during chronic viral infection.

Nature Immunology. 20: 701-210, June 2019, https://doi.org/10.1038/s41590-019-0397-y

Hatoon Baazim*, Martina Schweiger, Michael Moschinger, Haifeng Xu, Thomas Scherer, Alexandra Popa, Suchira Gallage, Adnan Ali, Kseniya Khamina, Lindsay Kosack, Bojan Vilagos, Mark Smyth, Alexander Lercher, Joachim Friske, Doron Merkler, Alan Aderem, Thomas H. Helbich, Mathias Heikenwälder, Philipp A. Lang, Rudolf Zechner & Andreas Bergthaler**

* First author

** Corresponding author

nature immunology

ARTICLES

https://doi.org/10.1038/s41590-019-0397-y

CD8+ T cells induce cachexia during chronic viral infection

Hatoon Baazim[1], Martina Schweiger[2,9], Michael Moschinger[1,9], Haifeng Xu[3], Thomas Scherer[4], Alexandra Popa[1], Suchira Gallage[5], Adnan Ali[5], Kseniya Khamina[1], Lindsay Kosack[1], Bojan Vilagos[1], Mark Smyth[1], Alexander Lercher[1], Joachim Friske[6], Doron Merkler[7], Alan Aderem[8], Thomas H. Helbich[6], Mathias Heikenwälder[5], Philipp A. Lang[3], Rudolf Zechner[2] and Andreas Bergthaler[1]*

Cachexia represents a leading cause of morbidity and mortality in various cancers, chronic inflammation and infections. Understanding of the mechanisms that drive cachexia has remained limited, especially for infection-associated cachexia (IAC). In the present paper we describe a model of reversible cachexia in mice with chronic viral infection and identify an essential role for CD8+ T cells in IAC. Cytokines linked to cancer-associated cachexia did not contribute to IAC. Instead, virus-specific CD8+ T cells caused morphologic and molecular changes in the adipose tissue, which led to depletion of lipid stores. These changes occurred at a time point that preceded the peak of the CD8+ T cell response and required T cell–intrinsic type I interferon signaling and antigen-specific priming. Our results link systemic antiviral immune responses to adipose-tissue remodeling and reveal an underappreciated role of CD8+ T cells in IAC.

Patients with chronic illnesses such as infections and malignancies are often confronted with cachexia, a multifactorial syndrome that aggravates the underlying disease and worsens prognosis[1,2]. Cachexia manifests with both behavioral and metabolic symptoms, the severity of which varies between diseases and individuals, making it difficult to define and diagnose[3,4]. Cachectic patients exhibit anorexia, anhedonia and lethargy, as well as unintentional loss of over 5% of their body weight[3,4]. This is caused by a rapid depletion of fat and lean mass, which not only impacts the patient's quality of life, but is also often a leading cause of morbidity and mortality[2,3,5]. Conventional nutritional support does not reverse cachexia. Although several treatment options such as agonists for the orexigenic hormone ghrelin are explored, standards of care to prevent or alleviate cachexia remain ill-defined[1,6].

The emergence of cachexia accompanies a surge of proinflammatory cytokines such as tumor necrosis factor (TNF), interferon (IFN)-γ, interleukin (IL)-6 and IL-1[7,8]. Depending on the disease model, these cytokines can be secreted by tumor cells, in the case of cancer, host immune cells and/or cells involved in metabolic regulation, such as adipocytes[9,10]. Murine models of cancer-associated cachexia (CAC) have greatly improved our understanding of the mechanisms contributing to weight loss[5,10,11]. However, appropriate mechanistic models to study cachexia in the context of infection are still underdeveloped. In the present study we employed a murine benchmark model of chronic viral infection to interrogate the molecular and cellular requirements for infection-associated cachexia (IAC). We designed an integrative approach of genetic, dietary and pharmacologic perturbations to uncover both the shared and the unique properties of CAC and IAC. This led to the characterization of morphologic, molecular and metabolic changes in adipose tissue, and identified the main immune drivers of IAC, providing much-needed molecular insights into the pathophysiology of cachexia.

Results

Infection with LCMV clone 13 leads to reversible cachexia. Wild-type C57BL/6J mice infected with 2×10^6 focus forming units (FFU) of the chronic strain clone 13 of the lymphocytic choriomeningitis virus (LCMV) exhibited 15–20% weight loss within the first week of infection (Fig. 1a). To assess whether this is a manifestation of cachexia or a direct result of anorexia, we fed uninfected, wild-type mice with the same amount of chow diet consumed by LCMV-infected mice for 2 weeks post-infection (pair feeding). Between 6 and 8 days after infection the pair-fed, uninfected group lost less than 3% of the initial weight compared with over 10% lost by infected mice (Fig. 1a,b), indicating that the anorectic feeding behavior could not account for the full extent of weight loss observed in the LCMV-infected mice. To characterize the infection-induced pathophysiology, we used metabolic cages to monitor LCMV-infected mice compared with age- and sex-matched uninfected mice. Between day 6 and day 8 after infection, mice exhibited signs of lethargy and showed reduced food and water intake, activity and energy expenditure compared with uninfected mice (Fig. 1b–d and Supplementary Fig. 1a). The respiratory exchange ratio (RER), calculated from the ratio of CO_2 emission to O_2 consumption, showed a significant reduction between day 6 and day 8 post-infection (Fig. 1d and Supplementary Fig. 1a), suggesting that LCMV-infected mice relied on fat metabolism as the main energy

[1]CeMM Research Center for Molecular Medicine of the Austrian Academy of Sciences, Vienna, Austria. [2]Institute of Molecular Biosciences, University of Graz, Graz, Austria. [3]Department of Molecular Medicine II, Heinrich Heine University, Düsseldorf, Germany. [4]Division of Endocrinology and Metabolism, Department of Medicine III, Medical University of Vienna, Vienna, Austria. [5]Division of Chronic Inflammation and Cancer, German Cancer Research Center, Heidelberg, Germany. [6]Department of Biomedical Imaging and Image-guided Therapy, Division of Gender and Molecular Imaging, Preclinical Imaging Laboratory, Medical University of Vienna, Vienna, Austria. [7]Department of Pathology and Immunology, University of Geneva, Geneva, Switzerland. [8]Center for Global Infectious Disease Research, Seattle Children's Research Institute, Seattle, WA, USA. [9]These authors contributed equally: Martina Schweiger, Michael Moschinger. *e-mail: abergthaler@cemm.oeaw.ac.at

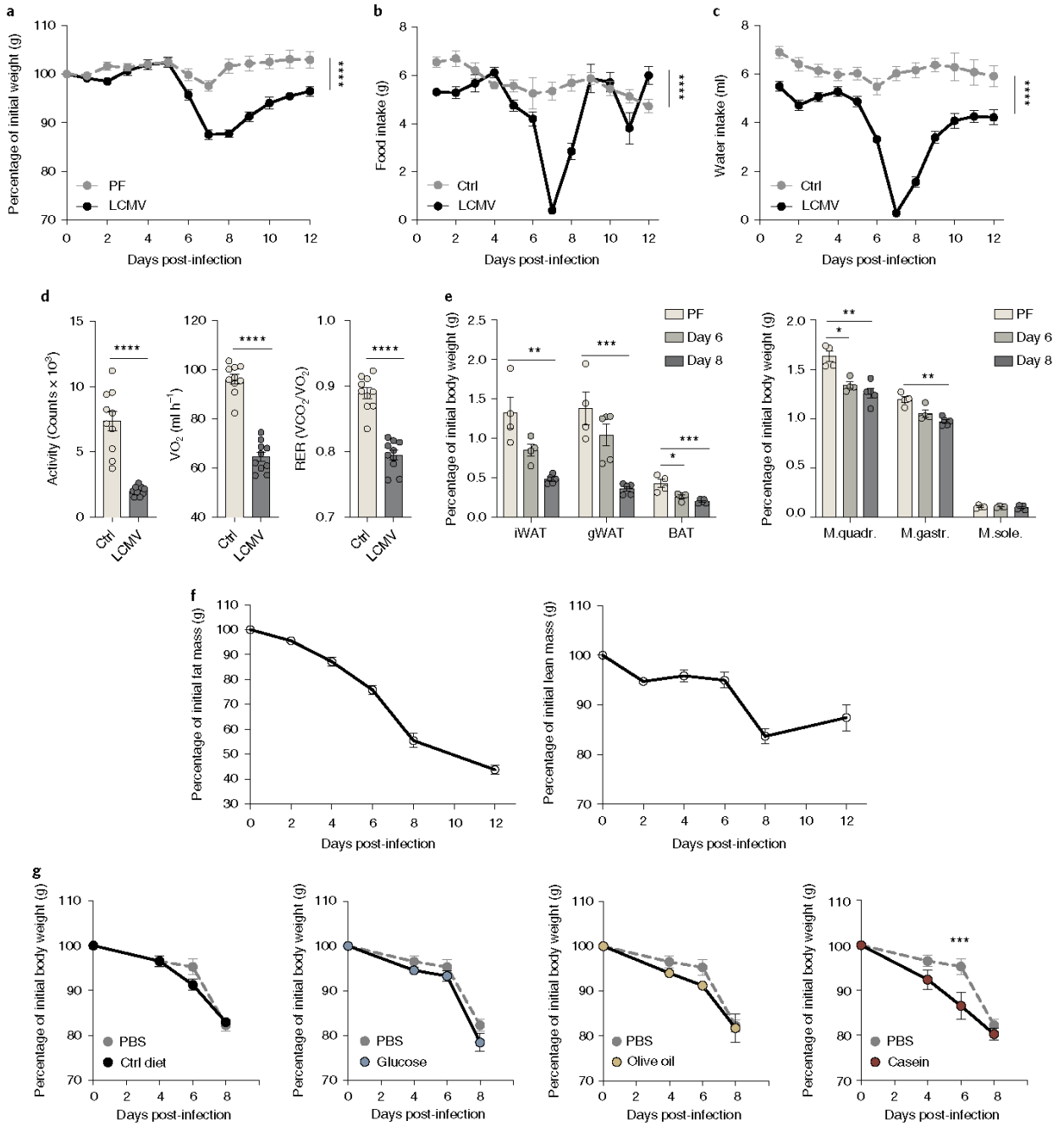

Fig. 1 | Infection with LCMV clone 13 leads to transient cachexia. a, Body weight kinetics for C57BL6/J wild-type mice infected with 2×10^6 FFU of LCMV clone 13, compared with pair-fed (PF) mice ($n=5$). **b**,**c**, Food intake (**b**) and water intake (**c**) of LCMV-infected mice compared with uninfected controls ($n=10$; $^{****}P<0.0001$, two-way analysis of variance (ANOVA)); data are representative of three independent experiments for **a** and **b**, and **c** represents a single experiment. **d**, Activity, oxygen consumption and RER in LCMV-infected mice compared with uninfected controls (Ctrl; $n=10$). Data shown represent the average of days 6, 7 and 8 post-infection ($^{****}P<0.0001$) from a single experiment. **e**, Percentage of tissue weight normalized to body weight before infection in inguinal, gonadal and interscapular brown adipose tissue ($^{**}P=0.002$, $^{***}P=0.0006$, $^{*}P=0.0172$, $^{***}P=0.0009$, unpaired, two-tailed, Student's *t*-test), as well as quadriceps (M.quadr.), gastrocnemius (M.gastr.) and soleus (M.sole.; $^{*}P=0.039$, $^{**}P=0.0035$, $^{***}P=0.0001$, unpaired, two-tailed, Student's *t*-test) at day 7 for pair-fed uninfected mice and days 6 and 8 post-infection for LCMV-infected mice ($n=5$). BAT, brown adipose tissue; iWAT, inguinal white adipose tissue; gWAT, gonadal white adipose tissue. **f**, Body composition as measured in live, un-anesthetized, LCMV-infected mice using EchoMRI ($n=5$). **e**,**f**, Representative data of two independent experiments. **g**, Body weight kinetics in LCMV-infected mice supplemented with the equivalent of 1 kcal of indicated diet through oral gavage daily between day 4 and day 7 post-infection ($n=4$; $^{***}P=0.0003$, two-way ANOVA, Bonferroni's correction). Data are representative of three independent experiments. All data show the mean ± s.e.m.

substrate. These pathophysiologic changes preceded the peak of the viral load and of the adaptive immune response, which happened at days 8–12 (see Supplementary Fig. 1b–d). After day 8 mice slowly started to regain weight, despite the continuous presence of the virus (Fig. 1a–c and Supplementary Fig. 1a–d)[12].

By comparing the body composition, we found that both the fat and the lean (muscle) masses were severely depleted in the first week after infection compared with the pair-fed, uninfected mice (Fig. 1e,f). The fat tissue, however, underwent an earlier and more severe depletion compared with muscles, starting 4 days post-infection (Fig. 1f). This depletion over time affected different fat depots, including the inguinal white adipose tissue, gonadal white adipose tissue and interscapular brown adipose tissue (Fig. 1e). To assess the loss of muscle mass we examined quadriceps, gastrocnemius and soleus, which represent both slow- and fast-twitch muscles. The muscle mass of quadriceps and gastrocnemius was reduced in infected mice compared with pair-fed mice (Fig. 1e). This was associated with decreased expression of the myoblast differentiation marker, *MyoD1*, and the increased expression of *Fbxo32* and *Trim63*, encoding Atrogin1 and Murf1, respectively, involved in proteasomal degradation in all three muscles in the infected mice compared with pair-fed mice (see Supplementary Fig. 1e–g).

To evaluate the relationship between the viral inoculum and the weight loss, we titrated the infection dose of LCMV clone 13, ranging from 2×10^6 FFU to 2×10^2 FFU. There was a marked amelioration of weight loss at the lower virus inocula; doses below 2×10^4 FFU showed little to no weight loss (see Supplementary Fig. 1h). These lower virus inocula are known to be associated with accelerated viral clearance[13]. Infection with the acute strain of LCMV resulted in similar weight kinetics to low-dose LCMV clone 13 infection (see Supplementary Fig. 1i), suggesting a possible link between determinants for viral persistence and the development of cachexia.

To examine whether weight loss was ameliorated by nutrient supplementation, we used oral gavage to administer a daily caloric intake of 1 kcal of a chow-like control diet, glucose, olive oil or casein to LCMV clone 13-infected mice between day 4 and day 8 post-infection. Oral gavage supplementation did not alleviate weight loss compared with the PBS-supplemented control (Fig. 1i). On the contrary, all gavage-supplemented groups recovered at a slower rate compared with PBS-supplemented, LCMV-infected mice (see Supplementary Fig. 1j), indicating that virus-induced weight loss cannot be prevented by nutritional supplementation. These results reveal several hallmarks of cachexia in LCMV clone 13-infected mice, including anorexia and metabolic dysfunction, as well as depleted fat and muscle mass that cannot be reversed by nutritional supplementation.

Viral infection triggers adipose tissue remodeling and lipolysis. Both subcutaneous and visceral compartments of the adipose tissue in LCMV-infected mice underwent depletion compared with uninfected controls (Fig. 2a). Using histologic analysis to examine the morphologic changes in the inguinal adipose tissue of LCMV-infected compared with uninfected mice, we observed a significant reduction in the size of adipocytes at days 6 and 8 post-infection (Fig. 2b,c). Next, we determined the protein abundance and activation status of adipose triglyceride lipase (ATGL) and hormone-sensitive lipase (HSL), two enzymes central to lipolysis[14], in inguinal adipose tissue at days 0, 4, 6 and 8 after LCMV infection. Expression of ATGL and HSL, as well as that of phosphorylated-HSL (pHSL), phosphorylated at residue Ser^{660}, were increased in inguinal adipose tissue during LCMV infection compared with uninfected mice (Fig. 2d), suggesting increased lipolysis peaking at day 6 post-infection. This was corroborated by elevated levels of non-esterified fatty acids (NEFAs) in the serum of LCMV-infected mice compared with uninfected controls (Fig. 2e). In addition, reduced messenger RNA expression of the lipoprotein lipase (*Lpl*) and, to a lesser extent, of the lipid-scavenging receptor *Cd36* in inguinal fat, together with the increased levels of triglyceride in the serum of LCMV-infected mice compared with pair-fed uninfected mice (Fig. 2e,f), indicated a reduction in the rate of lipid uptake in adipose tissue and/or lipid mobilization in the liver. Decreased mRNA expression of *Dgat2*, the rate-limiting enzyme in triglyceride biosynthesis (Fig. 2f), also suggested a lower rate of lipid synthesis in LCMV-infected mice[15]. Notably, inguinal fat pads in infected mice showed increased vascularization (see Supplementary Fig. 2b,c), which may be involved in inflammation-mediated tissue remodeling. Together, these data show that LCMV clone 13 infection leads to depletion of lipid stores in adipose tissue by modulating key regulators of lipid metabolism.

To investigate whether the virus-induced adipose tissue wasting followed similar mechanisms to CAC, we examined the mRNA expression of *Ucp1* as an indicator of adipose tissue beiging. The mRNA expression of *Ucp1* was marginally lower in the interscapular, inguinal and gonadal fat of infected mice compared with pair-fed mice (Fig. 2g). Based on models of cachexia in Lewis lung carcinoma and B16 melanoma in $Atgl^{-/-}$ and $Hsl^{-/-}$ mice[16], the absence of ATGL or HSL was sufficient to ameliorate weight loss in cachectic mice, and more profoundly in $Atgl^{-/-}$, indicating an essential role for ATGL and HSL in CAC. To determine whether these lipases were required for IAC, we infected $Atgl^{fl/fl}$ $Adipoq^{Cre/+}$ and $Hsl^{fl/fl}$ $Adipoq^{Cre/+}$ mice, which have a conditional ablation of ATGL and HSL in adipocytes driven by the adiponectin (Adipoq) promoter. We found that the ablation of either lipase did not reduce the extent of weight loss

Fig. 2 | Infection-associated cachexia triggers severe adipose tissue remodeling and increased lipolysis. a, Representative MRI cross-sections (left) and longitudinal sections (right). Displayed sections were selected to show iLNs on uninfected controls and LCMV-infected mice at 6 and 8 days post-infection. (Bottom) images show the fat compartment, after subtracting fat-suppressed acquisitions from the matching non-suppressed images. Images were acquired from a single experiment where $n=3$. **b**, Representative H&E staining of inguinal fat pads from uninfected controls and mice infected at 6 and 8 days post-infection. Images were acquired from a single experiment where $n=3$. **c**, Four to five images were collected from each inguinal fat pad, at 20× magnification ($n=3$). The diameter of each adipocyte was measured, and the distribution and median values were evaluated across all conditions. Violin plots represent the density of data points in each condition and the minimum and maximum values. The inner box plots are bound by the upper (75%) and lower (25%) quantiles, and the median is represented by an inner horizontal line. Cutoffs were set to include all cells between 10 and 100 µm in diameter (****$P<0.0001$, one-way ANOVA, Bonferroni's correction). **d**, Protein expression of HSL, pHSL and ATGL, within the inguinal fat pad of control and infected mice at indicated timepoints ($n=3$). Data are representative of three independent experiments. **e**, Serum NEFAs and triglyceride levels of control and infected mice 8 days post-infection ($n=3$). Data are representative of two independent experiments (**$P=0.002$, one-way ANOVA, Bonferroni's correction). **f**, Fold-change of inguinal fat pat mRNA expression of scavenger receptor (*Cd36*) ($n=7$), *Lpl* ($n=7$) and *Dgat2* ($n=8$), as measured by quantitative PCR from infected mice compared with pair-fed mice. Data are pooled from two independent experiments (**$P=0.0021$, 0.0038, 0.0069, *$P=0.0279$, two-way ANOVA, Bonferroni's correction). **g**, Fold-change of *Ucp1* mRNA expression of control and infected mice in indicated fat pads ($n=6$). Data are pooled from two independent experiments (***$P=0.0002$, unpaired, two-tailed, Student's *t*-test). **h,i**, Body weight kinetics in adipose tissue-specific knockouts of either ATGL ($n=3$) (**h**) or HSL ($n=4$) (**i**) compared with flox controls. Data are representative of two independent experiments. The means ± s.e.m. values are shown in **e**–**i**.

during LCMV infection compared with the floxed control group (Fig. 2h), suggesting that neither lipase was required for IAC.

The hormone ghrelin and adipokines such as leptin and adiponectin are considered active modulators of both metabolic and immune processes[11,17,18]. The amount of ghrelin in the serum and the expression of adiponectin in inguinal adipose tissue were similar in LCMV-infected and -uninfected mice (see Supplementary Fig. 2d,f). Notably, circulating leptin levels showed a reduction on LCMV infection, whereas mRNA expression of leptin was increased in inguinal adipose tissue at day 6 (see Supplementary Fig. 2e,f), suggesting leptin could be involved in mediating adipose tissue wasting during IAC. However, leptin-deficient $Lep^{Ob/Ob}$ mice lost weight at a similar rate to $Lep^{Ob/+}$ mice after LCMV infection, and displayed anorexia (see Supplementary Fig. 2g). We also quantified the loss of fat and lean mass over 8 days after infection in $Lep^{Ob/Ob}$ and $Lep^{Ob/+}$ mice, and found that fat and lean compartments were

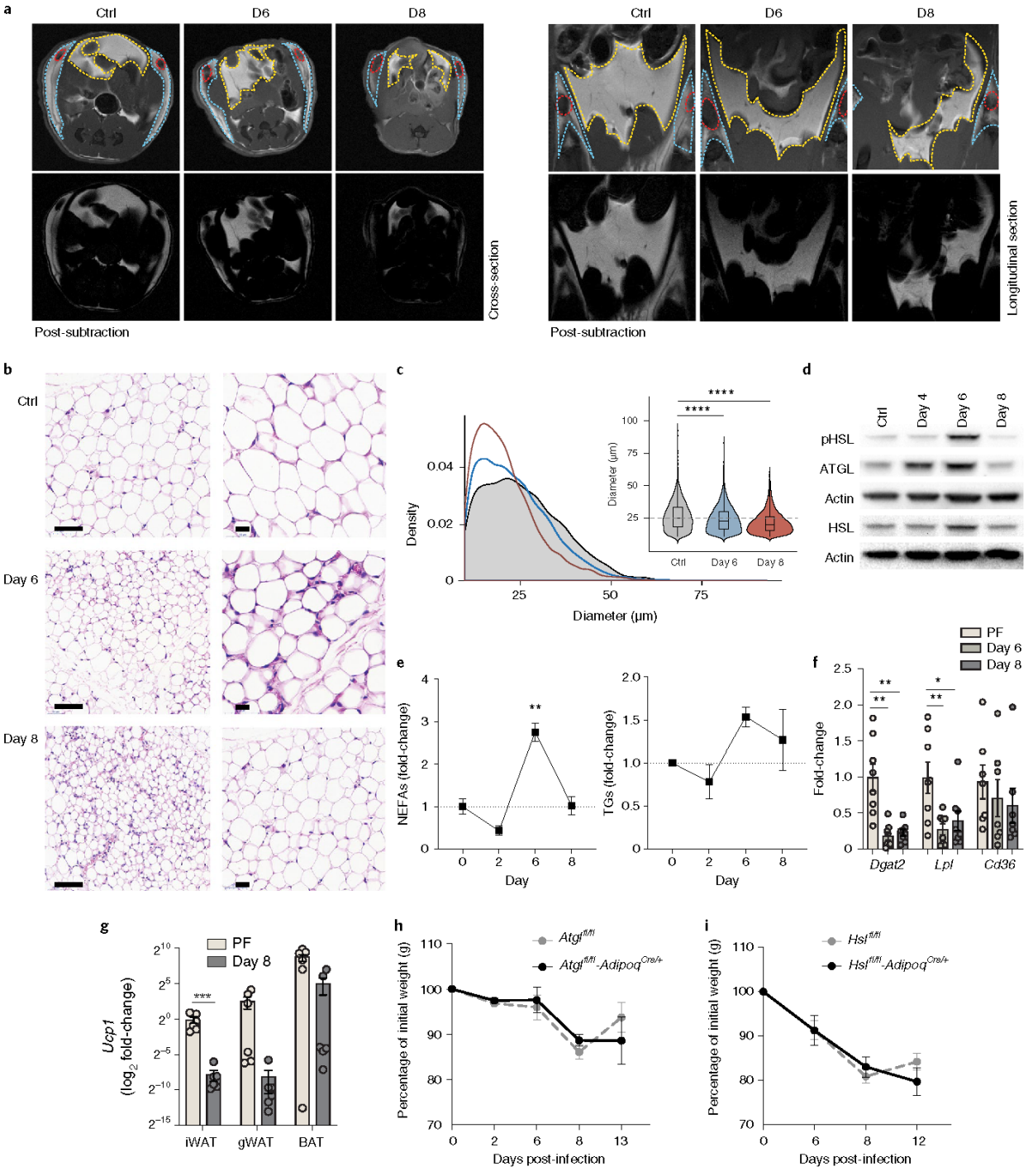

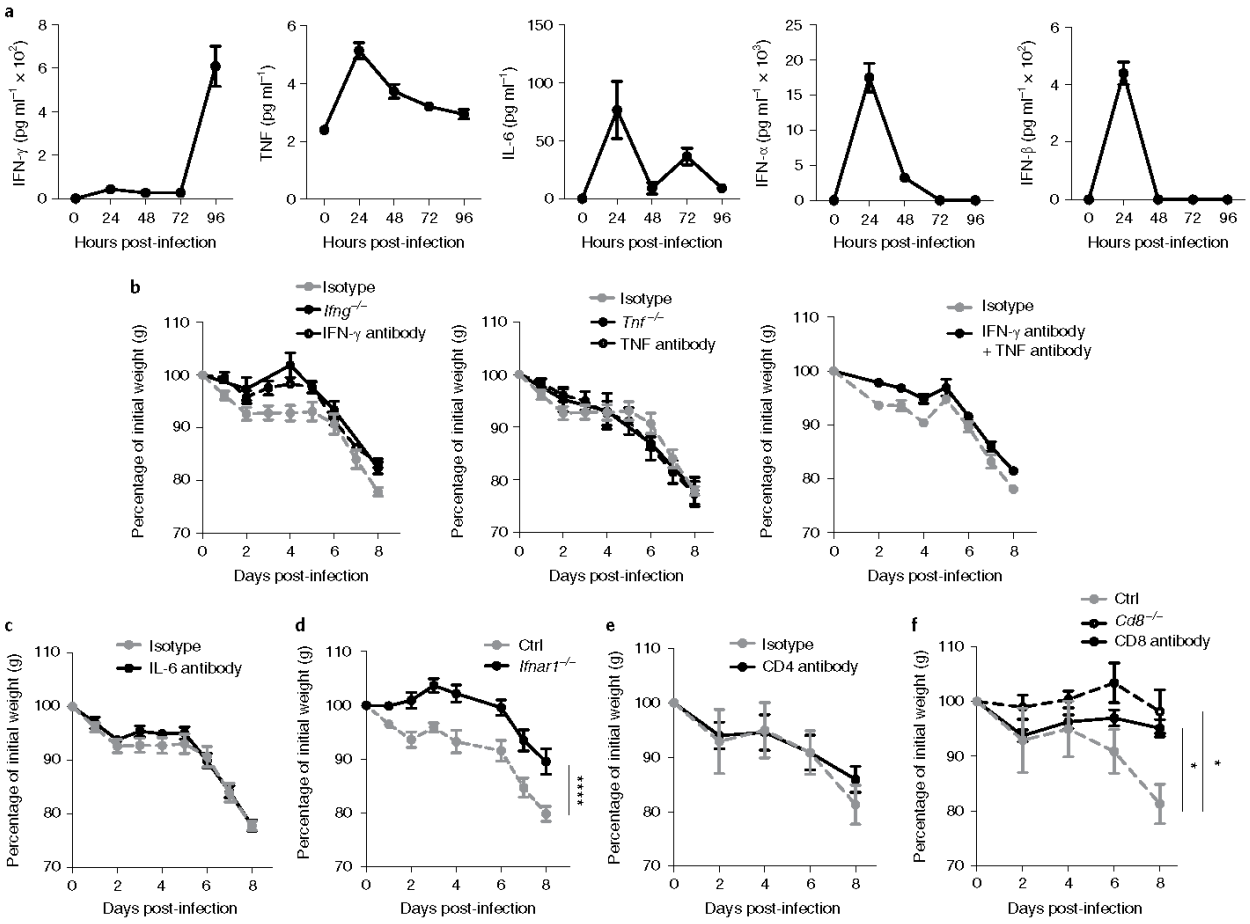

Fig. 3 | Type I IFN and CD8 T cells play critical roles in inducing infection-associated cachexia. a, Serum cytokine concentration of LCMV-infected wild-type mice ($n=4$). Data are representative of a single experiment. **b**, Body weight of LCMV-infected mice, either genetically ablated from IFN-γ or TNF ($n=4$), or treated with anti-IFN-γ- or anti-TNF-depleting antibodies ($n=5$), or a combination of both ($n=9$). Data are representative of a single experiment for genetic knockouts, two independent experiments for single antibody treatment and pooled data from two independent experiments for the double depletion of IFN-γ and TNF. **c**, Mice treated with anti-IL-6-depleting antibodies ($n=5$). **d**, *Ifnar1*$^{-/-}$ mice ($n=4$; $^{****}P<0.0001$, two-way ANOVA). **e**, Mice treated with anti-CD4-depleting antibodies ($n=4$). **f**, *Cd8*$^{-/-}$ mice and mice treated with anti-CD8-depleting antibodies ($n=4$;$^{*}P=0.027$, $^{*}P=0.046$, two-way ANOVA). **c**–**f**, These are representative of two independent experiments. The data show the mean ± s.e.m.

equally depleted in both groups (see Supplementary Fig. 2h), suggesting that, although leptin expression was increased in the adipose tissue, it did not mediate the activated lipolytic state or the disrupted feeding behavior during LCMV infection. These results indicate that IAC triggers structural and metabolic reprogramming in adipose tissue between day 6 and day 8 post-infection.

Infection-associated cachexia is driven by type I IFN and CD8$^+$ T cells. In various models of cachexia and adipose tissue remodeling, cytokines such as IFN-γ, TNF and IL-6 trigger weight loss, acting either independently or together with other cytokines and immune cells[8]. Bead-based multiplex assays for 32 cytokines, as well as ELISA assays for IFN-α and IFN-β, revealed a highly dynamic pattern for serum cytokines and indicated the induction of IFN-γ, TNF, IL-6, IFN-α and IFN-β, among others, within the first 96 h after LCMV clone 13 infection of wild-type mice (Fig. 3a and Supplementary Fig. 2a and Supplementary Table 1). Cytokines implicated in CAC, such as IL-1β and leukemia inhibitory factor[8,19], showed no increase in the serum of LCMV-infected mice (see Supplementary Fig. 3a and Supplementary Table 1). Pathways associated with proinflammatory cytokines such as IFN-γ, TNF and IL-6 have been linked to CAC[8,20]. Neutralization of IFN-γ, TNF and IL-6 by genetic ablation using *Ifng*$^{-/-}$, *Tnf*$^{-/-}$ and *TnfrI*$^{-/-}$ *mice* or antibody-mediated blockade initiated 1 day before infection, and then continued every second day, did not ameliorate weight loss in LCMV-infected mice (Fig. 3b,c). Infected mice, in which we simultaneously depleted IFN-γ and TNF using neutralizing antibodies, still lost up to 20% of their body weight by day 8 post-infection (Fig. 3b). Type 1 IFNs were detectable in the serum of LCMV-infected mice within the first 2 days of infection (Fig. 3a)[21]. Genetic ablation of IFN-α/β-receptor α chain (IFNAR) signaling using *Ifnar1*$^{-/-}$ mice resulted in ameliorated weight loss by approximately 10% at 8 days after infection compared with wild-type LCMV-infected mice (Fig. 3d and Supplementary Fig. 3b,c), implicating type I IFN responses in IAC.

Next, we determined whether a particular T cell population mediated weight loss during LCMV infection. This was done through the intravenous injection of depleting antibodies for CD8$^+$ T cells and CD4$^+$ T cells 2 days and 1 day, respectively, before LCMV infection (Fig. 3e,f) or infection of *Cd8*$^{-/-}$ mice (Fig. 3f). The depletion of CD4$^+$ T cells in LCMV-infected mice did not protect against weight loss (Fig. 3e and Supplementary Fig. 3d–f); however, depletion of

CD8$^+$ T cells resulted in little to no weight loss compared with wild-type controls (Fig. 3f and Supplementary Fig. 3d–f). These results suggested a key role for CD8$^+$ T cells in IAC.

To examine whether CD8$^+$ T cells drove weight loss in other viral infections, we infected *Rag2*$^{-/-}$ mice, which lack both T and B lymphocytes, with a sublethal dose of influenza virus strain PR/8. Although LCMV-infected *Rag2*$^{-/-}$ mice were protected from weight loss (see Supplementary Fig. 3g), PR/8-infected *Rag2*$^{-/-}$ mice continued to lose weight after 8 days and infected wild-type mice started to regain weight (see Supplementary Fig. 3h). These results indicated that weight loss during influenza virus infection occurs via different mechanisms compared with those mediating weight loss during LCMV infection. Uninfected wild-type mice fed the same amount of food as that consumed by PR/8-infected wild-type mice had identical weight loss to the infected group (see Supplementary Fig. 3i,j), suggesting that weight loss in PR/8-infected mice was due to anorexia. These findings highlight the variety of mechanisms by which weight loss occurs in different infection settings.

CD8$^+$ T cell–intrinsic IFNAR1 signaling alters lipid metabolism during infection. To further investigate the interrelationship of type I IFN signaling, CD8$^+$ T cells and the wasting of the adipose tissue, we used *Ifnar1*$^{fl/fl}$ *Adipoq*$^{Cre/+}$ mice, which lack IFNAR1 expression in adipocytes, and *Ifnar1*$^{fl/fl}$ *Cd4*$^{Cre/+}$ mice, in which IFNAR1 is specifically deleted in CD4$^+$ and CD8$^+$ T cells. The LCMV-infected *Ifnar1*$^{fl/fl}$ *Adipoq*$^{Cre/+}$ mice showed a similar weight loss to the floxed control group (see Supplementary Fig. 4a), whereas the LCMV-infected *Ifnar1*$^{fl/fl}$ *Cd4*$^{Cre/+}$ mice were protected from weight loss, and preserved both fat and lean mass (Fig. 4a,b), indicating that type I IFN signaling in CD8$^+$ T cells was required for IAC. LCMV-infected *Ifnar1*$^{fl/fl}$ and *Ifnar1*$^{fl/fl}$ *Cd4*$^{Cre/+}$ mice had comparable numbers of CD8$^+$ T cell in their spleens and inguinal lymph nodes (iLNs) at day 6 post-infection, the time point at which cachexia is initiated (see Supplementary Fig. 4b,c). However, *Ifnar1*$^{fl/fl}$ *Cd4*$^{Cre/+}$ CD8$^+$ T cells did not upregulate the activation marker CD44 and could not launch antigen-specific responses, as indicated by the absence of GP33$^+$ and NP396$^+$ CD8$^+$ T cells (see Supplementary Fig. 4b,c). Expansion of CD8$^+$ T cells was impaired at day 8 after LCMV infection in the spleens of *Ifnar1*$^{fl/fl}$ *Cd4*$^{Cre/+}$ compared with *Ifnar1*$^{fl/fl}$ mice (data not shown), indicating that CD8$^+$ T cell–intrinsic signaling through IFNAR was required for T cell activation and expansion[22,23].

To gain further insights into the changes taking place in the adipose tissue of LCMV-infected mice, we performed RNA-sequencing (RNA-seq) analysis of bulk adipose tissue from inguinal fat pads of *Ifnar1*$^{fl/fl}$ and *Ifnar1*$^{fl/fl}$ *Cd4*$^{cre/+}$ mice 6 days post-infection. Principal component analysis (PCA) showed differential clustering between uninfected and LCMV-infected mice on PC1 and between *Ifnar1*$^{fl/fl}$ and *Ifnar1*$^{fl/fl}$ *Cd4*$^{cre/+}$ on PC2 (Fig. 4c and Supplementary Fig. 4d). Pathway enrichment analysis of infection-induced gene modulation showed an increase in immune processes in *Ifnar1*$^{fl/fl}$ mice compared with *Ifnar1*$^{fl/fl}$ *Cd4*$^{cre/+}$ mice, and highlighted multiple changes in metabolic processes within the top five pathways downregulated (Fig. 4e). Metabolic pathway enrichment analysis with the Reactome metabolic database found that five of the top ten pathways enriched in *Ifnar1*$^{fl/fl}$ mice, compared with *Ifnar1*$^{fl/fl}$ *Cd4*$^{cre/+}$, during infection were involved in lipid metabolism (Fig. 4f). The expression of genes involved in the biosynthesis and uptake of lipids was predominantly downregulated in adipose tissue of LCMV-infected *Ifnar1*$^{fl/fl}$ compared with LCMV-infected *Ifnar1*$^{fl/fl}$ *Cd4*$^{cre/+}$ mice (Fig. 4g). Notably, the expression of *Dgat2*, the rate-limiting enzyme in triglyceride synthesis, showed the anticipated reduction of expression during infection in *Ifnar1*$^{fl/fl}$ mice and this was absent in infected *Ifnar1*$^{fl/fl}$ *Cd4*$^{cre/+}$ mice (Fig. 4g,h). Similarly, *Lpl* expression decreased during infection but not in *Ifnar1*$^{fl/fl}$ *Cd4*$^{cre/+}$ mice. Expression of *Cd36* was not affected in any condition (Fig. 4h). Circulating levels of NEFAs and triglycerides showed no increase during infection in *Ifnar1*$^{fl/fl}$ *Cd4*$^{cre/+}$ mice compared with *Ifnar1*$^{fl/fl}$ mice (Fig. 4i).

The lipolysis of adipose tissue is triggered by a variety of hormones and signaling molecules, such as glucocorticoids, which induce the expression of ATGL and HSL, thyroid-stimulating hormone and catecholamines; these all induce the phosphorylation of HSL by interacting with the thyroid-stimulating hormone receptor in the case of thyroid-stimulating hormone or with β-adrenergic receptors in the case of catecholamines[24]. Quantification of circulating cortisol and corticosterone, at day 6 after LCMV infection, indicated increased levels of cortisol and corticosterone in *Ifnar1*$^{fl/fl}$ mice compared with uninfected *Ifnar1*$^{fl/fl}$ mice, which was abrogated in *Ifnar1*$^{fl/fl}$*Cd4*$^{Cre/+}$ mice (Fig. 4j and Supplementary Fig. 4d). Circulating amounts of free thyroxine and free triiodothyronine remained relatively constant across all conditions (see Supplementary Fig. 4d). Furthermore, serum concentrations of norepinephrine were slightly reduced in *Ifnar1*$^{fl/fl}$ mice on infection, but were increased in infected *Ifnar1*$^{fl/fl}$*Cd4*$^{cre/+}$ mice compared with uninfected mice at day 6 post-infection (see Supplementary Fig. 4d). The amounts of norepinephrine in the inguinal adipose tissue remained relatively constant throughout all conditions (see Supplementary Fig. 4d). Downstream of these signaling hormones, expression of *Abrd2* mRNA (encoding the β-adrenergic receptors) was highly increased in the inguinal fat of LCMV-infected compared with uninfected *Ifnar1*$^{fl/fl}$ mice, as were protein levels of pHSL (see Supplementary Fig. 4d). Both increases were abrogated in the inguinal fat of *Ifnar1*$^{fl/fl}$ *Cd4*$^{cre/+}$ mice (see Supplementary Fig. 4d), consistent with reduced lipolysis in these mice. Expression of ATGL was increased, and expression of the lipid droplet-associated protein, perilipin, was decreased similarly in LCMV-infected *Ifnar1*$^{fl/fl}$ *Cd4*$^{Cre/+}$ and *Ifnar1*$^{fl/fl}$ mice (see Supplementary Fig. 4d). The hydrolytic activity of ATGL is controlled by its coactivator, CGI-58 (ref. [14]). Expression of *Abhd5* mRNA (encoding CGI-58) increased in inguinal adipose tissue of LCMV-infected *Ifnar1*$^{fl/fl}$ mice, but not in LCMV-infected *Ifnar1*$^{fl/fl}$*Cd4*$^{cre/+}$ mice compared with uninfected mice (see Supplementary Fig. 4d). These observations indicate that the correlation between the increased amounts of glucocorticoids in the serum and the upregulation of lipolysis in LCMV-infected mice was dependent on IFNAR signaling in CD8$^+$ T cells.

CD8$^+$ T cells trigger cachexia through antigen-specific activation. We next examined the kinetics of viral infection and T cell infiltration into the inguinal fat of LCMV-infected mice. Using immunofluorescent co-staining for the LCMV nucleoprotein (NP)$^+$ and CD8$^+$ T cells, we detected the presence of viral nucleoprotein and CD8$^+$ cells at day 6 and day 8 post-infection (Fig. 5a,b), consistent with the detection of LCMV-NP mRNA by quantitative PCR from inguinal, gonadal and brown adipose tissue of infected wild-type mice (see Supplementary Fig. 1c). To address the role of T cell infiltration into adipose tissue, we treated infected and control mice with the immunosuppressive drug FTY720, which transiently blocks the egress of lymphocytes from the lymphoid organs without interfering with T cell priming[25]. Flow cytometry indicated a reduction of virus-specific GP33$^+$ and NP396$^+$ CD8$^+$ T cells in the blood and spleen of FTY720-treated mice, and their accumulation in iLNs (Fig. 5c and Supplementary Fig. 5a–d). Treatment with FTY720 did not affect weight loss in infected mice compared with sham-treated mice (Fig. 5d), suggesting no role or only a minor role of local T cell infiltration in triggering adipose tissue wasting. In line with this, LCMV-infected *Prf1*$^{-/-}$ mice, which lack perforin, an important mediator of cytotoxic activity in CD8$^+$ T cells, had similar weight loss kinetics to the infected wild-type mice (Fig. 5e), suggesting that CD8$^+$ T cells triggered cachexia independently of cytotoxic cell-to-cell interaction.

To address whether CD8$^+$ T cells trigger adipose tissue wasting as a result of direct antigen stimulation, or in response to bystander

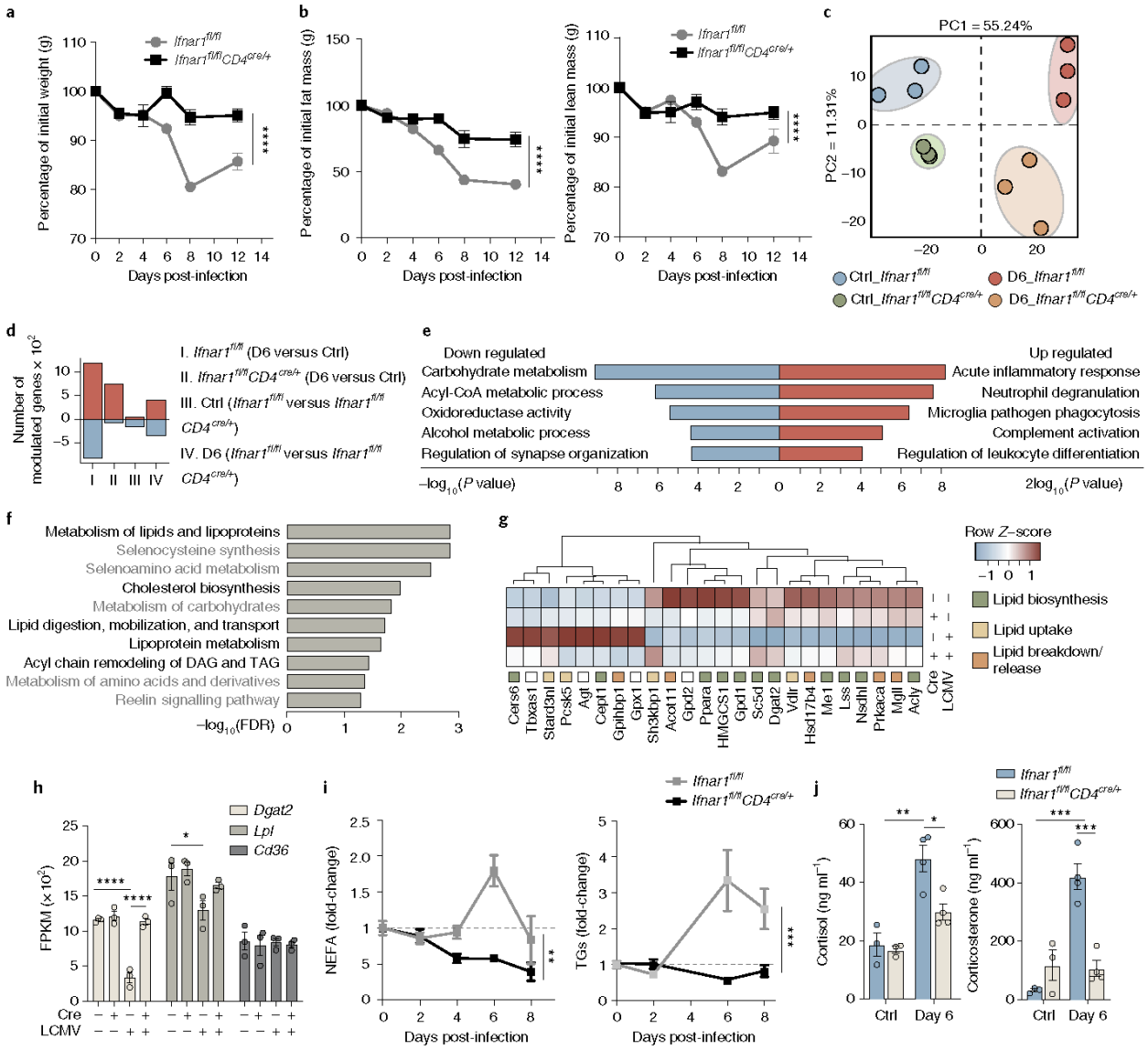

Fig. 4 | CD8 T cells modulate adipose tissue lipid metabolism in a type I IFN-dependent manner. a–j, Analysis of *Ifnar1*$^{fl/fl}$ *CD4*$^{cre/+}$ mice compared with *Ifnar1*$^{fl/fl}$ controls. **a**, Body weight kinetics of LCMV-infected mice ($n=4$; $^{****}P<0.0001$, two-way ANOVA). Data are representative of four independent experiments and show the mean ± s.e.m. **b**, Body composition as measured using EchoMRI in live, un-anesthetized, LCMV-infected mice ($n=4$; $^{****}P<0.0001$, two-way ANOVA). Data are representative of a single experiment and show the mean ± s.e.m. **c–h**, RNA-seq analysis of inguinal fat pads of LCMV-infected and uninfected *Ifnar1*$^{fl/fl}$ *CD4*$^{cre/+}$ mice compared with *Ifnar1*$^{fl/fl}$ controls at 6 days post-infection ($n=3$). Data show PCA (**c**), number of modulated genes (**d**) and significantly modulated genes (<0.05 adjusted *P*, log-fold-change > 0.7 or < −0.7) in the limma implementation of the 2 × 2 factorial interaction model. **e**, The top five enriched ClueGo pathways for up- and downregulated genes. **f**, Enrichment of top 10 modulated metabolic pathways. DAG, diacylglycerol; TAG, triacylglycerol. **g**, Heatmap of the top modulated genes involved in lipid biosynthesis, uptake, or breakdown and release. **h**, RNA expression of *Cd36*, *Lpl* and *Dgat2* ($^{****}P<0.0001$, $^{*}P=0.015$, two-way ANOVA, Bonferroni's correction). **i**, Serum triglyceride and NEFA levels ($n=4$; $^{**}P=0.0027$, $^{***}P=0.0004$, two-way ANOVA). **j**, Circulating levels of cortisol and corticosterone, as measured by ELISA ($n=4$; $^{**}P=0.0010$, $^{*}P=0.0185$, $^{***}P=0.0001$, $^{***}P=0.0004$, two-way ANOVA, Bonferroni's correction). **h–j**, The data are representative of two independent experiments and show the mean ± s.e.m.

activation induced by the inflammatory milieu, we generated mixed bone marrow chimeras. This was done using wild-type (CD45.2$^+$) recipients and congenic (CD45.1$^+$) donors, where the mice received mixed bone marrows at 1:1 ratios of either OT-I *Rag1*$^{-/-}$ and *Cd8*$^{-/-}$ or wild-type and *Cd8*$^{-/-}$. OT-I *Rag1*$^{-/-}$ mice carry a transgenic T cell receptor specific for the ovalbumin-derived peptide SIINFEKL ($OVA_{257-264}$) and do not have a residual antigen-specific repertoire due to loss of endogenous recombination events on the *Rag1*$^{-/-}$ background. The addition of bone marrow from *Cd8*$^{-/-}$ mice compensated for the lack of the CD4 T cells and B cells in the OT-I *Rag1*$^{-/-}$ mice. After confirming the success of the bone marrow reconstitution using congenic markers (see Supplementary Fig. 5e–f), chimeric mice were infected with LCMV clone 13 and monitored up to 12 days post-infection. Using FACS analysis, we confirmed the lack of

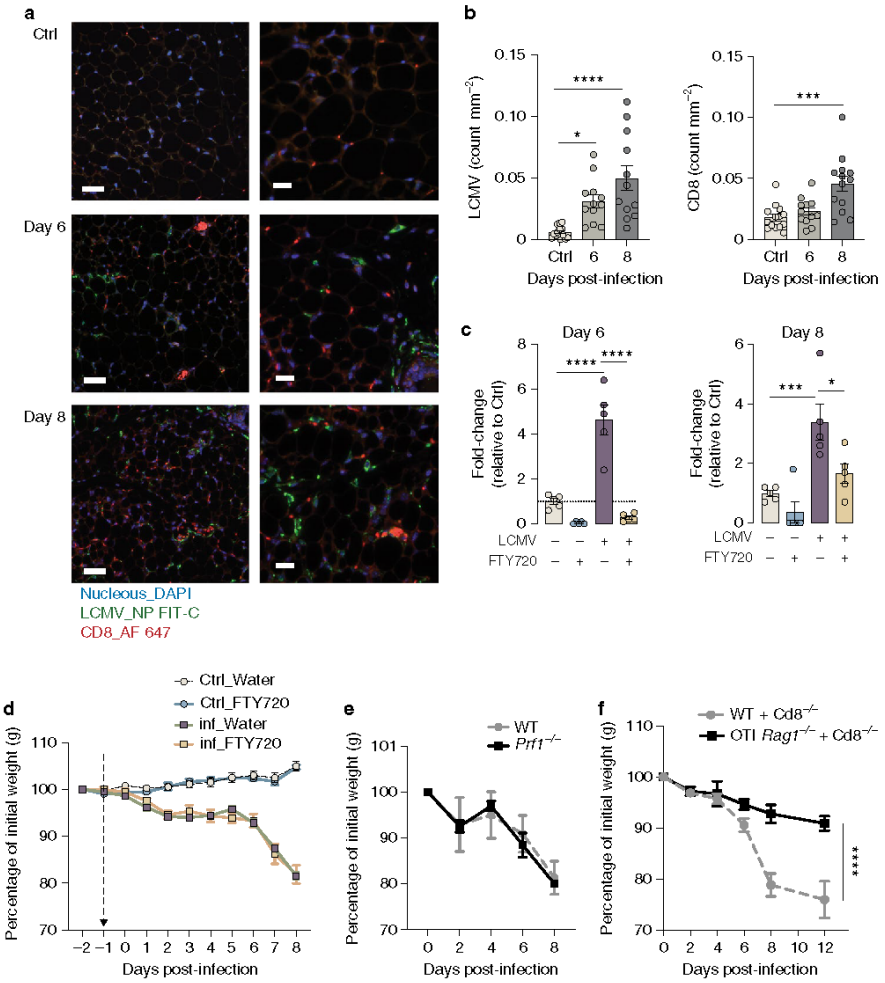

Fig. 5 | CD8 T cells trigger cachexia during the early stage of T cell priming and antigen recognition. a, Immunohistochemistry co-staining with DAPI, LCMV-NP (FITC) and CD8$^+$ T cells (Alexa Fluor 647) in inguinal fat pads of LCMV-infected mice at days 6 and 8 compared with uninfected mice ($n=3$). **b**, LCMV-NP$^+$ and CD8$^+$ staining from four to five images per inguinal fat pad ($n=3$), as quantified using cell profiler (*$P=0.0138$, ****$P<0.0001$, ***$P=0.0001$, one-way ANOVA, Bonferroni's correction). **a**,**b**, The data are representative of a single experiment. **c**, Fold-change in circulating CD8$^+$ T cells on days 6 and 8 post-infection relative to uninfected control after daily gavage administration of either FTY720 (0.3 mg kg^{-1}) or water ($n=5$; ****$P<0.0001$, ***$P=0.0004$, *$P=0.0143$, two-way ANOVA, Bonferroni's correction). **d**, Body weight kinetics of infected, FTY720-treated and water-treated mice, compared with uninfected controls ($n=5$). Data are representative of two independent experiments. **e**, Body weight kinetics of *Prf1*$^{-/-}$ mice compared with wild-type controls ($n=4$). Data are representative of a single experiment. **f**, Body weight kinetics in wild-type + *Cd8*$^{-/-}$ and OT-I *Rag1*$^{-/-}$ + *Cd8*$^{-/-}$ chimeric mice infected with LCMV ($n=6$). Data are pooled from two independent experiments. **b**–**f**, Data show the mean ± s.e.m.

LCMV-specific, CD8$^+$ GP33$^+$ T cells in the spleens of OT-I *Rag1*$^{-/-}$ + *Cd8*$^{-/-}$ mice compared with wild-type + *Cd8*$^{-/-}$ controls (see Supplementary Fig. 5g,h). *OT-I Rag1*$^{-/-}$ + *Cd8*$^{-/-}$ chimeric mice were completely protected against LCMV-induced weight loss, whereas the wild-type + *Cd8*$^{-/-}$ chimeric mice lost approximately 20% of their body weight (Fig. 5f,g), indicating that antigen-specific priming of CD8$^+$ T cells was required for LCMV-induced weight loss. Together, these data suggest that CD8 T cells triggered weight loss during the early stages of activation, following antigen-specific stimulation, and is likely to occur independent of direct cell-to-cell interaction.

Discussion

In the present study we employed a model of chronic viral infection to elucidate the inflammatory drivers of IAC.

IAC manifested 6 days after infection, preceding the peak of the adaptive immune response at day 12, then showed gradual resolution thereafter, which contrasts with the terminal course of CAC[3,5]. We reported in the present study on a role for type I IFNs and CD8$^+$ T cells in triggering IAC, but not IL-6, TNF and IFN-γ, cytokines that often mediate CAC[6,8]. The manifestation of IAC required IFNAR1 signaling specifically within T cells not adipocytes, in addition to antigen-specific CD8$^+$ T cell receptor priming. Deletion of the cytolytic effector molecule perforin or the pharmacologic blockade of T cell egress from lymphatic organs did not prevent cachexia, which suggested mechanisms other than classic CD8$^+$ T cell–mediated cytotoxicity.

During CAC, adipose lipid storage is depleted through increased ATGL- and HSL-mediated lipolysis, resulting in elevated circulating NEFAs, a process that we also observed during LCMV-induced cachexia[14,15]. In contrast to CAC, however, we did not observe increased adipose tissue beiging and thermogenesis[26,27]. We found a depletion of inguinal, gonadal and brown adipose tissue, accom-

panied by increased vascular density at 6 and 8 days post-infection, mainly in the inguinal compartment. Such remodeling may facilitate nutrient shuttling from the adipose tissue and modulate its exposure to metabolic and/or hormonal regulators, which could further amplify its depletion. Increased vascularization is one of several similar features between IAC and obesity[28], all of which could further influence systemic inflammation, dyslipidemia and metabolic dysfunctions across different organs[29].

Expression of leptin, a key regulator of appetite, lipolysis and the immune response[17], showed a marked increase in adipose tissue of infected mice. However, the genetic ablation of leptin in *Lep*$^{ob/ob}$ did not prevent weight loss and anorexia during LCMV infection. We observed a correlation between increased lipolysis and the increased circulating glucocorticoids, which are central drivers of the stress-response program, and can induce lipolysis by activating ATGL and HSL[24]. In addition, glucocorticoids have endogenous roles in regulating systemic metabolism and are well-known immunomodulatory molecules[30–32], which situates them as potential candidates in mediating immunometabolic crosstalk during IAC.

Previous studies examining LCMV-associated morbidity used intracranial infection with LCMV Armstrong, and reported weight loss that occurred as a direct result of anorexia mediated by major histocompatibility complex-II-restricted CD4$^+$ T cells[33–35], which contrasts the weight loss independent of the anorexia observed in our model. In the present study force feeding the mice during LCMV infection, or the supplementation with specific nutrients, did not alleviate weight loss, but rather hampered recovery, particularly on administration of glucose and casein. This is contrary to observations during infection with the influenza virus or injection of poly(I:C), in which administration of glucose and casein improved survival[36]. These differences may be due to distinct metabolic demands during different infections, influenced by viral life cycle, tropism and/or virus-induced immune responses, leading to either anorexia or cachexia. In line with this, *Rag2*$^{-/-}$ mice were not protected from weight loss during influenza infection. The detrimental effects of nutrient supplementation suggest that fasting metabolism is advantageous for efficient recovery. Fasting metabolism and caloric restriction had positive effects on survival and immune function in other models of bacterial infection and cancer[36,37], and may have beneficial effects for cancer patients[38,39]. The underlying mechanisms of nutrient redistribution during fasting in IAC and CAC warrant further investigations.

CD8$^+$ T cells are drivers of immunopathology in chronic infections such as LCMV and human immunodeficiency virus[40]. Studies have shown that virus clearance or persistence is determined during the early phase of infection, although the exact mechanisms are not well understood[12,41,42]. We speculate that the onset of cachexia during the early stages of infection with LCMV clone 13 may be linked to the establishment of viral persistence. To this point, mice infected with either the acute Armstrong strain of LCMV or with low doses of LCMV clone 13 did not show weight loss. These observations raise the question of the potential evolutionary advantages of cachexia. As a result of the correlation between cachexia and worsened prognosis in cancer patients, the syndrome has been presumed to be detrimental[7]. However, this assumption lacks a thorough mechanistic foundation and remains a matter of debate[43]. In infection, cachexia could serve an immunomodulatory role by tempering the immune response to limit immunopathology, similar to T cell exhaustion[44]. Alternatively, cachexia could facilitate a rapid increase of nutrient accessibility to fuel adaptive immune responses and/or other inflammatory processes. This would explain the excessive release of NEFAs at day 6 post-infection, a time point when energy metabolism shifts toward fat use. At the present time, relatively little is known about the regulation of nutrient redistribution across organs in inflammatory conditions, and how that may influence the immune response, metabolism and tissue repair[45].

The present study contributes to understanding the mechanisms that induce cachexia in different inflammatory and disease settings. Studies of cachexia and its context-dependent pathogenesis can improve the understanding of pathophysiological processes and systemic immunometabolism[46,47]. Comparative studies in infection and cancer could provide invaluable insights into the pathogenesis of cachexia and possible new therapeutic strategies.

Online content

Any methods, additional references, Nature Research reporting summaries, source data, statements of code and data availability and associated accession codes are available at https://doi.org/10.1038/s41590-019-0397-y.

Received: 4 December 2018; Accepted: 8 April 2019;
Published online: 20 May 2019

References

1. Von Haehling, S. & Anker, S. D. Treatment of cachexia: an overview of recent developments. *Int. J. Cardiol.* **184**, 726–742 (2014).
2. Baracos, V. E., Martin, L., Korc, M., Guttridge, D. C. & Fearon, K. C. H. Cancer-associated cachexia. *Nat. Rev. Dis. Primers* **4**, 1–18 (2018).
3. Fearon, K. et al. Definition and classifi cation of cancer cachexia: an international consensus. *Lancet Oncol.* **12**, 489–495 (2011).
4. Kotler, D. Challenges to diagnosis of HIV-associated wasting. *J. Acquir. Immune Defic. Syndr.* **37**, S280–S283 (2004).
5. Tisdale, M. J. Cachexia in cancer patients. *Nat. Rev. Cancer* **2**, 862–871 (2002).
6. Porporato, P. E. Understanding cachexia as a cancer metabolism syndrome. *Oncogenesis* **5**, 200 (2016).
7. Morley, J. E., Thomas, D. R. & Wilson, M.-M. G. Cachexia: pathophysiology and clinical relevance. *Am. J. Clin. Nutr.* **83**, 735–743 (2006).
8. Fearon, K. C. H., Glass, D. J. & Guttridge, D. C. Cancer cachexia: Mediators, signaling, and metabolic pathways. *Cell Metab.* **16**, 153–166 (2012).
9. Vaitkus, J. A. & Celi, F. S. The role of adipose tissue in cancer-associated cachexia. *Exp. Biol. Med.* **242**, 473–481 (2017).
10. Petruzzelli, M. & Wagner, E. F. Mechanisms of metabolic dysfunction in cancer-associated cachexia. *Genes Dev.* **30**, 489–501 (2016).
11. Flint, T. R., Fearon, D. T. & Janowitz, T. Connecting the metabolic and immune responses to cancer. *Trends Mol. Med.* **23**, 451–464 (2017).
12. Bergthaler, A. et al. Viral replicative capacity is the primary determinant of lymphocytic choriomeningitis virus persistence and immunosuppression. *Proc. Natl Acad. Sci. USA* **107**, 21641–21646 (2010).
13. Stamm, A., Valentine, L., Potts, R. & Premenko-Lanier, M. An intermediate dose of LCMV clone 13 causes prolonged morbidity that is maintained by CD4+T cells. *Virology* **425**, 122–132 (2012).
14. Zechner, R. et al. FAT SIGNALS—lipases and lipolysis in lipid metabolism and signaling. *Cell Metab.* **15**, 279–291 (2012).
15. Tsoli, M. et al. Depletion of white adipose tissue in cancer cachexia syndrome is associated with inflammatory signaling and disrupted circadian regulation. *PLoS ONE* **9**, e92966 (2014).
16. Das, S. K. et al. Adipose triglyceride lipase contributes to cancer-associated cachexia. *Science* **333**, 233–238 (2011).
17. Ruud, J. & Brüning, J. C. Metabolism: light on leptin link to lipolysis. *Nature* **527**, 43–44 (2015).
18. Baatar, D., Patel, K. & Taub, D. D. The effects of ghrelin on inflammation and the immune system. *Mol. Cell Endocrinol.* **340**, 44–58 (2011).
19. Kandarian, S. C. et al. Tumour-derived leukaemia inhibitory factor is a major driver of cancer cachexia and morbidity in C26 tumour-bearing mice. *J. Cachexia Sarcopenia Muscle* **9**, 1–12 (2018).
20. Patel, H. J. & Patel, B. M. TNF-α and cancer cachexia: molecular insights and clinical implications. *Life Sci.* **170**, 56–63 (2016).
21. Bhattacharya, A. et al. Superoxide dismutase 1 protects hepatocytes from type i interferon-driven oxidative damage. *Immunity* **43**, 974–986 (2015).
22. Curtsinger, J. M., Valenzuela, J. O., Agarwal, P., Lins, D. & Mescher, M. F. Cutting edge: type I IFNS provide a third signal to CD8 T cells to stimulate clonal expansion and differentiation. *J. Immunol.* **174**, 4465–4469 (2005).
23. Kolumam, G. A., Thomas, S., Thompson, L. J., Sprent, J. & Murali-Krishna, K. Type I interferons act directly on CD8 T cells to allow clonal expansion and memory formation in response to viral infection. *J. Exp. Med.* **202**, 637–650 (2005).
24. Xu, C. et al. Direct effect of glucocorticoids on lipolysis in adipocytes. *Mol. Endocrinol.* **23**, 1161–1170 (2009).
25. Pinschewer, D. D. et al. FTY720 immunosuppression impairs effector T cell peripheral homing without affecting induction, expansion, and memory. *J. Immunol.* **164**, 5761–5770 (2000).

26. Petruzzelli, M. et al. A switch from white to brown fat increases energy expenditure in cancer-associated cachexia. *Cell Metab.* **20**, 433–447 (2014).
27. Kir, S. et al. PTH/PTHrP receptor mediates cachexia in models of kidney failure and cancer. *Cell Metab.* **23**, 315–323 (2016).
28. Cao, Y. Angiogenesis and vascular functions in modulation of obesity, adipose metabolism, and insulin sensitivity. *Cell Metab.* **18**, 478–489 (2013).
29. Vegiopoulos, A., Rohm, M. & Herzig, S. Adipose tissue: between the extremes. *EMBO J.* **36**, 1999–2017 (2017).
30. Quatrini, L. et al. Endogenous glucocorticoids control host resistance to viral infection through the tissue-specific regulation of PD-1 expression on NK cells. *Nat. Immunol.* **19**, 954–962 (2018).
31. Miller, A. H. et al. Effects of viral infection on corticosterone secretion and glucocorticoid receptor binding in immune tissues. *Psychoneuroendocrinology* **22**, 455–474 (1997).
32. Jamieson, A. M., Yu, S., Annicelli, C. H. & Medzhitov, R. Influenza virus-induced glucocorticoids compromise innate host defense against a secondary bacterial infection. *Cell Host Microbe* **7**, 103–114 (2010).
33. Doherty, P. C., Hou, S. & Southern, P. J. Lymphocytic choriomeningitis virus induces a chronic wasting disease in mice lacking class I major histocompatibility complex glycoproteins. *J. Neuroimmunol.* **46**, 11–17 (1993).
34. Hildeman, D. & Muller, D. Immunopathologic weight loss in intracranial LCMV infection initiated by the anorexigenic effects of IL-1β. *Viral Immunol.* **13**, 273–285 (2000).
35. Kamperschroer, C. & Quinn, D. G. The role of proinflammatory cytokines in wasting disease during lymphocytic choriomeningitis virus infection. *J. Immunol.* **169**, 340–349 (2002).
36. Wang, A. et al. Opposing effects of fasting metabolism on tissue tolerance in bacterial and viral inflammation. *Cell* **166**, 1512–1525.e12 (2016).
37. Pietrocola, F. et al. Caloric restriction mimetics enhance anticancer immunosurveillance. *Cancer Cell* **30**, 147–160 (2016).
38. Nencioni, A., Caffa, I., Cortellino, S. & Longo, V. D. Fasting and cancer: molecular mechanisms and clinical application. *Nat. Rev. Cancer* **18**, 707–719 (2018).
39. Longo, V. D. & Mattson, M. P. Fasting: molecular mechanisms and clinical applications. *Cell Metab.* **19**, 181–192 (2014).
40. Rouse, B. T. & Sehrawat, S. Immunity and immunopathology to viruses: what decides the outcome? *Nat. Rev. Immunol.* **10**, 514–526 (2010).
41. Virgin, H. W., Wherry, E. J. & Ahmed, R. Redefining chronic viral infection. *Cell* **138**, 30–50 (2009).
42. Sullivan, B. M., Teijaro, J. R., De La Torre, J. C. & Oldstone, M. B. A. Early virus–host interactions dictate the course of a persistent infection. *PLoS Pathog.* **11**, 1004588 (2015).
43. Danai, L. V. et al. Altered exocrine function can drive adipose wasting in early pancreatic cancer. *Nature* **558**, 600–604 (2018).
44. Wherry, E. J. & Kurachi, M. Molecular and cellular insights into T cell exhaustion. *Nat. Rev. Immunol.* **15**, 486–499 (2015).
45. Perry, R. J. et al. Hepatic acetyl CoA links adipose tissue inflammation to hepatic insulin resistance and type 2 diabetes. *Cell* **160**, 745–758 (2015).
46. Norata, G. D. et al. The cellular and molecular basis of translational immunometabolism. *Immunity* **43**, P421–P434 (2015).
47. Buck, M. D., Sowell, R. T., Kaech, S. M. & Pearce, E. L. Metabolic instruction of immunity. *Cell* **169**, 570–586 (2017).

Acknowledgements

We thank S. Niggemeyer, S. Jungwirth and J. Riede for animal husbandry. The authors would like to thank L. Bakiri, V. Baracos, Y. Belkaid, R. Medzhitov, G. Superti-Furga, E. Wagner and R. M. Zinkernagel for valuable feedback and discussions. This project has received funding from the European Research Council under the European Union's Seventh Framework Programme and Horizon 2020 research and innovation program (grant agreement no. 677006, 'CMIL' to A.B., no. 340896 and 'LipoCheX' to R. Z.) from the German Research Council (grant nos. SFB974, KFO217, LA-2558/5-1 and Jürgen Manchot Graduate School MOI III to P.A.L.), from the Austrian Science Fund (grant no. FWF P26766 to T.S.) and from the US National Institutes of Health (grant nos. R01AI032972, U19AI100627 to A. Aderem). A.L. and M. Smyth are supported by DOC fellowships of the Austrian Academy of Sciences.

Author contributions

H.B. conceived the project, designed and performed experiments, analyzed the data and wrote the manuscript. M. Schweiger, T.S., B.V., A. Aderem and R.Z. contributed to the experimental design, shared reagents and/or contributed to data interpretation. M.M., H.X., K.K., L.K., M. Smyth, A.L. and P.A.L. designed, performed and/or analyzed experiments. A.P. performed the bioinformatic data analyses. S.G., A. Ali and M.H. performed metabolic cage measurements. J.F. and T.H.H. performed MRI. D.M. provided histologic and immunohistochemical staining. A.B. conceived the project, designed experiments, analyzed the data, wrote the manuscript and supervised the project.

Competing interests

The authors declare no competing interests.

Additional information

Supplementary information is available for this paper at https://doi.org/10.1038/s41590-019-0397-y.

Reprints and permissions information is available at www.nature.com/reprints.

Correspondence and requests for materials should be addressed to A.B.

Publisher's note: Springer Nature remains neutral with regard to jurisdictional claims in published maps and institutional affiliations.

Methods

Contact for resource and reagent sharing. Further information and requests for resources and reagents should be addressed to A.B. Additional experimental information can be found in the Nature Research Reporting Summary accompanying the present study.

Experimental model and subject details. *Mice.* In the present study we used both wild-type and genetically modified mouse models, all on a C57BL/6 background. These mice were bred under specific pathogen-free conditions at the Institute for Molecular Biotechnology of the Austrian Academy of Sciences, Vienna, Austria, as well as the Central Facility for Animal Research and Scientific Animal Welfare (ZETT) in Dusseldorf, Germany, and the Zentrales Tierlabor at the German Cancer Research Center (DKFZ) in Heidelberg. Genetically modified mice include: *Ifnγ*$^{-/-}$ (ref. [48]; 003288-JAX), *Tnf*$^{-/-}$ (ref. [49]; 005540-JAX), *Tnfr1*$^{-/-}$ (ref. [50]; 003242-JAX), *Ifnar1*$^{-/-}$ (ref. [51] ; 032045-JAX), *Ifnar1*$^{fl/fl}$ (ref. [52]; 028256-JAX), *Ifnar1*$^{fl/fl}$-*Adipoq*$^{Cre/+}$, *Atgl*$^{fl/fl}$-*Adipoq*$^{Cre/+}$ (refs. [53,54]; 024278-JAX, 010803-JAX), *Hsl*$^{fl/fl}$-*Adipoq*$^{Cre/+}$ (ref. [54]; 010803-JAX), *Ifnar1*$^{fl/fl}$-*Cd4*$^{Cre/+}$ (ref. [55]; 017336-JAX), *Ob/+ and Ob/Ob* (ref. [56]; 000632-JAX), *Cd45.1* (ref. [57]; MGI:4819849), *Cd8*$^{-/-}$ (ref. [58]; 002665-JAX), *Rag2*$^{-/-}$ (ref. [59]; 008449-JAX), OT-I *Rag1*$^{-/-}$ CD45.1 (refs. [60,61]; 003831-JAX and 002216-JAX) and *Prf1*$^{-/-}$ (ref. [62]; 002407-JAX). The *Ifnar1*$^{fl/fl}$-*Cd4*$^{Cre/+}$ mice were kindly provided by the laboratory of D. Pinschewer in Zurich, Switzerland. *Lep*$^{Ob/+}$ and *Lep*$^{Ob/Ob}$ mice were purchased from Jackson Laboratories. *Ifnar1*$^{fl/fl}$-*Adipoq*$^{Cre/+}$ mice were generated in house by crossing *Ifnar1*$^{fl/fl}$ mice to *Hsl*$^{fl/fl}$-*Adipoq*$^{Cre/+}$ mice, and then crossing out the *Hsl*$^{fl/fl}$ allele. Animal experiments were performed at the Department for Biomedical Research of the Medical University of Vienna, Vienna, Austria, the ZETT in Dusseldorf, Germany, the Division of Chronic Inflammation and Cancer, DKFZ, Heidelberg, Germany and the Institute of Systems Biology in Seattle, USA. Mice were housed in individually ventilated cages, and experiments were performed in compliance with the respective animal experimental licenses (BMWFW-66.009/0199-WF/V/3b/2015, BMWFW-66.009/0395-WF/V/3b/2015, BMWFW-66.009/0379-WF/V/3b/2016, BMWFW-66.009/0360-WF/V/3b/2017 BMWFW-66.009/0318-II/3b/2012, A25, A504, A479, A424, respectively, 35-9185.81/G-152/16, 35-9185.81/G-152/16, 01.24 A.10), approved by the institutional ethical committees and guidelines of the Austrian institutions, the German animal protection law and the state of Baden-Württemberg, as well as the Institutional Animal Care and Use Committees of the Institute of Systems Biology in Seattle. Within each experiment, mice were both age and sex matched; however, male and female mice were used interchangeably between experiments, and results showed no sex-dependent differences in any of the measured parameters. To generate chimeric mice, bone marrow cells were isolated from donor mice by flushing the femur and tibia with 10% FCS, β-mercaptoethanol, 1% penicillin–streptomycin and 2 mM L-glutamine. Cells were ran through a strainer, centrifuged and then frozen in 10% DMSO, 75% FCS and 15% media, consisting of RPMI (10% FCS, β-mercaptoethanol, 1% penicillin–streptomycin and 2 mM L-glutamine). The cells were then stored at −80 °C until transfer. Recipient mice were subjected to 10.5 Gy irradiation using BIOBEAM GM 2000 (Gamma Medical Services); 1 day post-irradiation, mice received 1×10^7 cells from donor mice in a 1:1 ratio. Mice were then allowed a period of recovery, before receiving two rounds of 200 μg of anti-CD90 treatment. To examine the efficiency of the procedure, we performed FACS analysis of a CD45.1:CD45.2 ratio.

Virus. C57BL/6 mice were infected intravenously with high-dose (2×10^6 FFU) LCMV strain clone 13, except when indicated otherwise. For the dose titration experiment, the virus was titrated by a factor of 10 to get the following inocula: 2×10^6 FFU, 2×10^5 FFU, 2×10^4 FFU, 2×10^3 FFU and 2×10^2 FFU. For acute LCMV infection, mice were infected with high-dose 2×10^6 FFU of LCMV strain Armstrong. Viral loads were determined using a focal-forming assay[12], or via quantitative PCR of LCMV nuclear protein. Probe: [6FAM]-CTTGCCGACCTCTTCAATGCGCAA-[BHQ1]; forward primer: ACTGACGAGGTCAACCCGG; reverse primer: CAAGTACTCACACGGCATGGA. Influenza infections were performed using $10^{10.2}$ 50% egg infective dose per ml titer of the PR8 strain of influenza.

Mouse calorimetry. Mice were individually placed in the PhenoMaster (TSE Systems) cages 2 days before infection and allowed to acclimatize to the new environment. After infection, metabolic parameters such as food and water intake, oxygen consumption, carbon dioxide production, RER and activity were measured every 12 min (5 measurements every hour) for 12 consecutive days.

Feeding experiments. During pair-feeding experiments, all mice were placed in single housing for a minimum of 3 days before the start of the experiment, and monitored daily throughout the course of the experiment. Each day the food intake of LCMV-infected mice was measured (ad libitum diet), and a matching amount was given to the pair-fed control mice (restricted diet) up to the point of harvest. For gavage feeding experiments, mice were weighed before infection and, subsequently, infected at the same time. The gavage took place starting from 4 days until 7 days post-infection with continuous free access to a chow diet. During the gavage period mice received 0.5 ml of either PBS or a respective diet twice a day, constituting a supplementation of 1 kcal day^{-1}. Abbot Promote-high protein diet (1 kcal ml^{-1}) was used as the control diet due to the high compatibility with the nutritional profile of chow diet (Abbot Promote, calorie composition: 25% protein, 23% fat and 52% carbohydrates; chow diet, calorie composition: 24% protein, 18% fat and 58% carbohydrates)[36].

Antibodies and pharmacologic treatments. The antibodies used were: Rat IgG1 isotype (MOPC-21, BE0083-BioXcell), Hamster IgG1 isotype (BE0091-BioXcell), anti-TNF-α (XT3.11, Rat IgG1, BE0058-BioXcell), anti-IFN-γ (XMG1.2, Rat IgG1, BE0055-BioXcell), anti-IL-1α (ALF-161, Hamster IgG1, BE0243-BioXcell), anti-IL-6 (MP5-20F3, Rat IgG1, BE0046-BioXcell), anti-CD4 (YTS191, Rat IgG2b, BE0119-BioXcell), anti-CD8 (YTS169.4, Rat IgG2b, BE0117-BioXcell) and anti-CD90 (T24, Rat IgG2b, BE0212-BioXcell). Anti-IFN-γ, anti-TNF-α, anti-IL-6 neutralizing antibodies (0.5 mg), and their Rat IgG1 isotype control, were intraperitoneally injected 1 day before LCMV infection, and were re-administered every second day up to 7 days post-infection. For anti-IL-1α, and its Hamster IgG1 isotype control, 0.2 mg was intraperitoneally injected every 3 days, starting 2 days before LCMV infection. For antibody depletion of CD4 and CD8 T cells, 0.2 mg of monoclonal antibodies was injected iintravenously 2 days and 1 day before infection. FACS analysis was performed on blood to confirm the efficiency to CD4$^+$ and CD8$^+$ T cell depletion.

FTY720 administration was performed as described in a previous paper[25]. Mice received a daily gavage of 0.3 mg kg^{-1} of FTY720 (SML0700, Sigma-Aldrich) dissolved in sterile water. The treatment was administered 1 day before infection and carried on until 8 days post-infection. Blood samples were drawn at 6 and 8 days post-infection, and mice were scarified at 8 days post-infection via cervical dislocation. Spleen and iLNs were subsequently taken for FACS analysis.

Imaging. We used the EchoMRI-100H (EchoMRI LCC) to longitudinally monitor body composition in a non-invasive manner in awake un-anesthetized mice. The results displayed show the average of three consecutive measurements for each mouse within an experimental group, during each time point. For magnetic resonance imaging (MRI), mice were euthanized using cervical dislocation before imaging and kept at 4 °C until imaged. MRI measurements were performed on a 9.4 T animal MRI (BioSpec 94/30USR Bruker Biospin) equipped with a B-GA12SHP gradient and an ^{1}H volume coil with an inner diameter of 40 mm (RFRES 400 1 H 075/040 QSN TR, Bruker Biospin). A multi-spin echo sequence (repetition time = 500 ms, echo time = 7.86 ms, average = 4) was used, with and without fat suppression (fat suppression bandwidth = 1401.17 Hz). A set of 24 slices was acquired in a coronal direction with a resolution of 100 μm^2 in plain and a slice thickness of 1 mm. Total acquisition time was 16 min. To evaluate the size of the fat compartments, the fat-suppressed images are subtracted from corresponding images without fat suppression. Postprocessing was performed using ParaVision v.6 (Bruker Biospin).

Histology. Mice were anesthetized using 15% ketamine and 5% xylazine in PBS, and then perfused with 20 ml of 4% paraformaldehyde in PBS. Isolated tissue was then incubated in 4% paraformaldehyde in PBS, before being transferred to PBS.

For H&E staining, histologic evaluation was performed on 3-μm-thick sections stained with H&E. Four to five representative images (20× magnification) were collected from each fat pad for quantitative analysis using ImageJ-Adiposoft plugin. Cutoffs were set to include all cells larger than 10 μm and smaller than 100 μm in diameter. Images were run through the automated Adiposoft analysis and then manually adjusted as needed.

For immunofluorescence staining, heat-induced antigen retrieval (citrate buffer, pH 6) and unspecific binding blocking (FCS block plus goat anti-mouse Fab block) was performed on paraformaldehyde-fixed sections. Sections were subsequently incubated with the following primary antibodies: rabbit anti-LCMV nucleoprotein sera (1:4,000, generated by prime-boost immunization against purified LCMV-NP) and rat anti-CD8a (1:1000, eBioscience, no. 4SM15) diluted in DAKO Real Antibody Diluent (no. S2022). Bound antibodies were visualized with appropriate species-specific Alexa Fluor 647 anti-rat and Alexa Fluor 488 anti-rabbit (1:200, Jackson ImmunoResearch). Nuclei were stained with 4′,6-diamidino-2-phenylindole (DAPI; 1:2,000, Invitrogen). Immunostained sections were scanned using a Pannoramic 250 FLASH II (3DHISTECH) Digital Slide Scanner with objective magnification of 20×. Four to five representative images were captured at 20× magnification and the image analysis was done using Cell Profiler v.3.0.

Serum measures. Blood samples were collected via the tail vein for longitudinal measurements. For end-point measurements, animals were anesthetized using 15% ketamine and 5% xylazine in PBS, blood was immediately drawn from the vena cava, and the animals where then euthanized via cervical dislocation. Triglyceride levels in the serum were determined using a Cobas C311 Analyzer (Roche). The NEFA content was evaluated enzymatically using NEFA kit (Wako Chemicals: reagents: 434-91795, standard 270-77000).

We used the MILLIPLEX MAP Mouse Cytokine/Chemokine Magnetic Bead Panel-Premixed 32 Plex (MCYTMAG-70K-PX32, Millipore) to quantify a wide range of circulating cytokines and chemokines. Analysis was done following the manufacturer's instructions. To detect circulating levels of IFN-α, we performed ELISA using rat anti-mIFN-α capture antibody (PBL Interferon Source,

no. 22100-1), rabbit anti-mIFN-α detection antibody (PBL Interferon Source, no. 32100-1), anti-rabbit horseradish peroxidase secondary antibody (Jackson ImmunoResearch, no. 711-036-152) and 3,3′,5,5′-tetramethylbenzidine (TMB) solution (Life Technologies, no. 002023). For IFN-β measurements, we used rat anti-mIFN-β capture antibody (PBL Interferon Source, no. 22400-1), rabbit anti-mIFN-β detection antibody (PBL Interferon Source, no. 32400-1), anti-rabbit horseradish peroxidase secondary antibody (Jackson ImmunoResearch, no. 711-036-152) and TMB solution (Life Technologies, no. 002023).

Different ELISA kits were used to measure leptin, cortisol, corticosterone, free triiodothyronine, free thyroxine and norepinephrine, according to the manufacturer's instructions: leptin (PK-EL-68232DM, PromoCell), cortisol (EIAHCOR, Thermo Scientific), corticosterone (ADI-900-097, Enzo Biochem), free triiodothyronine (KET0004, Abbkine), free thyroxine (CSB-E05080m, Cusabio) and norepinephrine (BA E-5200, Labor Diagnostika Nord).

Tissue measures. After euthanasia by cervical dislocation, all harvested tissue was instantly rinsed in PBS and then snap frozen in liquid nitrogen, until further processing. Importantly, iLNs were always separated from the inguinal adipose tissue during the harvest. RNA was isolated from adipose tissue for real-time PCR analysis using QIAzol lysis reagent following the manufacturer's instructions (Qiagen). However, after homogenization, an additional centrifugation step was required to remove any excess oil layer. We then reverse transcribed the RNA samples into complementary DNA using the First Strand cDNA synthesis Kit (Fermentas). After this, we used TaqMan Fast Universal PCR Mastermix and TaqMan Gene Assays for *Rplp0* (no. Mm00725448_s1), *Cd36* (no. Mm00432403_m1), *Lpl* (no. Mm00434764_m1), *Dgat2* (no. Mm00515643_m1), *Ucp1* (no. Mm01244861_m1), *Lep* (no. Mm00434759_m1) and *Adipoq* (no. Mm00456425_m1).

For protein isolation from adipose tissue, samples were homogenized in 1 ml sucrose buffer (250 mM sucrose, 1 mM dithiothreitol, 1 mM ethylenediaminetetraacetic acid, 1:1,000 protease inhibitor cocktail, pH 7), then centrifuged at 4 °C, 1,000*g* for 10 min. The infranatant layer was collected, and protein content was determined using Coomassie Plus Bradford Assay Kit (Thermo Scientific). Protein, 20–40 μg, was used for sodium dodecylsulfate/polyacrylamide gel electrophoresis analysis using NuPAGE Novex 4–12% Bis-Tris Gels (Life Technologies), Westran Clear signal PVDF membranes (Whatman) and the following primary antibodies: anti-ATGL (no. 2138S, Cell Signaling), anti-HSL (no. 4107S, Cell Signaling), anti-pHSL Ser^{660} (no. 4126S, Cell Signaling), anti-D418-Perlipin (3470S, Cell Signaling) and anti-β-actin (no. ab8224, Abcam). As a secondary antibody, we used horseradish peroxidase-conjugated, anti-rabbit antibody (no. P0448, Dako). Detection of the luminescence signal was performed using the ChemiDoc XRS+ (Bio-Rad Laboratories), following the immunoreaction using Pierce ECL-Western blotting detection reagent (Thermo Scientific) and Amersham ECL select western blotting detection reagent (GE Healthcare Life Sciences).

To quantify norepinephrine levels in inguinal white adipose tissue, fat tissue was first weighed, cut into smaller pieces with scissors and then homogenized in norepinephrine extraction buffer (1 mM ethylenediaminetetraacetic acid, 10 mM HCl, 4 mM sodium metabisulfite) using a mixer mill (TissueLyser II, Qiagen). Homogenates were rested for 1 h at 4 °C and adjusted to the same weight per volume percentage by adding deionized water (final volume per sample was 1 ml). To this mixture 200 μl chloroform was added and centrifugation was performed for 15 min at 13,000*g* and 4 °C. The aqueous supernatant was quantified for norepinephrine using the corresponding ELISA kit.

Flow cytometry analysis. Single cell suspensions of iLNs and spleen were prepared through mechanical disruption against 40- to 70-μm cell strainers. Total cell count was quantify minimum essential medium-heparin (1,000 U), and treated with red blood cell lysis buffer (eBioscience). Samples were then treated with anti-CD16/32 FcR-Block (clone 93, eBioscience), and subsequently stained with the respective antibodies as indicated for each experiment: CD8b.2: Pacific Blue (clone 53-5.8); CD8a: PE-Cy7 (clone 53-6.7), PerCP-Cy5 (clone 53-6.7), fluorescein isothiocyanate (FITC; clone 53-6.7), AF700 (clone 53-6.7); CD4: Pacific Blue (clone RM4-4); CD3: APC (clone 17A2), PE-Cy7 (clone 145-2C11); CD45.1: Pacific Blue (clone: A20), PE-Cy7 (clone A20); CD45.2: PE (clone 104), APC (clone 104); CD44: BV605 (clone IM7); Fixable Viability Dye eFluor 780 (APC-Cy7, Life Technologies). To enumerate the number of virus-specific $CD8^+$ T cells, samples were incubated with a fluorophore-labeled, GP33-specific tetramer at 37 °C for 15 min before FcR-block treatment. GP33-specific tetramers were obtained through the NIH Tetramer Core Facility. To quantify the blood (cell μl^{-1}), a precise amount was either directly pipetted into minimum essential medium-heparin or collected in ethylenediaminetetraacetic acid-coated tubes and then transferred to minimum essential medium-heparin; 123count eBeads Counting Beads (no. 01-1234, Invitrogen) were used to quantify cell numbers according to the manufacturer's instructions.

RNA-seq and data processing. To establish the best quality of RNA for RNA-seq analysis, and avoid RNA degradation as a result of the heat generated from homogenization, lymph node-free inguinal adipose tissue was smashed into powder over dry ice, using a pre-cooled BioMasher (Kimble and Chase). After this 1 ml of QIAzol lysis reagent (Qiagen) was added, and RNA was isolated following the manufacturer's instructions, with an additional starting centrifugation step to remove the oil layer. Total RNA was quantified using a Qubit 2.0 Fluorometric Quantitation system (Life Technologies), whereas the RNA integrity number was determined using the Experion Automated Electrophoresis System (Bio-Rad).

The sequencing libraries for the 12 samples were pooled and sequenced on an Illumina HiSeq 3000/4000 instrument using 50-base-pair single-end chemistry. Calling of the bases, using the Illumina Realtime Analysis software, was converted into a BAM format using Illumina2bam and de-multiplexed using BamIndexDecoder (https://github.com/wtsi-npg/illumina2bam). The Tuxedo suite was performed for the RNA-seq analysis pipeline. Reads were mapped on the mouse reference genome (*Mus musculus*, Ensembl e87) using TopHat2 v.2.0.10. Cufflinks v.2.2.1 was employed to assemble transcripts from spliced read alignments, using the Ensembl e87 transcriptome as the reference, as well as new assembly of transcript models. Furthermore, differential analysis of gene expression was quantified using Cuffdiff v.2.2.1. Transcriptome sets of all replicates for each sample group were combined with Cuffmerge. Expression values in graphs are reported as FPKM (fragments per kilobase of transcript per million). Genes are considered expressed when they have FPKM values ≥ 1.

PCA was performed on the gene set with a minimum average expression level across conditions of 5 FPKM. Only the 10% most variable (computed on the coefficient of variance) genes were considered for the PCA analysis. Heatmaps of FPKM expression values of different gene sets were performed using Pearson's distance measure with an average clustering method.

An additional RNA-seq analysis was performed at the transcriptome level to implement an interaction model (2 × 2 factorial design). The gene expression on the mouse Ensembl e87 transcripts was quantified from the previously TopHat2-mapped reads with featureCounts v.1.5.3. Raw read counts are further normalized with the voom function of the limma package[53]. Normalized expression values, reported as $\log_2$ counts per million, were further processed through limma's empirical Bayes models. We implemented limma's interaction model as a 2 × 2 factorial design of uninfected T cell–$Ifnar1^{+/+}$, uninfected T cell–$Ifnar1^{\Delta/\Delta}$ and uninfected, 6 days post-LCMV-infected. Genes differentially modulated in the interaction model were selected based on a minimum $\log_2$ counts per million of 0, a minimum $\log_2$ fold-change absolute value of 0.6 and a maximum adjusted *P* value of 0.05.

We performed enrichment analyses on the genes differentially modulated in the interaction model. Separately, up- and downregulated genes were analyzed with Cytoscape ClueGO v.2.3.3, based on GO (Biological Processes, Molecular Functions, Immune System Process), InterPro, KEGG, Reactome and Wiki Pathways. Terms were called enriched based on a maximum *P* value of 0.05 and a minimum of 3% gene overlap. GO Term Fusion and grouping were performed. Enriched groups were further ranked according to the group, Bonferroni's step-down-adjusted *P* value. Group lead terms were defined inside each group as the term with the lowest adjusted *P* value of enrichment. In-depth metabolic Reactome pathway enrichment was performed with a Cytoscape Reactome Functional Interaction app. Pathways with a maximum false discovery rate of 0.05 were retained.

Quantification and statistical analysis. Results are displayed as mean ± s.e.m. and were statistically analyzed as detailed in the figure legends using GraphPad Prism v.7.0. Statistically significant *P* values were indicated as follows: $*P \leq 0.05$, $**P \leq 0.01$, $***P \leq 0.001$, $****P \leq 0.0001$.

Reporting Summary. Further information on research design is available in the Nature Research Reporting Summary linked to this article.

Data availability

The accession number for the raw data of the RNA-seq is GSE118819.

References

48. Huang, S. et al. Immune response in mice that lack the interferon-gamma receptor. *Science* **259**, 1742–1745 (1993).
49. Pasparakis, M., Alexopoulou, L., Episkopou, V. & Kollias, G. Immune and inflammatory responses in TNF alpha-deficient mice: a critical requirement for TNF alpha in the formation of primary B cell follicles, follicular dendritic cell networks and germinal centers, and in the maturation of the humoral immune response. *J. Exp. Med.* **184**, 1397–1411 (1996).
50. Peschon, J. J. et al. TNF receptor-deficient mice reveal divergent roles for p55 and p75 in several models of inflammation. *J. Immunol.* **160**, 943–952 (1998).
51. Muller, U. et al. Functional role of type I and type II interferons in antiviral defense. *Science* **264**, 1918–1921 (1994).
52. Prigge, J. R. et al. Type I IFNs act upon hematopoietic progenitors to protect and maintain hematopoiesis during pneumocystis lung infection in mice. *J. Immunol.* **195**, 5347–5357 (2015).
53. Sitnick, M. T. et al. Skeletal muscle triacylglycerol hydrolysis does not influence metabolic complications of obesity. *Diabetes* **62**, 3350–3361 (2013).

54. Eguchi, J. et al. Transcriptional control of adipose lipid handling by IRF4. *Cell Metab.* **13**, 249–259 (2011).
55. Sawada, S., Scarborough, J. D., Killeen, N. & Littman, D. R. A lineage-specific transcriptional silencer regulates CD4 gene expression during T lymphocyte development. *Cell* **77**, 917–929 (1994).
56. Coleman, D. L. & Hummel, K. The influence of genetic background on the expression of the obese (Ob) gene in the mouse. *Diabetologia* **9**, 287–293 (1973).
57. Komuro, K., Itakura, K., Boyse, E. A. & John, M. Ly-5: a new T-lymphocyte antigen system. *Immunogenetics* **1**, 452–456 (1974).
58. Fung-Leung, W. et al. CD8 is needed for development of cytotoxic T but not helper T cells. *Cell* **65**, 443–449 (1991).
59. Shinkai, Y. et al. RAG-2-deficient mice lack mature lymphocytes owing to inability to initiate V(D)J rearrangement. *Cell* **68**, 855–867 (1992).
60. Hogquist, K. A. et al. T cell receptor antagonist peptides induce positive selection. *Cell* **76**, 17–27 (1994).
61. Mombaerts, P. et al. RAG-l-deficient mice have no mature B and T lymphocytes. *Cell* **68**, 869–877 (1992).
62. Kägi, D. et al. Cytotoxicity mediated by T cells and natural killer cells is greatly impaired in perforin-deficient mice. *Nature* **369**, 31–37 (1994).
63. Smyth, G. K. Linear models and empirical Bayes methods for assessing differential expression in microarray experiments. *Stat. Appl. Genet. Mol. Biol.* **3**, 1–25 (2004).

nature research

Corresponding author(s): Bergthaler

Last updated by author(s): 02/04/2019

Reporting Summary

Nature Research wishes to improve the reproducibility of the work that we publish. This form provides structure for consistency and transparency in reporting. For further information on Nature Research policies, see Authors & Referees and the Editorial Policy Checklist.

Statistics

For all statistical analyses, confirm that the following items are present in the figure legend, table legend, main text, or Methods section.

n/a	Confirmed
☐	☒ The exact sample size (*n*) for each experimental group/condition, given as a discrete number and unit of measurement
☐	☒ A statement on whether measurements were taken from distinct samples or whether the same sample was measured repeatedly
☐	☒ The statistical test(s) used AND whether they are one- or two-sided *Only common tests should be described solely by name; describe more complex techniques in the Methods section.*
☐	☒ A description of all covariates tested
☐	☒ A description of any assumptions or corrections, such as tests of normality and adjustment for multiple comparisons
☐	☒ A full description of the statistical parameters including central tendency (e.g. means) or other basic estimates (e.g. regression coefficient) AND variation (e.g. standard deviation) or associated estimates of uncertainty (e.g. confidence intervals)
☐	☒ For null hypothesis testing, the test statistic (e.g. *F*, *t*, *r*) with confidence intervals, effect sizes, degrees of freedom and *P* value noted *Give P values as exact values whenever suitable.*
☒	☐ For Bayesian analysis, information on the choice of priors and Markov chain Monte Carlo settings
☐	☒ For hierarchical and complex designs, identification of the appropriate level for tests and full reporting of outcomes
☒	☐ Estimates of effect sizes (e.g. Cohen's *d*, Pearson's *r*), indicating how they were calculated

Our web collection on statistics for biologists contains articles on many of the points above.

Software and code

Policy information about availability of computer code

Data collection	EchMRI-TM-130 Analyzer was used to record body composition data acquired using EchoMRI-TM-100H. MRI Analysis was done using a multi spin echo (MSME) sequence (repetition time[TR]= 500 ms, echo time[TE]=7.86 ms, averages =4) with and without fat suppression (fat suppression bandwidth=1401.17 Hz). BD FACS Diva 8.0.1 was used for data collection during flow cytometry analysis.
Data analysis	Graph design and statistical analysis was performed using GraphPad Prism V7.0. Postprocessing of MRI data was performed using ParaVision V6 Quantitative analysis of adipose tissue H/E staining was performed using ImageJ-Adiposoft plugin V1.15. Immunohistochemistry stained sections were scanned using Pannoramic 250 FLAH II (3DHISTECH) Digital Slide Scanner. The images were then analyzed using Cell Profiler V3.0. For flow cytometry data analysis we used FlowJo V10.4.2. For RNA-sequencing data was quinfified and analyzed using the TopHat2 (v2.0.10). Cufflinks (v2.2.1), Cuffdiff (v2.2.1) and the Cuffmerge pipeline. Enrichment analysis was performed with Cytoscape ClueGO 82 (v2.3.3).

For manuscripts utilizing custom algorithms or software that are central to the research but not yet described in published literature, software must be made available to editors/reviewers. We strongly encourage code deposition in a community repository (e.g. GitHub). See the Nature Research guidelines for submitting code & software for further information.

Data

Policy information about availability of data

All manuscripts must include a data availability statement. This statement should provide the following information, where applicable:

- Accession codes, unique identifiers, or web links for publicly available datasets
- A list of figures that have associated raw data
- A description of any restrictions on data availability

Accession number for the row data of the RNAseq: GSE118819.

Field-specific reporting

Please select the one below that is the best fit for your research. If you are not sure, read the appropriate sections before making your selection.

☒ Life sciences ☐ Behavioural & social sciences ☐ Ecological, evolutionary & environmental sciences

For a reference copy of the document with all sections, see nature.com/documents/nr-reporting-summary-flat.pdf

Life sciences study design

All studies must disclose on these points even when the disclosure is negative.

Sample size	All experiments described in this study were done using a sample size varying between n=3-5 as indicated in figure legends.
Data exclusions	No data was excluded from the analysis.
Replication	All data shown are either representative or pooled data from at least two successful independent experiments. In the case of RNA-sequencing data and histology (H/E data and immunofluorescent data), a single experiment was performed, quality control measures were taken to insure the validity of the experiment, this include measurement of viral load and body weight of LCMV-infected mice.
Randomization	age- and sex-matched mice were randomly assigned to the experimental groups prior to the start of the experiment.
Blinding	*Describe whether the investigators were blinded to group allocation during data collection and/or analysis. If blinding was not possible, describe why OR explain why blinding was not relevant to your study.*

Reporting for specific materials, systems and methods

We require information from authors about some types of materials, experimental systems and methods used in many studies. Here, indicate whether each material, system or method listed is relevant to your study. If you are not sure if a list item applies to your research, read the appropriate section before selecting a response.

Materials & experimental systems

n/a	Involved in the study
☐	☒ Antibodies
☒	☐ Eukaryotic cell lines
☒	☐ Palaeontology
☐	☒ Animals and other organisms
☒	☐ Human research participants
☒	☐ Clinical data

Methods

n/a	Involved in the study
☒	☐ ChIP-seq
☐	☒ Flow cytometry
☒	☐ MRI-based neuroimaging

Antibodies

Antibodies used

Rat IgG1 isptype, clone: MOPC-21 (0.5mg) BioXcell BE0083
Hamster IgG1 isotype, clone: N/A (0.2mg) BioXcell BE0091
Rat IgG1 anti-TNFα, clone: XT3.11 (0.5mg) BioXcell BE0058
Rat IgG1 anti-IFNγ, clone: XMG1.2 (0.5mg) BioXcell BE0055
Hamster IgG1 anti-IL1α, clone: ALF-161 (0.2mg) BioXcell BE0243
Rat IgG1 anti-IL6, clone: MP5-20F3 (0.5mg) BioXcell BE0046
Rat IgG2b anti-CD4, clone:YTS191 (0.2mg) BioXcell BE0119
Rat IgG2b anti-CD8, clone: YTS169.4 (0.2mg) BioXcell BE0117
Rat IgG2b anti-CD90, clone: T24 (200μg) BioXcell BE0212
Rat anti-CD16/CD32, clone: 93 (1:200) eBioscience #14-0161-82
Anti-mouse CD8b.2 Pacific Blue, clone: 53-5.8 (1:200) Biolegend #140414
Anti-mouse CD8a PE-Cy7, clone: 53-6.7 (1:200) Biolegend #100721

Anti-mouse CD8a PerCP-Cy5, clone:53-6.7 (1:200) Biolegend #100733
Anti-mouse CD8a FITC , clone: 53-6.7 (1:200) Biolegend #100803
Anti-mouse CD8a AF700, clone: 53-6.7 (1:200) Biolegend #100729
Anti-mouse CD4 Pacific Blue, clone: RM4-4 (1:200) Biolegend #116007
Anti-mouse CD3 APC, clone: 17A2 (1:200) Biolegend #100235
Anti-mouse CD3 PE-Cy7, clone: 145-2C11 (1:200) Biolegend #100319
Anti-mouse CD45.1 Pacific Blue, clone: A20 (1:200) Biolegend #110721
Anti-mouse CD45.1PE-Cy7, clone:A20 (1:200) Biolegend #110729
Anti-mouse CD45.2 PE, clone 104 (1:200) Biolegend #109807
Anti-mouse CD45.2 APC, clone:104 (1:200) Biolegend #109813
Anti-mouse CD44 BV605, clone: IM7 (1:200) Biolegend #103047
Anti-ATGL, (1:1000) Cell Signaling #2138S
Anti-HSL, (1:1000) Cell Signaling #4107S
Anti-phospho HSL Ser660, (1:1000) Cell Signaling #4126S
Anti-D418-Perlipin, (1:1000) Cell Signaling #3470S
Anti-β-Actin, (1:1000) Abcam ab8224
HRP-conjugated anti-rabbit antibody, (1:4000) Dako P0448
Rat anti-mIFN-α capture antibody, (1:54) PBL Interferon Source 22100-1
Rabbit anti-mIFN-α detection antibody, (1:738) PBL Interferon Source 32100-1
Anti-rabbit HRP secondary antibody, (1:5000) Jackson ImmunoResearch 711-036-152
Rat anti-mIFN-β capture antibody, (1:1000) PBL Interferon Source 22400-1
Rabbit anti-mIFN-β detection antibody, (1:1000) PBL Interferon Source 32400-1
Rat anti-CD8a Alexa Fluor 647, clone:4SM15 (1:1000) eBioscience #4SM15
Alexa Fluor 488 anti-LCMV_NP, (1:4000)

Validation

All antibodies were validated as per manufacturer instruction. For FACS antibodies unstained samples were included in every run, to control for auto-fluorescence. The LCMV_NP Alexa Fluor antibody has been previously validation in Kosak et al. Sci Rep. 2017 Sep 12;7(1):11289. DOI: 10.1038/s41598-017-10637-y

Animals and other organisms

Policy information about studies involving animals; ARRIVE guidelines recommended for reporting animal research

Laboratory animals

Mouse: C57BL/6, The Jackson Laboratory JAX: 000664
Mouse: Ifnγ-/-:B6.129S7-Ifngr1tm1Agt/J, The Jackson Laboratory JAX: 003288
Mouse: Tnf-/-: B6.129S-Tnftm1gkl/J, The Jackson Laboratory JAX: 005540
Mouse: Tnfrl-/-: C57BL/6- Tnfrsf1atm1/mx/J, The Jackson Laboratory JAX: 003242
Mouse: Ifnar1-/-: B6.129S2-Ifnar1tm1Agt/Mmjax, The Jackson Laboratory JAX: 032045
Mouse: Ifnar1fl/fl: B6(Cg)-Ifnar1tm1.1Ees/J, The Jackson Laboratory JAX: 028256
Mouse: AdipoqCre/+: B6;FVB-Tg(Adipoq-cre)1Evdr/J, The Jackson Laboratory JAX: 010803
Mouse: Atglfl/fl: B6N.129S-Pnpla2tm1Eek/J, The Jackson Laboratory JAX: 024278
Mouse: Hslfl/fl: B6.129P2-Lipetm1Rze/J, Laboratory of Rudolf Zechner, Graz, Austria. N/A
Mouse: Cd4Cre/+: STOCK Tg(Cd4-cre)1Cwi/BfluJ, The Jackson Laboratory JAX: 017336
Mouse: Ob/Ob: B6.Cg-Lepob/J, The Jackson Laboratory JAX: 000632
Mouse: Cd45.1, Ly5a, PtprcSJL Komuro et al., 1974 MGI:4819849
Mouse: Cd8-/-: B6.129S2-Cd8atm1Mak/J, The Jackson Laboratory JAX: 002665
Mouse: Rag2-/-: B6(Cg)-Rag2tm1.1Cgn/J, The Jackson Laboratory JAX: 008449
Mouse: OT-I Rag1-/- CD45.1: C57BL/6-Tg(Tcratcrb)1100Mjb/J, B6.129S7-Rag1tm1Mom/J, The Jackson Laboratory JAX: 003831, 002216
Mouse: Prf1-/-: CD57BL/6-Prf1tm1Sdz/J, The Jackson Laboratory JAX: 002407

All animals within each experiment were age- and sex-matched. Animals were 8-12 weeks old by the start of the experiment. Between different experiments males and females were used interchangeably, as no sex-specific differences were observed in relevant parameters.

Wild animals

The study did not involve wild animals.

Field-collected samples

The study did not involve field-collected samples.

Ethics oversight

Ethical approval was obtained from the Department of Biomedical Research of the Medical University of Vienna, Vienna, Austria, as well as the Central Facility for Animal Research and Scientific Animal Welfare (ZETT) in Dusseldorf, Germany, the state of Beden-Wurttemberg, Germany, and the Institutional Animal Case and Use Committees of the Institute of Systems Biology in Seattle.

Note that full information on the approval of the study protocol must also be provided in the manuscript.

Flow Cytometry

Plots

Confirm that:

☒ The axis labels state the marker and fluorochrome used (e.g. CD4-FITC).

☒ The axis scales are clearly visible. Include numbers along axes only for bottom left plot of group (a 'group' is an analysis of identical markers).

☐ All plots are contour plots with outliers or pseudocolor plots.

☒ A numerical value for number of cells or percentage (with statistics) is provided.

Methodology

Sample preparation	For flow cytometry analysis samples were obtained from either blood, spleen or inguinal lymph nodes. Blood samples were collected in MEM-1000UHeparin, then treated with RBC lysis buffer. Spleens and lymph nodes were collected in PBS-2%FCS on ice, then mechanically distrupted against 40-70μm cell trainers.
Instrument	Flow cytometry data was collected using LSRFortessa.
Software	BD FACS Diva 8.0.1 was used for data collection. For data analysis we used FlowJo V10.4.2.
Cell population abundance	No cell sorting was performed in this study.
Gating strategy	Among live, single cells: CD4 T cells were gated as: CD3+CD8+ CD8 T cells were gated as: CD3+CD8+ or CD44+ CD8+ Virus-specific CD8 T cells were gated as: CD3+ CD8+ and either GP33+ or NP396+ For Chimeric mice: endogenous CD8 T cells were gated as: CD45.2+CD8+ the transferred CD8 T cells were gated as CD45.1+CD8+

☒ Tick this box to confirm that a figure exemplifying the gating strategy is provided in the Supplementary Information.

nature immunology

SUPPLEMENTARY INFORMATION

https://doi.org/10.1038/s41590-019-0397-y

In the format provided by the authors and unedited.

CD8+ T cells induce cachexia during chronic viral infection

Hatoon Baazim[1], Martina Schweiger[2,9], Michael Moschinger[1,9], Haifeng Xu[3], Thomas Scherer[4], Alexandra Popa[1], Suchira Gallage[5], Adnan Ali[5], Kseniya Khamina[1], Lindsay Kosack[1], Bojan Vilagos[1], Mark Smyth[1], Alexander Lercher[1], Joachim Friske[6], Doron Merkler[7], Alan Aderem[8], Thomas H. Helbich[6], Mathias Heikenwälder[5], Philipp A. Lang[3], Rudolf Zechner[2] and Andreas Bergthaler[1]*

[1]CeMM Research Center for Molecular Medicine of the Austrian Academy of Sciences, Vienna, Austria. [2]Institute of Molecular Biosciences, University of Graz, Graz, Austria. [3]Department of Molecular Medicine II, Heinrich Heine University, Düsseldorf, Germany. [4]Division of Endocrinology and Metabolism, Department of Medicine III, Medical University of Vienna, Vienna, Austria. [5]Division of Chronic Inflammation and Cancer, German Cancer Research Center, Heidelberg, Germany. [6]Department of Biomedical Imaging and Image-guided Therapy, Division of Gender and Molecular Imaging, Preclinical Imaging Laboratory, Medical University of Vienna, Vienna, Austria. [7]Department of Pathology and Immunology, University of Geneva, Geneva, Switzerland. [8]Center for Global Infectious Disease Research, Seattle Children's Research Institute, Seattle, WA, USA. [9]These authors contributed equally: Martina Schweiger, Michael Moschinger. *e-mail: abergthaler@cemm.oeaw.ac.at

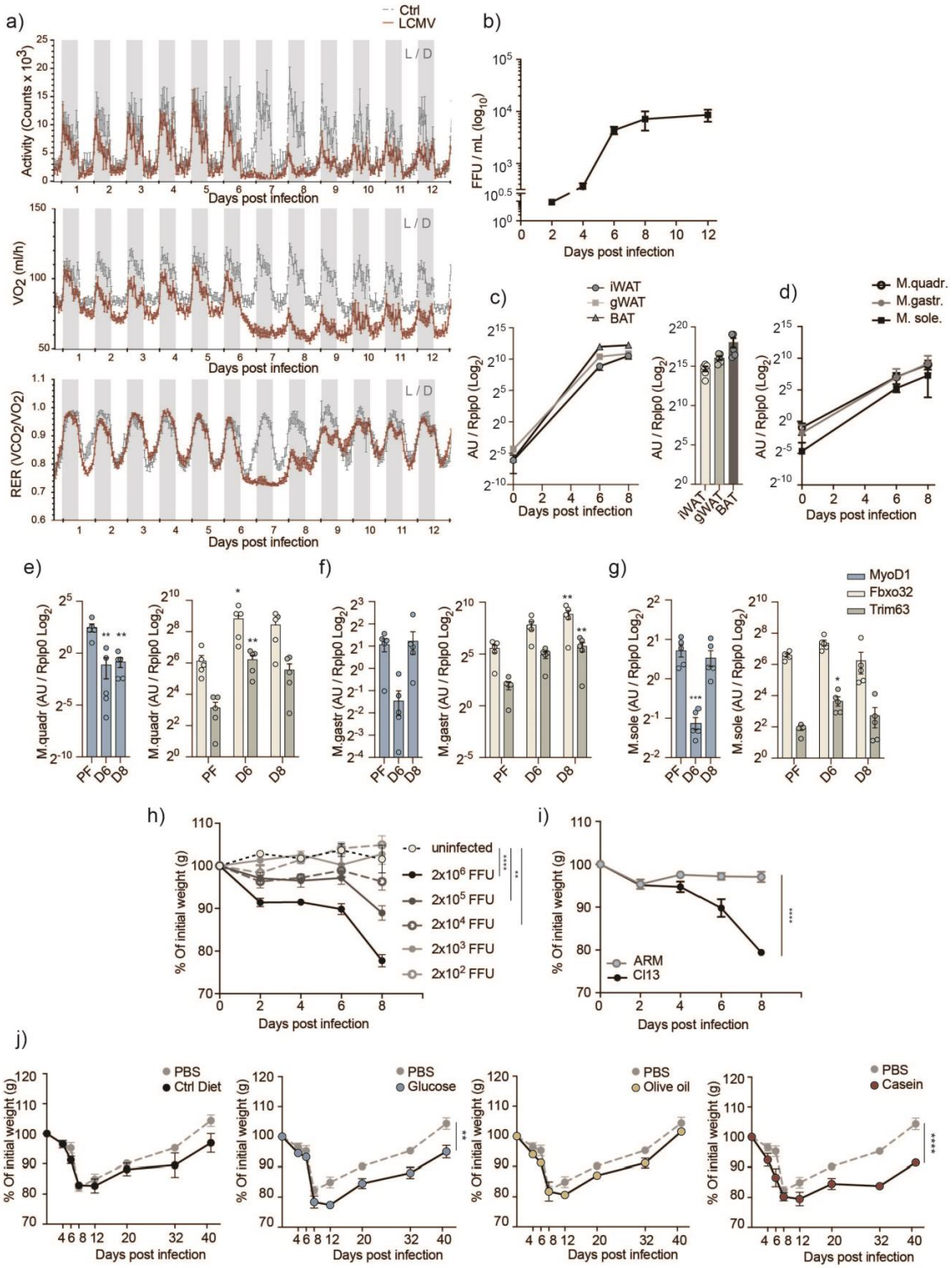
a)
Ctrl
LCMV
L / D
Activity (Counts x 10^3)
VO2 (ml/h)
RER (VCO2/VO2)
Days post infection
b)
FFU / mL (log10)
Days post infection
c)
iWAT
gWAT
BAT
AU / Rplp0 (Log2)
d)
M.quadr.
M.gastr.
M. sole.
e)
M.quadr (AU / Rplp0 Log2)
f)
M.gastr (AU / Rplp0 Log2)
g)
MyoD1
Fbxo32
Trim63
M.sole (AU / Rplp0 Log2)
PF
D6
D8
h)
% Of initial weight (g)
uninfected
2x10^6 FFU
2x10^5 FFU
2x10^4 FFU
2x10^3 FFU
2x10^2 FFU
i)
ARM
Cl13
j)
PBS
Ctrl Diet
Glucose
Olive oil
Casein

Supplementary Figure 1

Characterization of the pathophysiological changes induced by IAC.

a) Activity, oxygen consumption (VO_2) and respiratory exchange ratio (RER) of LCMV-infected mice compared to uninfected controls (n=10). Data are representative of a single experiment.

b) Circulating viral load of LCMV-infected mice, measured using focus-forming assay (n=4). Data are representative of two independent experiments

c,d) LCMV nuclear protein as measured by qPCR from tissue homogenate of inguinal, gonadal, and interscapular-brown adipose tissue up to 8 days post-infection, and 17 days post-infection (column graph) (n=5), representative of three independent experiments (c), as well as quadriceps, gastrocnemius and soleus muscles (n=5) representative of two independent experiments.

e-g) RNA expression of myoblast differentiation 1 (MoyD1), and the proteasomal degradation markers Atrogin1 (Fbxo32) and Murf1 (Trim63) in the indicated muscle compartment (n=5) (p-values: **0.0025 , **0.0029, *0.0252, **0.0059 (e), **0.0087 , **0.0071 (f), ***0.0003 , *0.0295 (g) one-way ANOVA, Bonferroni correction).

h) Body weight kinetics of mice infected with a titrated dose of LCMV-Cl13, ranging from $2x10^6$ FFU to $2x10^2$ FFU (n=3), (p-values: **** < 0.0001, **0.0021 two-way ANOVA).

i) Body weight kinetics of mice infected with high dose LCMV-Cl13 compared to LCMV-ARM (n=4), (p-values: ****< 0.0001 two-way ANOVA). h-i) data are representative of three independent experiments.

j) Body weight kinetics Of LCMV-infected mice after gavage supplementation of indicated diet between 4 and 7 days after infection (n=4) (p-values: **0.0029, ****< 0.0001, two-way ANOVA) Data are representative of a single experiment.

All data shows mean ± s.e.m.

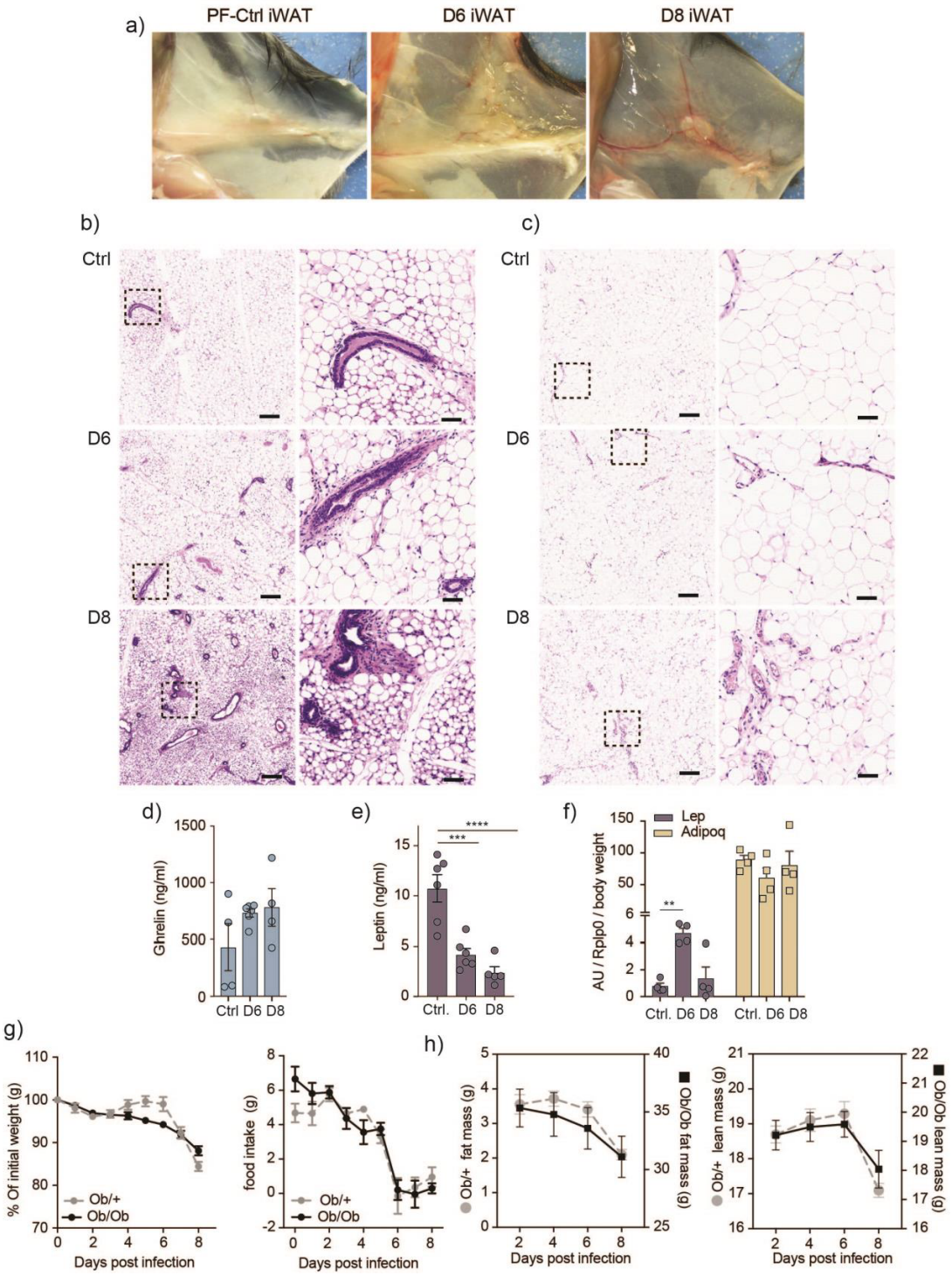
a)
PF-Ctrl iWAT
D6 iWAT
D8 iWAT
b)
c)
Ctrl
D6
D8
d)
Ghrelin (ng/ml)
Ctrl D6 D8
e)
Leptin (ng/ml)
Ctrl. D6 D8
f)
Lep
Adipoq
AU / Rplp0 / body weight
Ctrl. D6 D8 Ctrl. D6 D8
g)
% Of initial weight (g)
Ob/+
Ob/Ob
Days post infection
food intake (g)
Days post infection
h)
Ob/+ fat mass (g)
Ob/Ob fat mass (g)
Days post infection
Ob/+ lean mass (g)
Ob/Ob lean mass (g)
Days post infection

Supplementary Figure 2

IAC triggers severe adipose tissue remodeling and alters leptin expression and concentration.

a) Inguinal fat pad in LCMV-infected mice at 6 and 8 days post-infection compared to pair-fed mice. Similar results were observed across all experiments using LCMV-infected wild-type mice.

b,c) Representative H/E staining taken from inguinal fat pad (b) and gonadal fat pad (c) at 6 and 8 days post-infection compared to uninfected controls (n=3).

d,e) Serum concentration of ghrelin (n=5) (d) and leptin (n=6) (e) as measured by ELISA in infected and uninfected mice (p-values: ***0.0002, ****<0.00001 one-way ANOVA, Bonferroni correction). Data are pooled from two independent experiments.

f) Leptin (*Lep*) and Adiponectin (*Adipoq*) mRNA expression in inguinal fat pad of infected and uninfected mice, calculated from arbitrary units normalized to Ribosomal protein (*Rplp0*) and body weight (n=4) (p-values: **0.0018 one-way ANOVA, Bonferroni correction). Data are representative of a single experiment.

g,h) Infection of leptin knockout mice ($Lep^{Ob/Ob}$) and heterogeneous control ($Lep^{Ob/+}$) showing body weight kinetics and food intake (n=4), representative of two independent experiments (g) and body composition as measured in live un-anesthetized mice using EchoMRI (n=4), representative of a single experiment (h).

d-h) data shows mean ± s.e.m.

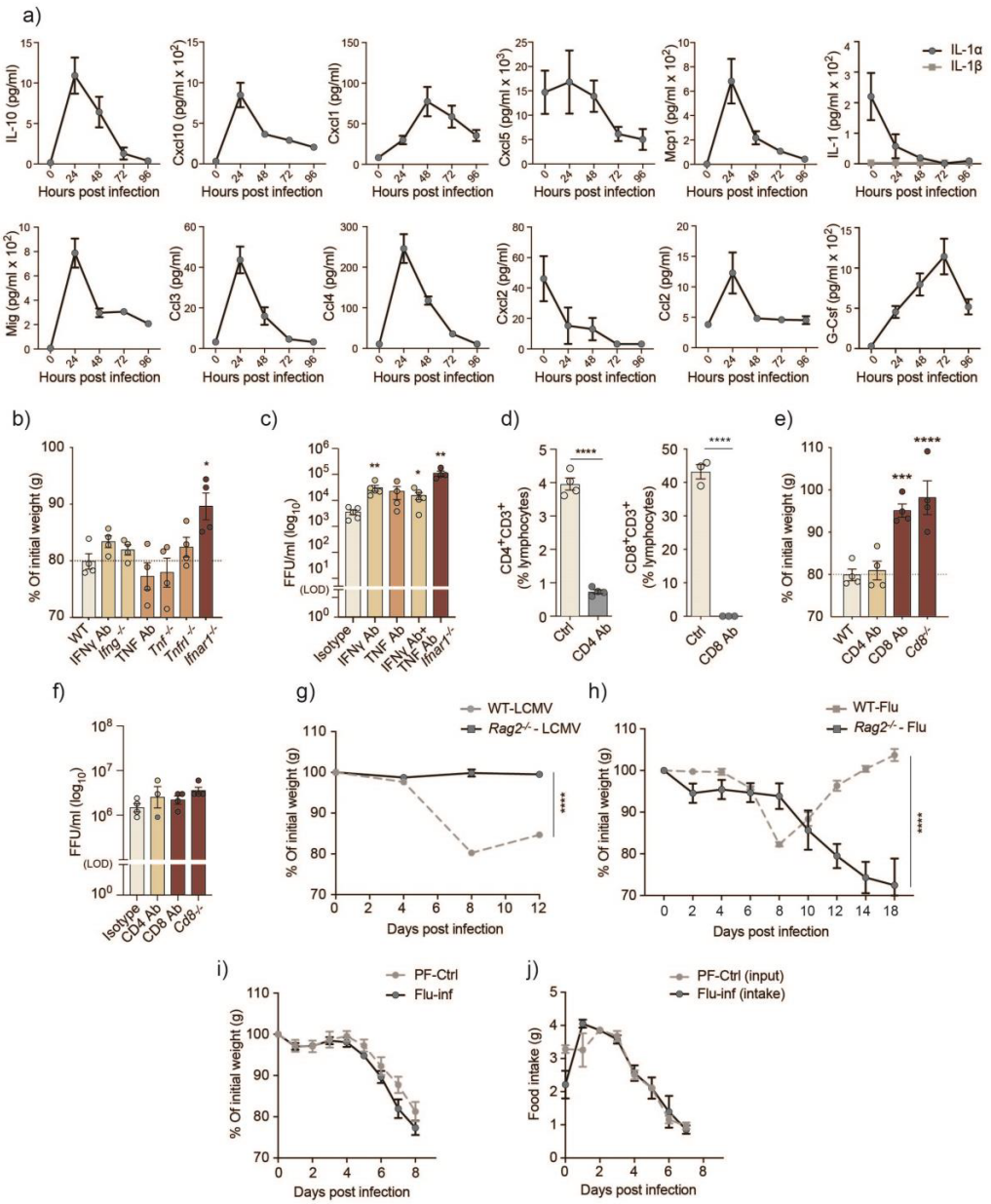

Supplementary Figure 3

The role of infection-induced proinflammatory cytokines and T cells in mediating weight loss during LCMV Cl13 and influenza infection.

a) Serum cytokines of LCMV-infected mice measured using Luminex multiplexing immunoassays (n=4). Data are representative of a single experiment.

b) Percent of initial body weight at 8 days post infection in genetic knockout and neutralizing antibody-treated mice for the indicated

cytokines and cytokine receptors (n=4) (p-values: *0.0122 unpaired two-tailed Student's t-test). Data shows a summary of figure 2b-2d.

c) Circulating viral load as measured using focus-forming assay at 8 days after infection. (n=5) for antibody depletion and (n=4) for *Ifnar1*$^{-/-}$ (p-values: **0.0092, *0.0371, **0.0015 unpaired two-tailed t-test).

d) Percent of circulating CD4^{+} T cells or CD8^{+} as indicated, following treatment with either CD4 blocking antibody (n=3) or CD8 blocking antibody (n=4) respectively.

e) Percent of initial body weight of mice treated with either anti-CD4 or anti-CD8 depleting antibodies, as well as CD8$^{-/-}$ (n=4).

f) Splenic viral load as measured with focus-forming assay at 8 days after infection. (n=3) for anti-CD4 treated mice and (n=4) for others. c-f) Data are representative of two independent experiments for antibody depletions and *Ifnar1*$^{-/-}$, and a single experiment for *Ifng*$^{-/-}$, *Tnf*$^{-/-}$, *Tnfrf*$^{-/-}$ and *Cd8*$^{-/-}$.

g,h) Body weight kinetics of WT and *Rag2*$^{-/-}$ mice infected with LCMV-Cl13 (n=5) (g) or Influenza PR/8 (n=4) (h) (p-values: ****< 0.0001 two-way ANOVA). Data are representative of two independent experiments.

i) Body weight kinetics and j) food intake of influenza-infected mice compared to pair-fed uninfected mice up to 8 days post-infection (n=4), data represent a single experiment.

Data shows mean ± s.e.m.

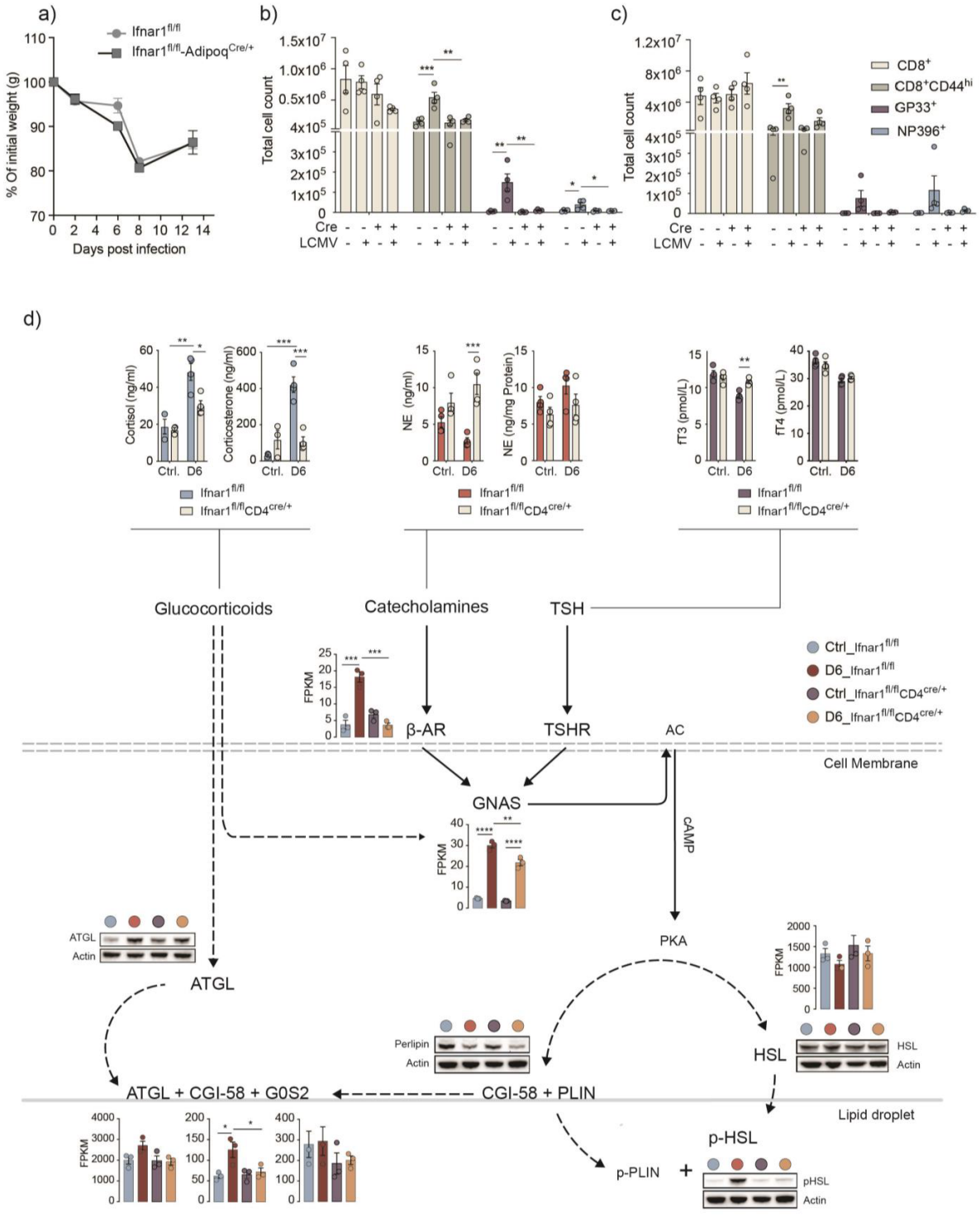
a)
Ifnar1fl/fl
Ifnar1fl/fl-AdipoqCre/+
% Of initial weight (g)
Days post infection
b)
Total cell count
Cre
LCMV
c)
CD8+
CD8+CD44hi
GP33+
NP396+
d)
Cortisol (ng/ml)
Corticosterone (ng/ml)
NE (ng/ml)
NE (ng/mg Protein)
fT3 (pmol/L)
fT4 (pmol/L)
Ctrl.
D6
Ifnar1fl/fl
Ifnar1fl/flCD4cre/+
Glucocorticoids
Catecholamines
TSH
β-AR
TSHR
AC
Cell Membrane
GNAS
cAMP
PKA
Ctrl_Ifnar1fl/fl
D6_Ifnar1fl/fl
Ctrl_Ifnar1fl/flCD4cre/+
D6_Ifnar1fl/flCD4cre/+
FPKM
ATGL
Actin
Perlipin
HSL
pHSL
p-HSL
p-PLIN
ATGL + CGI-58 + G0S2
CGI-58 + PLIN
Lipid droplet

Supplementary Figure 4

Loss of T cell–intrinsic type I IFN signaling abrogates infection-induced adipose tissue lipolysis.

a) Body weight kinetics of *Ifnar1*$^{fl/fl}$Adipoq$^{Cre/+}$ mice in comparison to *Ifnar1*$^{fl/fl}$ controls (n=4) Data are representative of two independent experiments.

b,c) FACS analysis of CD8^{+} T cells in spleen (n=4) (p-values: ***0.0005 , **0.0017 , **0.0059 , *0.0124 two-way ANOVA, Bonferroni correction) (b) and inguinal LN (n=4) (p-values: **0.0049 two-way ANOVA, Bonferroni correction) (c), harvested on 6 days post-infection from *Ifnar1*$^{fl/fl}$CD4$^{Cre/+}$ and *Ifnar1*$^{fl/fl}$ controls. Data represents a single experiment.

d) Schematic representation of fasting lipolysis, showing circulating cortisol (p-values: **0.0010, *0.137 two-way ANOVA, Bonferroni correction), corticosterone (p-values: ***0.0001, ***0.0004 two-way ANOVA, Bonferroni correction), norepinephrine (p-values: ***0.0004 two-way ANOVA, Bonferroni correction), free T3 (p-values: **0.0036 two-way ANOVA, Bonferroni correction) and free T4 levels, as well as adipose tissue norepinephrine (n=3). Data are representative of two independent experiments. RNA-seq data (n=3) shows mRNA expression of β-AR (Abrd2) (p-values: ***0.0001 one way ANOVA, Bonferroni correction), GNAS (p-values: ****< 0.0001, **0.0014 one-way ANOVA, Bonferroni correction), ATGL (Pnpla2), CGI-58 (Abhd5) (p-values: *0.0271, *0.048 one-way ANOVA, Bonferroni correction), G0S2 (G0s2) and HSL (Lipe), in addition to protein expression of ATGL, HSL, pHSL and Perilipin. Western blot data are representative of two independent experiments were (n=3).

Data shows mean ± s.e.m. for bar graphs and (a).

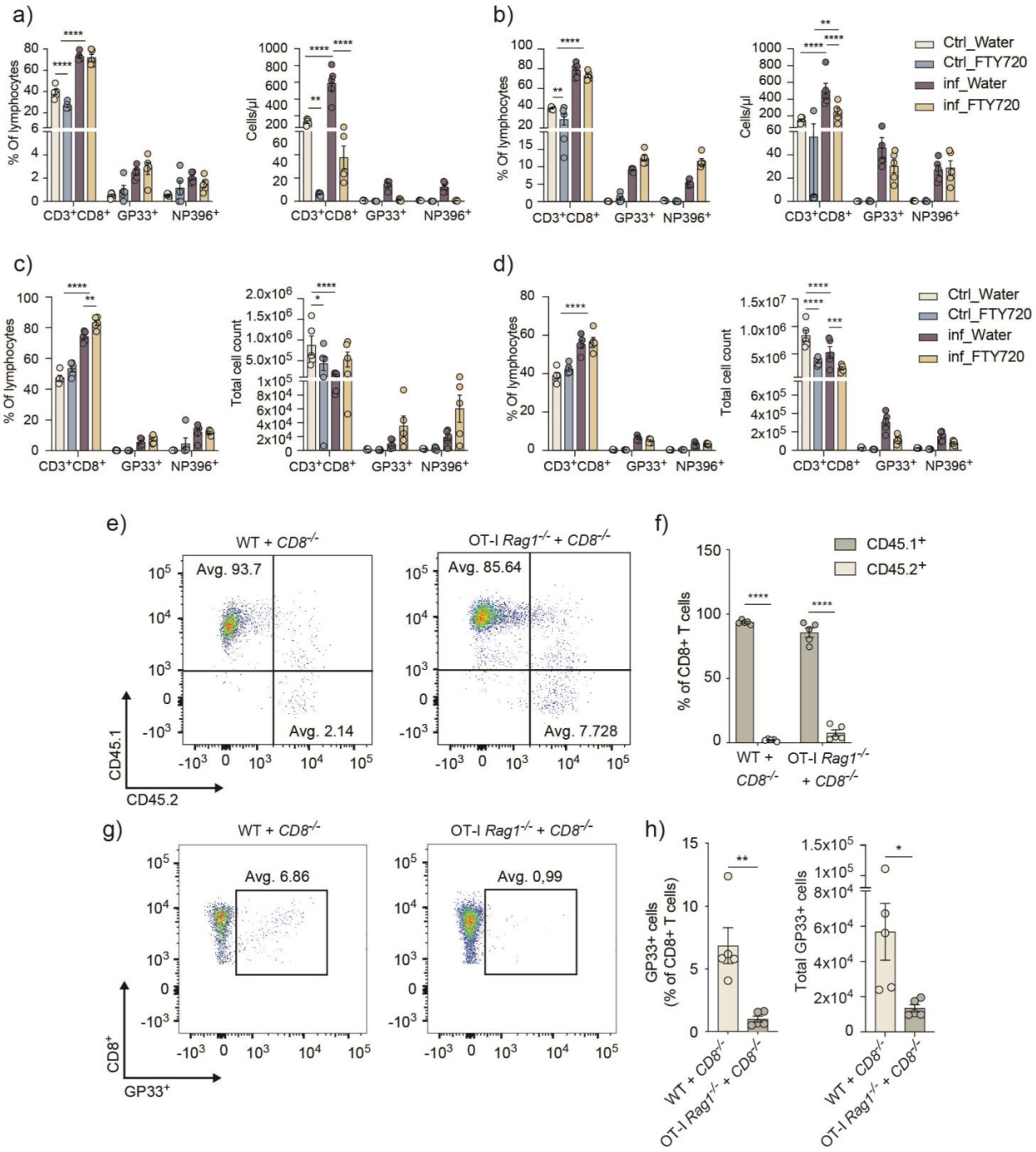
a)
b)
c)
d)
% Of lymphocytes
Cells/µl
Total cell count
CD3+CD8+
GP33+
NP396+
Ctrl_Water
Ctrl_FTY720
inf_Water
inf_FTY720
e)
WT + CD8-/-
OT-I Rag1-/- + CD8-/-
Avg. 93.7
Avg. 2.14
Avg. 85.64
Avg. 7.728
CD45.1
CD45.2
f)
CD45.1+
CD45.2+
% of CD8+ T cells
g)
Avg. 6.86
Avg. 0,99
CD8+
GP33+
h)
GP33+ cells (% of CD8+ T cells)
Total GP33+ cells

Supplementary Figure 5

CD8 T cell egress from lymph nodes is dispensable for the induction of IAC, but antigen-specific activation is required.

a-d) Virus-specific $CD3^+CD8^+$ T cells of LCMV-infected and uninfected mice after daily gavage administration of either FTY720 or water. Cell were isolated from blood at day 6 (n=5) (p-values: **** < 0.0001, **0.0083 two-way ANOVA, Bonferroni correction) (a) and day 8 post infection (n=5) (p-values: ****<0.0001, **0.0013, **0.0012 two-way ANOVA, Bonferroni correction) (b). At day 8 post-infection, cells were also isolated from inguinal LN (n=5) (p-values: **** < 0.0001, **0.0036, *0.0142 two way ANOVA, Bonferroni correction) (c) and spleen (n=5) (p-values: **** < 0.0001, ***0.0002 two way ANOVA, Bonferroni correction) (d).

e,f) Flow cytometry analysis showing the percent of $CD8^+$ T cells carrying $CD45.1^+$ vs $CD45.2^+$ congenic markers after bone marrow reconstitution in indicated chimeras (n=6) (p-values: ****< 0.0001 unpaired two-tailed Student's t-test).

g,h) Percentage and total number of $GP33^+CD8^+$ T cells in chimeric mice at 12 days after LCMV infection (n=6) (p-values: **0.0038, *0.0282 unpaired two-tailed Student's t-test).

e-h) Data are pooled from two independent experiments. All data shows mean ± s.e.m.

Fig. 2d

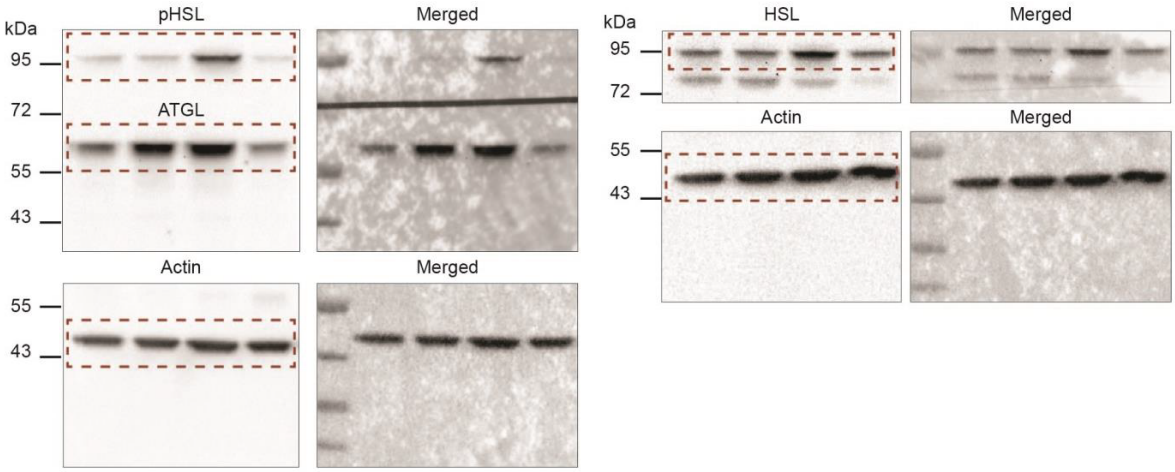

Supplementary Fig. 4d

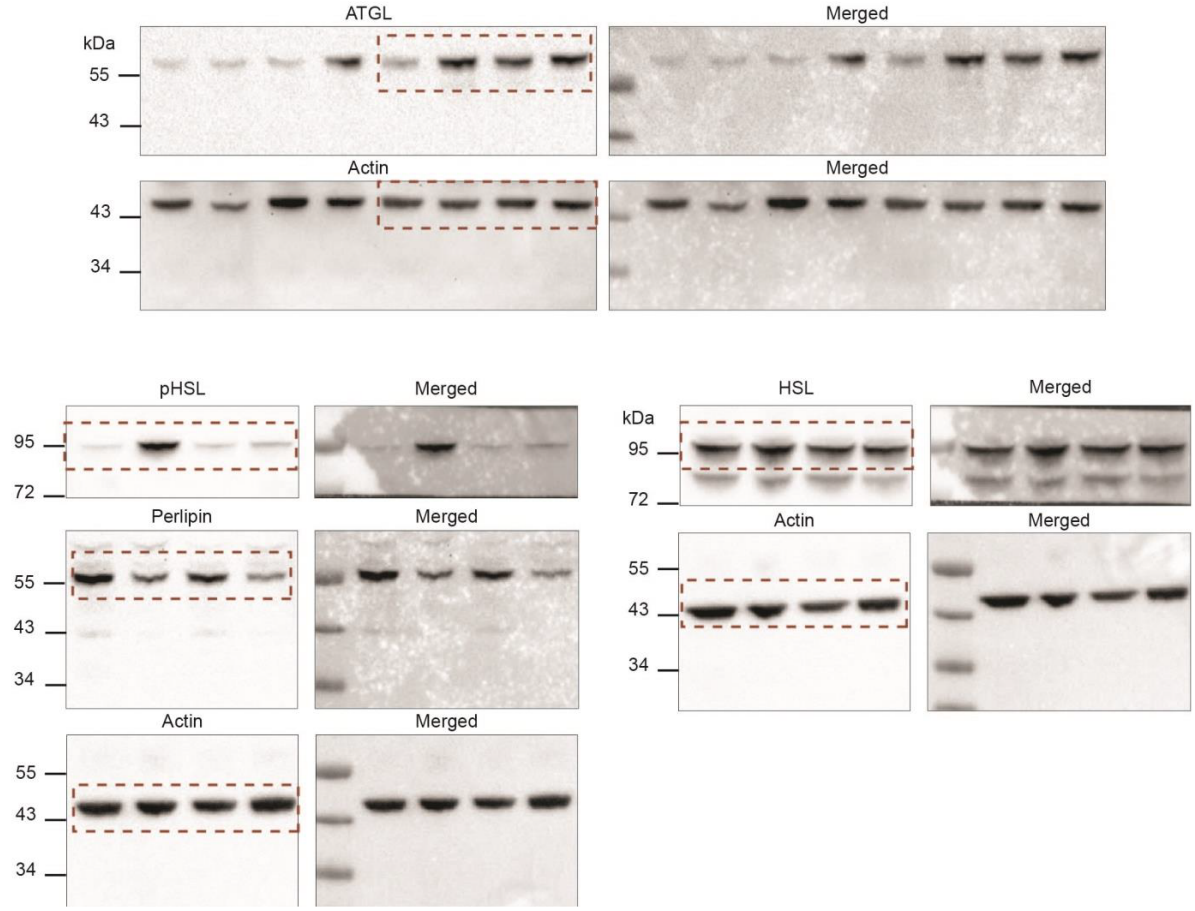

Supplementary Figure 6

Unprocessed images of all western blots.

(left) unprocessed image acquired for indicated antibodies. (right) merge images show the chemo-luminescence image automatically merged with ladder image as acquired using Bio-Rad ChemiDoc™ XRS+ system.

Supplementary Table 1:

	Ctrl		16h		24h		36h		48h		72h		96h	
	Mean	STDEV	Mean	STDEV	Mean	STDEV	Mean	STDEV	Mean	STDEV	Mean	STDEV	Mean	STDEV
Eotaxin	127,62	65,85	92,14	21,08	88,78	28,14	120,81	12,30	52,96	12,55	60,27	6,07	50,36	8,25
G-CSF	30,69	20,70	234,08	21,15	454,48	145,76	805,23	104,87	795,97	273,36	1142,98	441,38	518,19	188,38
GM-CSF	<3,2	-	<3,2	-	6,86	7,31	<3,2	-	<3,2	-	<3,2	-	<3,2	-
IFN-g	<0,63	-	37,80	7,00	43,16	6,16	8,51	4,24	26,17	11,59	608,70	184,96	684,16	173,48
IL-1a	220,43	154,36	14,36	12,73	57,25	79,16	64,04	15,98	19,50	16,01	1,64	0,43	9,60	16,55
IL-1b	<3,2	-	<3,2	-	<3,2	-	<3,2	-	<3,2	-	<3,2	-	<3,2	-
IL-2	<2,1	-	<2,1	-	<2,1	-	<2,1	-	<2,1	-	<2,1	-	<2,1	-
IL-3	1,31	0,17	1,52	0,16	1,44	0,14	1,55	0,04	1,45	0,09	1,45	0,13	1,41	0,10
IL-4	<1,34	-	<1,34	-	<1,34	-	<1,34	-	<1,34	-	<1,34	-	<1,34	-
IL-5	<1,99	-	5,22	3,81	3,69	3,40	<1,99	-	<1,99	-	34,67	26,11	81,84	20,03
IL-6	<0,09	-	125,68	32,68	76,53	49,49	25,30	15,28	9,19	10,32	36,41	14,35	9,04	3,64
IL-7	<0,01	-	<0,01	-	0,05	0,07	0,41	0,79	0,11	0,21	1,29	2,14	2,21	2,32
IL-9	<3,2	-	9,84	13,29	<3,2	-	<3,2	-	<3,2	-	<3,2	-	<3,2	-
IL-10	<0,18	-	9,71	4,92	10,92	4,45	14,59	3,81	6,41	3,81	1,30	1,46	0,39	0,42
IL-12(p40)	<0,27	-	<0,27	-	<0,27	-	<0,27	-	<0,27	-	<0,27	-	<0,27	-
IL-12(p70)	<1,86	-	<1,86	-	<1,86	-	<1,86	-	<1,86	-	<1,86	-	<1,86	-
IL-13	<3,2	-	<3,2	-	<3,2	-	<3,2	-	<3,2	-	<3,2	-	<3,2	-
IL-15	<0,69	-	3,51	5,64	1,65	1,93	5,39	9,39	3,61	5,84	10,36	19,34	8,86	16,35
IL-17	<0,57	-	<0,57	-	<0,57	-	<0,57	-	<0,57	-	<0,57	-	<0,57	-
IP-10	32,40	16,58	1646,91	262,30	847,57	301,22	622,68	63,25	366,53	37,61	290,25	27,11	205,53	26,91
KC	8,27	4,95	91,42	15,25	29,95	10,35	90,01	26,23	77,32	36,22	58,68	27,25	35,38	13,74
LIF	<0,84	-	<0,84	-	<0,84	-	<0,84	-	<0,84	-	<0,84	-	<0,84	-
LIX	14715,35	8875,36	11556,72	1589,85	16804,59	12982,59	21163,26	2643,70	13903,63	6421,48	6156,22	2932,71	5047,71	4304,10
MCP-1	<2,37	-	415,61	207,18	682,21	366,05	507,79	227,31	218,12	106,24	108,14	25,15	43,25	7,31
M-CSF	134,55	267,86	41,13	58,97	114,62	102,94	68,60	70,72	9,11	10,61	<0,62	-	<0,62	-
MIG	6,72	2,01	278,46	99,73	787,21	239,24	803,43	136,96	297,24	71,03	306,87	37,09	208,29	23,48
MIP-1A	<3,2	-	68,68	7,58	43,60	13,23	37,87	9,36	15,94	8,67	4,58	2,75	<3,2	-
MIP-1B	<3,2	-	434,73	97,49	245,80	71,52	194,26	23,23	117,56	20,12	35,69	12,19	10,62	14,85
MIP2	46,14	29,67	10,39	14,38	15,19	23,98	15,82	17,39	13,01	14,64	<3,2	-	<3,2	-
RANTES	3,82	0,46	11,60	4,82	12,28	6,78	9,69	2,93	4,84	0,62	4,62	0,50	4,53	1,29
TNF	2,40	0,24	5,18	0,76	5,14	0,57	5,20	0,50	3,73	0,49	3,21	0,21	2,94	0,33
VEGF	1,40	0,18	1,34	0,04	1,36	0,09	1,32	0,05	1,29	0,05	1,27	0,05	1,25	0,05
IFNa	<0,000	-	12483,90	2142,65	17450,51	4101,07	11505,30	1800,13	3216,97	1014,99	<0,000	-	<0,000	-
IFNb	<0,000	-	1071,96	214,65	439,38	78,04	<0,000	-	<0,000	-	<0,000	-	<0,000	-

4. Discussion.

Cachexia is a debilitating syndrome that impacts a wide range of patients, yet remains poorly diagnosed and, in the majority of cases, unsuccessfully managed (Baracos *et al*, 2018; Aoyagi *et al*, 2015). Patients suffering from cancer, chronic inflammation and infection, are at risk of manifesting cachexia during terminal stages of disease, and as such cachexia often correlates with increased morbidity and mortality (Lok, 2015).

In this study, I investigated the inflammatory and metabolic drivers of infection-associated cachexia, using a benchmark model of chronic viral infection. We report that infection with high dose LCMV-Cl13 results in a transient cachexia triggered by antigen-specific $CD8^+$ T cell response, and requires $CD8^+$ T cell-intrinsic type I IFN signaling. The decline in body weight accompanies a reduction in food and water intake, decreased physical activity, as well as a shift in systemic metabolism towards fat utilization. A closer examination of adipose tissue revealed severe structural remodeling, metabolic reprogramming and increased lipolysis. Within multiple models of cachexia, adipose tissue wasting was shown to precede muscle atrophy, and is thought to potentially predispose to it (Bing & Trayhurn, 2008; Das *et al*, 2011; Fukawa *et al*, 2016). The wasting affected fat depots in the whole organism, though the inguinal compartment showed a slightly earlier wasting. Additionally, fat remodeling was associated with an increase in the density of vascular structures, mainly in the inguinal fat pad, a feature that has not been previously described during cachexia. It's important to note that the true nature of this vasculature remains unknown and requires further characterization. Some similarities might be drawn between obesity and cachexia, in terms of the adipose tissue inflammatory milieu and metabolic changes which can promote systemic inflammation, dyslipidemia and metabolic dysfunctions (Vegiopoulos *et al*, 2017). Increased vascularization is a known feature of obesity, during which the expanding mass of adipocytes increases their distance to blood vessels, thereby triggering hypoxia-induced angiogenesis (Cao, 2013). Additionally, the differences in tissue remodeling of the inguinal and gonadal compartment could provide important clues into the molecular underpinnings of cachexia and may be attributed to the fat pad localization and/or the presence of lymph nodes, both of which are factors that can alter the tissue's metabolic and inflammatory state (Bjørndal *et al*, 2011). For instance, if the cachectic signals that link virus-specific $CD8^+$ T cells and adipocytes are transmitted from lymph nodes to peri-lymphatic adipose depots, the affected fat pads might then indirectly induce wasting in other depots. Though cross-fat pad communication networks are poorly understood, depot-specific manipulations in rodents highlight their presence and ability to affect the lipolytic and cell proliferative state (Shi & Bartness, 2005).

When viewing cachexia under the light of metabolic adaptation, the available evidence remains insufficient to definitively classify cachexia as a maladaptive syndrome. Cachectic patient have been reported to exhibit cardiac and respiratory complications that can result in

death (Fearon *et al*, 2011; Baracos *et al*, 2018). However, these complications mostly occur at very advanced stages of disease, and it is difficult to disentangle whether they occur as a result of the cachexia-program, or due to the underlying illness. Additionally, a study investigating cachexia during pancreatic ductal adenocarcinoma (PDAC), performed a review of clinical data from PDAC patients. This study showed no correlation between peripheral tissue wasting during cachexia and the patient's survival (Danai *et al*, 2018).

The syndrome as a whole occurs in three pathophysiological stages: pre-cachexia, cachexia, and refractory cachexia (Fearon *et al*, 2011). During pre-cachexia, subtle changes are observed in feeding behavior and glucose tolerance, which might not have a significant effect on weight loss (Muscaritoli *et al*, 2010). Patients are then classified as cachectic, when their weight loss exceeds 5% of their initial weight over 6 months and present with sarcopenia (Baracos *et al*, 2018; Tisdale, 2002). They enter a state refractory cachexia when the extent of illness prevents medical intervention and limits their life expectancy (Fearon *et al*, 2011). These stages could be viewed as a reflection of the adaptive state of the progression of cachexia programs as they progress in response to the inflammatory environment (Figure 6).

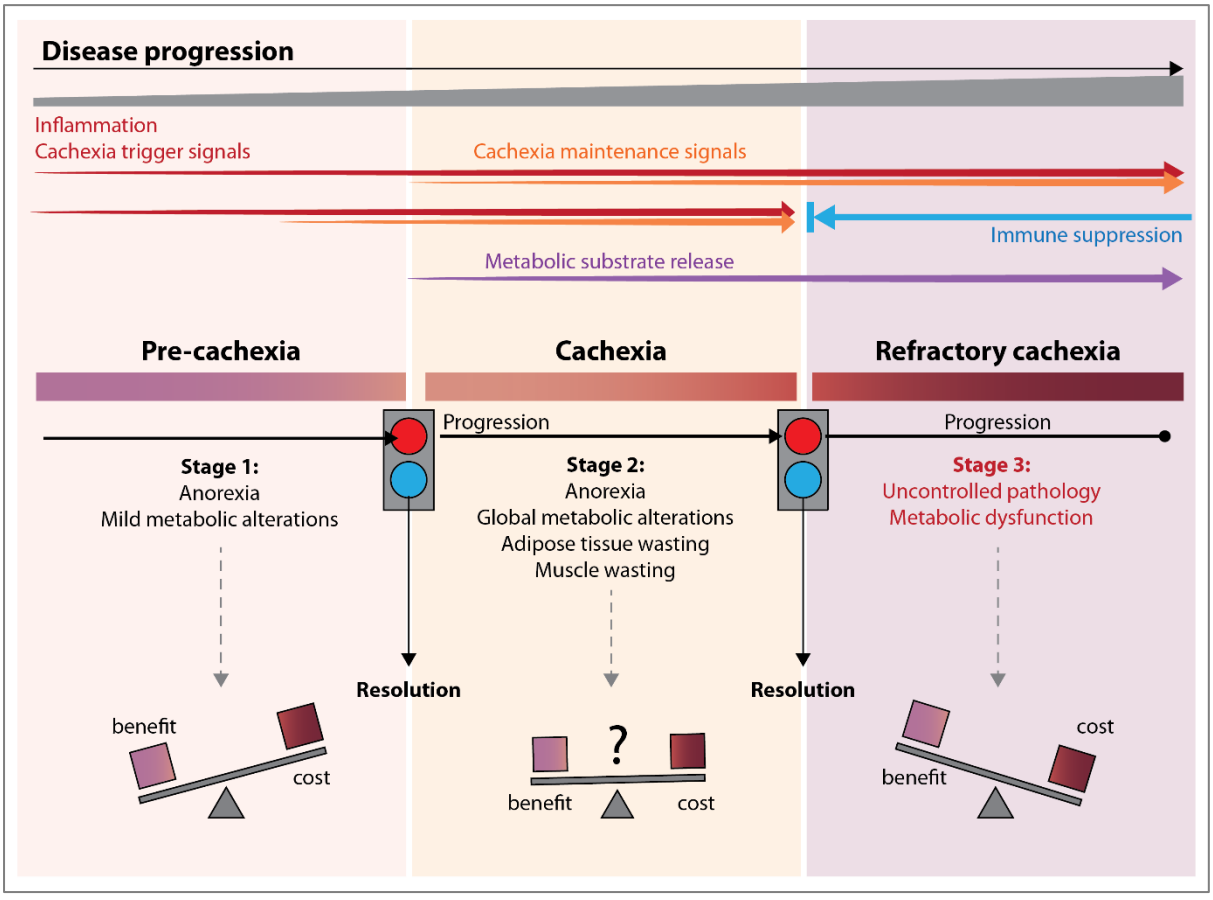

Figure 6: A model representing stages of cachexia along disease progression.

If we super-impose this progression on our model, we can point towards day 6 after infection as the transition point between pre-cachexia and cachexia, where the alterations in feeding behavior and lipid metabolism start to have global impacts. At day 8 post infection, the weight loss reaches a threshold of 15-20%, the progression of cachexia slows down and weight recovery begins. This threshold is likely to represent the dividing line between transient or terminal cachexia. It is reasonable to hypothesize that during transient cachexia, recovery starts either due to the resolution of the underlying illness (Arends *et al*, 2017), or due to the activation of immunomodulatory pathway that dampens the cachexia-programs (Wherry, 2011; Rouse & Sehrawat, 2010; Moseman & McGavern, 2013). If these immunomodulatory pathways fail to control the signals that either trigger or maintain cachexia, or if the underlying illness continued to progress, this could result in an uncontrolled pathology and refractory cachexia.

A better understanding of the trade-off mechanisms by which cachexia is influenced is still massively underexplored (Wang & Medzhitov, 2019). Our work provides a reliable model for comparative analyses, where viral infection-associated cachexia, could be compared to parasitic infection-associated cachexia and cancer-associated cachexia. Such comparative analyses would be crucial in the future to strip away the disease-specific variations and identify the main modulatory elements of cachexia. This could be valuable for the design of new therapeutic strategies, that are specialized to the respective context.

5. References.

Aoyagi T, Terracina KP, Raza A, Matsubara H & Takabe K (2015) Cancer cachexia, mechanism and treatment. *World J. Gastrointest. Oncol.* **7:** 17–29 Available at: http://www.ncbi.nlm.nih.gov/pubmed/25897346 [Accessed August 2, 2019]

Arends J, Bachmann P, Baracos V, Barthelemy N, Bertz H, Bozzetti F, Fearon K, Hütterer E, Isenring E, Kaasa S, Krznaric Z, Laird B, Larsson M, Laviano A, Mühlebach S, Muscaritoli M, Oldervoll L, Ravasco P, Solheim T, Strasser F, et al (2017) ESPEN guidelines on nutrition in cancer patients. *Clin. Nutr.* **36:** 11–48 Available at: http://dx.doi.org/10.1016/j.clnu.2016.07.015 [Accessed October 14, 2018]

Argilés JM, Busquets S, Toledo M & López-Soriano FJ (2009) The role of cytokines in cancer cachexia. *Curr. Opin. Support. Palliat. Care* **3:** 263–268

Argilés JM, López-Soriano FJ, Stemmler B & Busquets S (2017) Novel targeted therapies for cancer cachexia. *Biochem. J.* **474:** 2663–2678 Available at: http://www.biochemj.org.ez.srv.meduniwien.ac.at/content/ppbiochemj/474/16/2663.full.pdf [Accessed October 11, 2018]

Argilés JM, Stemmler B, López-Soriano FJ & Busquets S (2018) Inter-tissue communication in cancer cachexia. *Nat. Rev. Endocrinol.* **15:** 9–20 Available at: www.nature.com/nrendo [Accessed July 1, 2019]

Arner P, Bernard S, Salehpour M, Possnert G, Liebl J, Steier P, Buchholz BA, Eriksson M, Arner E, Hauner H, Skurk T, Rydén M, Frayn KN & Spalding KL (2011) Dynamics of human adipose lipid turnover in health and metabolic disease. *Nature* **478:** 110–113 Available at: http://www.nature.com/articles/nature10426 [Accessed July 30, 2019]

Arner P & Langin D (2014) Lipolysis in lipid turnover, cancer cachexia, and obesity-induced insulin resistance. *Trends Endocrinol. Metab.* **25:** 255–262 Available at: http://dx.doi.org/10.1016/j.tem.2014.03.002

Attia E (2010) Anorexia Nervosa: Current Status and Future Directions. *Annu. Rev. Med.* **61:** 425–435 Available at: http://www.annualreviews.org/doi/10.1146/annurev.med.050208.200745 [Accessed July 30, 2019]

Ayres JS & Schneider DS (2012) Tolerance of Infections. *Annu. Rev. Immunol.* **30:** 271–294 Available at: http://www.annualreviews.org/doi/10.1146/annurev-immunol-020711-075030 [Accessed July 29, 2019]

Baazim H, Schweiger M, Moschinger M, Xu H, Scherer T, Popa A, Gallage S, Ali A, Khamina K, Kosack L, Vilagos B, Smyth M, Lercher A, Friske J, Merkler D, Aderem A, Helbich TH, Heikenwälder M, Lang PA, Zechner R, et al (2019) CD8+ T cells induce cachexia during chronic viral infection. *Nat. Immunol.* **20:** 701–710 Available at:

http://www.nature.com/articles/s41590-019-0397-y [Accessed July 30, 2019]

Balaban S, Lee LS, Schreuder M & Hoy AJ (2015) Obesity and cancer progression: is there a role of fatty acid metabolism? *Biomed Res. Int.* **2015:** 274585 Available at: http://www.hindawi.com/journals/bmri/2015/274585/ [Accessed July 29, 2019]

Baltgalvis KA, Berger FG, Peña MMO, Mark Davis J, White JP & Carson JA (2010) Activity level, apoptosis, and development of cachexia in Apc(Min/+) mice. *J. Appl. Physiol.* **109:** 1155–61 Available at: http://www.physiology.org/doi/10.1152/japplphysiol.00442.2010 [Accessed July 12, 2019]

Baracos VE, Martin L, Korc M, Guttridge DC & Fearon KCH (2018) Cancer-associated cachexia. *Nat. Rev. Dis. Prim.* **4:** 1–18 Available at: http://dx.doi.org/10.1038/nrdp.2017.105

Barkhudaryan A, Scherbakov N, Springer J & Doehner W (2017) Cardiac muscle wasting in individuals with cancer cachexia. *ESC Hear. Fail.* **4:** 458–467 Available at: http://www.ncbi.nlm.nih.gov/pubmed/29154433 [Accessed July 13, 2019]

Battegay M, Moskophidis D, Waldner H, Bründler MA, Fung-Leung WP, Mak TW, Hengartner H & Zinkernagel RM (1993) Impairment and delay of neutralizing antiviral antibody responses by virus-specific cytotoxic T cells. *J. Immunol.* **151:** 5408–15 Available at: http://www.ncbi.nlm.nih.gov/pubmed/7693811 [Accessed September 6, 2019]

Bell E (2005) Intracellular trafficking, IRF7 and type-I-IFN responses. *Nat. Rev. Immunol.* **5:** 361–361 Available at: http://www.nature.com/articles/nri1625 [Accessed July 25, 2019]

Belury M, Nishijima Y, Asp ML, Stout MB, Reiser PJ & Belury MA (2010) Cardiac alterations in cancer-induced cachexia in mice. *Int. J. Oncol.* **37:** 347–53 Available at: http://www.ncbi.nlm.nih.gov/pubmed/20596662 [Accessed July 13, 2019]

Bergthaler A, Flatz L, Hegazy AN, Johnson S, Horvath E, Lohning M & Pinschewer DD (2010) Viral replicative capacity is the primary determinant of lymphocytic choriomeningitis virus persistence and immunosuppression. *Proc. Natl. Acad. Sci.* **107:** 21641–21646 Available at: http://www.ncbi.nlm.nih.gov/pubmed/21098292 [Accessed June 13, 2018]

Bergthaler A, Merkler D, Horvath E, Bestmann L & Pinschewer D (2007) Contributions of the lymphocytic choriomeningitis virus glycoprotein and polymerase to strain-specific differences in murine liver pathogenicity. *J. Gen. Virol.* **88:** 592–603 Available at: http://www.microbiologyresearch.org/docserver/fulltext/jgv/88/2/592.pdf?expires=1528903181&id=id&accname=guest&checksum=221ED5280A8C4F87D66B34FA2C54A3EA [Accessed June 13, 2018]

Bing C & Trayhurn P (2008) Regulation of adipose tissue metabolism in cancer cachexia.

Curr. Opin. Clin. Nutr. Metab. Care **11:** 201–207

Bird L (2019) Cachexia by T cells. *Nat. Rev. Immunol.***:** 1 Available at: http://www.nature.com/articles/s41577-019-0186-8 [Accessed June 7, 2019]

Bjørndal B, Burri L, Staalesen V, Skorve J & Berge RK (2011) Different adipose depots: Their role in the development of metabolic syndrome and mitochondrial response to hypolipidemic agents. *J. Obes.* **2011:**

Bossola M, Marzetti E, Rosa F & Pacelli F (2016) Skeletal muscle regeneration in cancer cachexia. *Clin. Exp. Pharmacol. Physiol.* **43:** 522–7 Available at: http://doi.wiley.com/10.1111/1440-1681.12559 [Accessed July 13, 2019]

Braun TP, Zhu X, Szumowski M, Scott GD, Grossberg AJ, Levasseur PR, Graham K, Khan S, Damaraju S, Colmers WF, Baracos VE & Marks DL (2011) Central nervous system inflammation induces muscle atrophy via activation of the hypothalamic-pituitary-adrenal axis. *J. Exp. Med.* **208:** 2449–63 Available at: http://www.jem.org/lookup/doi/10.1084/jem.20111020 [Accessed July 17, 2019]

Buchmeier M, de la Torre J, Peters C, Del la Torre J & Bowen M (2007) Arenaviridae: the viruses and their replication. Available at: https://www.scienceopen.com/document?vid=4cfb6de1-1bb9-44e9-8e72-f49898d3007c [Accessed September 3, 2019]

Buck MD, Sowell RT, Kaech SM & Pearce EL (2017) Metabolic Instruction of Immunity. *Cell* **169:** 570–586 Available at: http://dx.doi.org/10.1016/j.cell.2017.04.004

Burfeind KG, Michaelis KA & Marks DL (2016) The central role of hypothalamic inflammation in the acute illness response and cachexia. *Semin. Cell Dev. Biol.* **54:** 42–52 Available at: https://www.ncbi.nlm.nih.gov/pmc/articles/PMC4872506/pdf/nihms-782102.pdf [Accessed July 16, 2019]

Calder PC (2012) Fatty acids: Long-chain fatty acids and inflammation. *Proc. Nutr. Soc.* **71:** 284–289

Cao Y (2013) Angiogenesis and vascular functions in modulation of obesity, adipose metabolism, and insulin sensitivity. *Cell Metab.* **18:** 478–489 Available at: http://dx.doi.org/10.1016/j.cmet.2013.08.008

Cava A La & Matarese G (2004) The weight of leptin in immunity. *Nat. Rev. Immunol.* **4:** 371–379 Available at: http://www.nature.com/doifinder/10.1038/nri1350

Cerny A, Sutter S, Bazin H, Hengartner H & Zinkernagel RM (1988) Clearance of lymphocytic choriomeningitis virus in antibody- and B-cell-deprived mice. *J. Virol.* **62:** 1803–7 Available at: http://www.ncbi.nlm.nih.gov/pubmed/3258641 [Accessed September 4, 2019]

Chang SW, Pan WS, Lozano Beltran D, Oleyda Baldelomar L, Solano MA, Tuero I, Friedland JS, Torrico F & Gilman RH (2013) Gut Hormones, Appetite Suppression and

Cachexia in Patients with Pulmonary TB. *PLoS One* **8:** Available at: www.plosone.org [Accessed July 29, 2019]

Cheung WW, Paik KH & Mak RH (2010) Inflammation and cachexia in chronic kidney disease. *Pediatr. Nephrol.* **25:** 711–724

Cohen S, Nathan JA & Goldberg AL (2014) Muscle wasting in disease: Molecular mechanisms and promising therapies. *Nat. Rev. Drug Discov.* **14:** 58–74 Available at: http://dx.doi.org/10.1038/nrd4467

Coleman RA, Lewin TM, Van Horn CG & Gonzalez-Baró MR (2002) Do Long-Chain Acyl-CoA Synthetases Regulate Fatty Acid Entry into Synthetic Versus Degradative Pathways? *J. Nutr.* **132:** 2123–2126 Available at: http://www.ncbi.nlm.nih.gov/pubmed/12163649 [Accessed July 29, 2019]

Cone RD, Cowley MA, Butler AA, Fan W, Marks DL & Low MJ (2001) The arcuate nucleus as a conduit for diverse signals relevant to energy homeostasis. *Int. J. Obes. Relat. Metab. Disord.* **25 Suppl 5:** S63-7 Available at: http://www.nature.com/articles/0801913 [Accessed July 16, 2019]

Corbett TH, Griswold DP, Roberts BJ, Peckham JC & Schabel FM (1975) Tumor induction relationships in development of transplantable cancers of the colon in mice for chemotherapy assays, with a note on carcinogen structure. *Cancer Res.* **35:** 2434–9 Available at: http://www.ncbi.nlm.nih.gov/pubmed/1149045 [Accessed July 12, 2019]

Cornberg M, Kenney LL, Chen AT, Waggoner SN, Kim SK, Dienes HP, Welsh RM & Selin LK (2013) Clonal exhaustion as a mechanism to protect against severe immunopathology and death from an overwhelming CD8 T cell response. *Front. Immunol.* **4:** Available at: www.frontiersin.org [Accessed September 25, 2018]

Curtsinger JM, Valenzuela JO, Agarwal P, Lins D & Mescher MF (2005) Type I IFNs Provide a Third Signal to CD8 T Cells to Stimulate Clonal Expansion and Differentiation. *J. Immunol.* **174:** 4465–4469 Available at: http://www.jimmunol.org/cgi/doi/10.4049/jimmunol.174.8.4465

Danai L V., Babic A, Rosenthal MH, Dennstedt EA, Muir A, Lien EC, Mayers JR, Tai K, Lau AN, Jones-Sali P, Prado CM, Petersen GM, Takahashi N, Sugimoto M, Yeh JJ, Lopez N, Bardeesy N, Fernandez-Del Castillo C, Liss AS, Koong AC, et al (2018) Altered exocrine function can drive adipose wasting in early pancreatic cancer. *Nature* **558:** 600–604 Available at: https://doi.org/10.1038/s41586-018-0235-7 [Accessed July 18, 2018]

Das SK, Eder S, Schauer S, Diwoky C, Temmel H, Guertl B, Gorkiewicz G, Tamilarasan KP, Kumari P, Trauner M, Zimmermann R, Vesely P, Haemmerle G, Zechner R & Hoefler G (2011) Adipose triglyceride lipase contributes to cancer-associated cachexia. *Science (80-.).* **333:** 233–238

DeBoer MD (2009) Animal models of anorexia and cachexia. *Expert Opin. Drug Discov.* **4:** 1145–1155 Available at: https://www.ncbi.nlm.nih.gov/pmc/articles/PMC2771941/pdf/nihms147732.pdf [Accessed July 12, 2019]

DeBoer MD (2011) Ghrelin and cachexia: Will treatment with GHSR-1a agonists make a difference for patients suffering from chronic wasting syndromes? *Mol. Cell. Endocrinol.* **340:** 97–105 Available at: http://www.ncbi.nlm.nih.gov/pubmed/21354462 [Accessed June 25, 2019]

Deboer MD, Zhu X, Levasseur PR, Inui A, Hu Z, Han G, Mitch WE, Taylor JE, Halem HA, Dong JZ, Datta R, Culler MD & Marks DL (2008) Ghrelin treatment of chronic kidney disease: improvements in lean body mass and cytokine profile. *Endocrinology* **149:** 827–35 Available at: https://academic.oup.com/endo/article-lookup/doi/10.1210/en.2007-1046 [Accessed July 12, 2019]

Djouder N, Tuerk RD, Suter M, Salvioni P, Thali RF, Scholz R, Vaahtomeri K, Auchli Y, Rechsteiner H, Brunisholz RA, Viollet B, Mäkelä TP, Wallimann T, Neumann D & Krek W (2010) PKA phosphorylates and inactivates AMPKα to promote efficient lipolysis. *EMBO J.* **29:** 469–481 Available at: http://emboj.embopress.org/cgi/doi/10.1038/emboj.2009.339 [Accessed July 30, 2019]

Duncan RE, Ahmadian M, Jaworski K, Sarkadi-Nagy E & Sul HS (2007) Regulation of Lipolysis in Adipocytes. *Annu. Rev. Nutr.* **27:** 79–101 Available at: http://www.annualreviews.org/doi/10.1146/annurev.nutr.27.061406.093734 [Accessed July 30, 2019]

Fearon K, Strasser F, Anker SD, Bosaeus I, Bruera E, Fainsinger RL, Jatoi A, Loprinzi C, MacDonald N, Mantovani G, Davis M, Muscaritoli M, Ottery F, Radbruch L, Ravaso P, Walsh D, Wilcock A, Kaasa S & Baracos VE (2011) Definition and classification of cancer cachexia: an international consensus. *Lancet Oncol.* **12:** 489–495 Available at: www.thelancet.com/oncology [Accessed October 16, 2018]

Fearon KCH, Glass DJ & Guttridge DC (2012) Cancer cachexia: Mediators, signaling, and metabolic pathways. *Cell Metab.* **16:** 153–166

Filiano AJ, Xu Y, Tustison NJ, Marsh RL, Baker W, Smirnov I, Overall CC, Gadani SP, Turner SD, Weng Z, Peerzade SN, Chen H, Lee KS, Scott MM, Beenhakker MP, Litvak V & Kipnis J (2016) Unexpected role of interferon-γ 3 in regulating neuronal connectivity and social behaviour. *Nature* **535:** 425–429 Available at: https://www.nature.com/articles/nature18626.pdf [Accessed July 29, 2019]

Flatz L, Bergthaler A, de la Torre JC & Pinschewer DD (2006) Recovery of an arenavirus entirely from RNA polymerase I/II-driven cDNA. *Proc. Natl. Acad. Sci. U. S. A.* **103:** 4663–8 Available at: http://www.ncbi.nlm.nih.gov/pubmed/16537369 [Accessed July 15,

2019]

Di Francesco A, Di Germanio C, Bernier M & De Cabo R (2018) A time to fast. *Science (80-.).* **362:** 770–775 Available at: http://science.sciencemag.org/ [Accessed November 21, 2018]

Friedman JM & Halaas JL (1998) Leptin and the regulation of body weight in mammals. *Nature* **395:** 763–770

Fukawa T, Yan-Jiang BC, Min-Wen JC, Jun-Hao ET, Huang D, Qian CN, Ong P, Li Z, Chen S, Mak SY, Lim WJ, Kanayama HO, Mohan RE, Wang RR, Lai JH, Chua C, Ong HS, Tan KK, Ho YS, Tan IB, et al (2016) Excessive fatty acid oxidation induces muscle atrophy in cancer cachexia. *Nat. Med.* **22:** 666–671 Available at: http://dx.doi.org/10.1038/nm.4093

Ganeshan K, Nikkanen J, Man K, Leong YA, Sogawa Y, Maschek JA, Van Ry T, Chagwedera DN, Cox JE & Chawla A (2019) Energetic Trade-Offs and Hypometabolic States Promote Disease Tolerance. *Cell***:** 1–15 Available at: https://doi.org/10.1016/j.cell.2019.01.050

Geltink RIK, Kyle RL & Pearce EL (2018) Unraveling the Complex Interplay Between T Cell Metabolism and Function. *Annu. Rev. Immunol.***:** 461–488 Available at: http://doi.org/10.1146/annurev-immunol-042617-053019

Glass DJ (2005) Skeletal muscle hypertrophy and atrophy signaling pathways. *Int. J. Biochem. Cell Biol.* **37:** 1974–1984 Available at: http://www.ncbi.nlm.nih.gov/pubmed/16087388 [Accessed July 13, 2019]

Grossberg AJ, Scarlett JM & Marks DL (2010) Hypothalamic mechanisms in cachexia. *Physiol. Behav.* **100:** 478–489 Available at: http://dx.doi.org/10.1016/j.physbeh.2010.03.011

Guttridge DC, Mayo MW, Madrid L V., Wang CY & Baldwin J (2000) NF-κB-induced loss of MyoD messenger RNA: Possible role in muscle decay and cachexia. *Science (80-.).* **289:** 2363–2365 Available at: http://www.sciencemag.org/cgi/doi/10.1126/science.289.5488.2363 [Accessed July 13, 2019]

Von Haehling S & Anker SD (2014) Treatment of cachexia: An overview of recent developments. *Int. J. Cardiol.* **184:** 726–742 Available at: http://dx.doi.org/10.1016/j.jamda.2014.09.007

Von Haehling S, Ebner N, Dos Santos MR, Springer J & Anker SD (2017) Muscle wasting and cachexia in heart failure: Mechanisms and therapies. *Nat. Rev. Cardiol.* **14:** 323–341 Available at: www.nature.com/nrcardio [Accessed October 11, 2018]

Harden LM, Kent S, Pittman QJ & Roth J (2015) Fever and sickness behavior: Friend or foe? *Brain. Behav. Immun.* **50:** 322–333 Available at:

https://www.sciencedirect.com/science/article/pii/S0889159115004079 [Accessed July 29, 2019]

Haschemi A, Kosma P, Gille L, Evans CR, Burant CF, Starkl P, Knapp B, Haas R, Schmid JA, Jandl C, Amir S, Lubec G, Park J, Esterbauer H, Bilban M, Brizuela L, Pospisilik JA, Otterbein LE & Wagner O (2012) The sedoheptulose kinase CARKL directs macrophage polarization through control of glucose metabolism. *Cell Metab.* **15:** 813–26 Available at: https://linkinghub.elsevier.com/retrieve/pii/S1550413112001933 [Accessed July 29, 2019]

Hatter JA, Kouche YM, Melchor SJ, Ng K, Bouley DM, Boothroyd JC & Ewald SE (2018) Toxoplasma gondii infection triggers chronic cachexia and sustained commensal dysbiosis in mice. *PLoS One* **13:** Available at: https://doi.org/10.1371/journal.pone.0204895 [Accessed April 18, 2019]

Hayward AD, Rickard IJ & Lummaa V (2013) Influence of early-life nutrition on mortality and reproductive success during a subsequent famine in a preindustrial population. *Proc. Natl. Acad. Sci.* **110:** 13886–13891 Available at: www.pnas.org/cgi/doi/10.1073/pnas.1301817110 [Accessed July 29, 2019]

Hotamisligil GS (2017) Inflammation, metaflammation and immunometabolic disorders. *Nature* **542:** 177–185

Hotchin J & Benson L (1963) The Pathogenesis of Lymphocytic Choriomeningitis in Mice: the Effects of Different Inoculation Routes and the Footpad Response. *J. Immunol.* **91:** 460–8 Available at: http://www.ncbi.nlm.nih.gov/pubmed/14082033 [Accessed July 15, 2019]

Jelen S, Wacker S, Aponte-Santamaría C, Skott M, Rojek A, Johanson U, Kjellbom P, Nielsen S, de Groot BL & Rützler M (2011) Aquaporin-9 protein is the primary route of hepatocyte glycerol uptake for glycerol gluconeogenesis in mice. *J. Biol. Chem.* **286:** 44319–25 Available at: http://www.ncbi.nlm.nih.gov/pubmed/22081610 [Accessed July 30, 2019]

Jenkins MK & Johnson JG (1993) Molecules involved in T-cell costimulation. *Curr. Opin. Immunol.* **5:** 361–7 Available at: http://www.ncbi.nlm.nih.gov/pubmed/7688514 [Accessed July 26, 2019]

John K, Marino JS, Sanchez ER, Hinds TD & Jr HT (2016) The glucocorticoid receptor: cause of or cure for obesity? *Am J Physiol Endocrinol Metab* **310:** 249–257 Available at: http://www.ajpendo.org [Accessed September 4, 2018]

Katsuura G, Gottschall PE, Dahl RR & Arimura A (1988) Adrenocorticotropin release induced by intracerebroventricular injection of recombinant human interleukin-1 in rats: Possible involvement of prostaglandin. *Endocrinology* **122:** 1773–1779 Available at: http://www.ncbi.nlm.nih.gov/pubmed/2834174 [Accessed July 17, 2019]

Keithley JK & Swanson B (2013) HIV-Associated Wasting. *J. Assoc. Nurses AIDS Care* **24:** S103–S111 Available at: http://dx.doi.org/10.1016/j.jana.2012.06.013

Kir S, White JP, Kleiner S, Kazak L, Cohen P, Baracos VE & Spiegelman BM (2014) Tumour-derived PTH-related protein triggers adipose tissue browning and cancer cachexia. *Nature* **513:** 100–104 Available at: http://www.nature.com.ez.srv.meduniwien.ac.at/articles/nature13528.pdf [Accessed October 4, 2018]

Konishi M, Ebner N, von Haehling S, Anker SD & Springer J (2015) Developing models for cachexia and their implications in drug discovery. *Expert Opin. Drug Discov.* **10:** 743–752

Kotler D (2004) Challenges to Diagnosis of HIV-Associated Wasting. *JAIDS J. Acquir. Immune Defic. Syndr.* **37:** S280–S283 Available at: https://insights.ovid.com/crossref?an=00126334-200412015-00004 [Accessed August 28, 2018]

Krauss M, Schaller S, Borchers S, Findeisen R, Lippert J & Kuepfer L (2012) Integrating Cellular Metabolism into a Multiscale Whole-Body Model. *PLoS Comput. Biol.* **8:**

Krawczyk CM, Holowka T, Sun J, Blagih J, Amiel E, DeBerardinis RJ, Cross JR, Jung E, Thompson CB, Jones RG & Pearce EJ (2010) Toll-like receptor-induced changes in glycolytic metabolism regulate dendritic cell activation. *Blood* **115:** 4742–9 Available at: http://www.bloodjournal.org/cgi/doi/10.1182/blood-2009-10-249540 [Accessed July 29, 2019]

Lass A, Zimmermann R, Haemmerle G, Riederer M, Schoiswohl G, Schweiger M, Kienesberger P, Strauss JG, Gorkiewicz G & Zechner R (2006) Adipose triglyceride lipase-mediated lipolysis of cellular fat stores is activated by CGI-58 and defective in Chanarin-Dorfman Syndrome. *Cell Metab.* **3:** 309–319 Available at: http://www.ncbi.nlm.nih.gov/pubmed/16679289 [Accessed July 30, 2019]

Lee KJ, Perez M, Pinschewer DD & de la Torre JC (2002) Identification of the lymphocytic choriomeningitis virus (LCMV) proteins required to rescue LCMV RNA analogs into LCMV-like particles. *J. Virol.* **76:** 6393–7 Available at: http://www.ncbi.nlm.nih.gov/pubmed/1376367 [Accessed September 3, 2019]

Lempradl A, Pospisilik JA & Penninger JM (2015) Exploring the emerging complexity in transcriptional regulation of energy homeostasis. *Nat. Rev. Genet.* **16:** 665–681 Available at: http://dx.doi.org/10.1038/nrg3941

Liang C-, Yen E, Stone SJ, Koliwad S, Harris C & Farese R V (2008) Glycerolipids DGAT enzymes and triacylglycerol biosynthesis. *J. Lipid Res.* **49:** 2283 Available at: http://www.jlr.org [Accessed July 11, 2019]

Lok C (2015) Cachexia: The last illness. *Nature* **528:** 182–183 Available at:

http://www.nature.com/doifinder/10.1038/528182a [Accessed September 7, 2018]

Lu X, Yang X & Liu J (2010) Differential control of ATGL-mediated lipid droplet degradation by CGI-58 and G0S2. *Cell Cycle* **9:** 2719–25 Available at: http://www.tandfonline.com/doi/abs/10.4161/cc.9.14.12181 [Accessed July 30, 2019]

MacAl M, Lewis GM, Kunz S, Flavell R, Harker JA & Zúñiga EI (2012) Plasmacytoid dendritic cells are productively infected and activated through TLR-7 early after arenavirus infection. *Cell Host Microbe* **11:** 617–630 Available at: https://www.sciencedirect.com/science/article/pii/S1931312812001643?via%3Dihub [Accessed July 24, 2019]

Martin L (2016) Diagnostic criteria for cancer cachexia: Data versus dogma. *Curr. Opin. Clin. Nutr. Metab. Care* **19:** 188–198

Martin L, Birdsell L, Macdonald N, Reiman T, Clandinin MT, McCargar LJ, Murphy R, Ghosh S, Sawyer MB & Baracos VE (2013) Cancer cachexia in the age of obesity: skeletal muscle depletion is a powerful prognostic factor, independent of body mass index. *J. Clin. Oncol.* **31:** 1539–47 Available at: http://ascopubs.org/doi/10.1200/JCO.2012.45.2722 [Accessed June 25, 2019]

Martinez-Sobrido L, Zuniga EI, Rosario D, Garcia-Sastre A & de la Torre JC (2006) Inhibition of the Type I Interferon Response by the Nucleoprotein of the Prototypic Arenavirus Lymphocytic Choriomeningitis Virus. *J. Virol.* **80:** 9192–9199 Available at: http://www.ncbi.nlm.nih.gov/pubmed/16940530 [Accessed July 26, 2019]

Mathis D (2019) Organismal immunometabolism: advances in both directions. *Nat. Rev. Immunol.* **19:** 8–9 Available at: http://www.nature.com/articles/s41577-018-0118-z

Matsuyama T, Ishikawa T, Okayama T, Oka K, Adachi S, Mizushima K, Kimura R, Okajima M, Sakai H, Sakamoto N, Katada K, Kamada K, Uchiyama K, Handa O, Takagi T, Kokura S, Naito Y & Itoh Y (2015) Tumor inoculation site affects the development of cancer cachexia and muscle wasting. *Int. J. Cancer* **137:** 2558–2565 Available at: http://doi.wiley.com/10.1002/ijc.29620 [Accessed July 12, 2019]

Medzhitov R, Schneider DS & Soares MP (2012) Disease tolerance as a defense strategy Available at: http://science.sciencemag.org/ [Accessed July 29, 2019]

Michalek RD, Gerriets VA, Jacobs SR, Macintyre AN, MacIver NJ, Mason EF, Sullivan SA, Nichols AG & Rathmell JC (2011) Cutting Edge: Distinct Glycolytic and Lipid Oxidative Metabolic Programs Are Essential for Effector and Regulatory CD4+ T Cell Subsets. *J. Immunol.* **186:** 3299–3303 Available at: http://www.jimmunol.org/cgi/doi/10.4049/jimmunol.1003613

Miki K, Maekura R, Nagaya N, Nakazato M, Kimura H, Murakami S, Ohnishi S, Hiraga T, Miki M, Kitada S, Yoshimura K, Tateishi Y, Arimura Y, Matsumoto N, Yoshikawa M, Yamahara K & Kangawa K (2012) Ghrelin Treatment of Cachectic Patients with

Chronic Obstructive Pulmonary Disease: A Multicenter, Randomized, Double-Blind, Placebo-Controlled Trial. *PLoS One* **7:** e35708 Available at: http://dx.plos.org/10.1371/journal.pone.0035708 [Accessed June 25, 2019]

Molloy MJ, Grainger JR, Bouladoux N, Hand TW, Koo LY, Naik S, Quinones M, Dzutsev AK, Gao J-L, Trinchieri G, Murphy PM & Belkaid Y (2013) Intraluminal containment of commensal outgrowth in the gut during infection-induced dysbiosis. *Cell Host Microbe* **14:** 318–28 Available at: http://www.ncbi.nlm.nih.gov/pubmed/24034617 [Accessed July 12, 2019]

Morrison CD (2009) Leptin signaling in brain: A link between nutrition and cognition? *Biochim. Biophys. Acta - Mol. Basis Dis.* **1792:** 401–408 Available at: http://dx.doi.org/10.1016/j.bbadis.2008.12.004

Moseman EA & McGavern DB (2013) The great balancing act: Regulation and fate of antiviral T-cell interactions. *Immunol. Rev.* **255:** 110–124 Available at: https://www-ncbi-nlm-nih-gov.ez.srv.meduniwien.ac.at/pmc/articles/PMC3748617/pdf/nihms496423.pdf [Accessed September 4, 2018]

Moskophidis D, Lechner F, Pircher H & Zinkernagel RM (1993) Virus persistence in acutely infected immunocompetent mice by exhaustion of antiviral cytotoxic effector T cells. *Nature* **362:** 758–761 Available at: http://www.nature.com/doifinder/10.1038/362758a0 [Accessed December 4, 2018]

Muscaritoli M, Anker SD, Argilés J, Aversa Z, Bauer JM, Biolo G, Boirie Y, Bosaeus I, Cederholm T, Costelli P, Fearon KC, Laviano A, Maggio M, Fanelli FR, Schneider SM, Schols A & Sieber CC (2010) Consensus definition of sarcopenia, cachexia and pre-cachexia: Joint document elaborated by Special Interest Groups (SIG) "cachexia-anorexia in chronic wasting diseases" and "nutrition in geriatrics". *Clin. Nutr.* **29:** 154–159 Available at: http://www.ncbi.nlm.nih.gov/pubmed/20060626 [Accessed August 6, 2019]

Nielsen TS, Jessen N, Jørgensen JOL, Møller N & Lund S (2014) Dissecting adipose tissue lipolysis: Molecular regulation and implications for metabolic disease. *J. Mol. Endocrinol.* **52:**

Ning S, Pagano JS & Barber GN (2011) IRF7: Activation, regulation, modification and function. *Genes Immun.* **12:** 399–414 Available at: http://www.ncbi.nlm.nih.gov/pubmed/21490621 [Accessed July 24, 2019]

Norata GD, Caligiuri G, Chavakis T, Matarese G, Netea MG, Nicoletti A, O'Neill LAJ & Marelli-Berg FM (2015) The Cellular and Molecular Basis of Translational Immunometabolism. *Immunity* **43:** 421–434 Available at: http://dx.doi.org/10.1016/j.immuni.2015.08.023 [Accessed October 10, 2018]

O'Neill LAJ, Kishton RJ & Rathmell J (2016) A guide to immunometabolism for

immunologists. *Nat. Rev. Immunol.* **16:** 553–565 Available at: http://dx.doi.org/10.1038/nri.2016.70

Olivan M, Springer J, Busquets S, Tschirner A, Figueras M, Toledo M, Fontes-Oliveira C, Genovese MI, Ventura da Silva P, Sette A, López-Soriano FJ, Anker S & Argilés JM (2012) Theophylline is able to partially revert cachexia in tumour-bearing rats. *Nutr. Metab. (Lond).* **9:** 76 Available at: http://nutritionandmetabolism.biomedcentral.com/articles/10.1186/1743-7075-9-76 [Accessed July 13, 2019]

Patel HJ & Patel BM (2016) TNF-α and cancer cachexia: Molecular insights and clinical implications. *Life Sci.* **170:** 56–63 Available at: https://ac-els-cdn-com.ez.srv.meduniwien.ac.at/S0024320516306853/1-s2.0-S0024320516306853-main.pdf?_tid=f279033b-78c7-4ca4-a49e-2aa59b4e309e&acdnat=1528895914_86245bdee82da51c1e6bf1561fea0df7 [Accessed June 13, 2018]

Penna F, Busquets S & Argilés JM (2016) Experimental cancer cachexia: Evolving strategies for getting closer to the human scenario. *Semin. Cell Dev. Biol.* **54:** 20–27 Available at: http://dx.doi.org/10.1016/j.semcdb.2015.09.002 [Accessed July 11, 2019]

Petruzzelli M, Schweiger M, Schreiber R, Campos-Olivas R, Tsoli M, Allen J, Swarbrick M, Rose-John S, Rincon M, Robertson G, Zechner R & Wagner EF (2014) A switch from white to brown fat increases energy expenditure in cancer-associated cachexia. *Cell Metab.* **20:** 433–447 Available at: http://dx.doi.org/10.1016/j.cmet.2014.06.011

Pfau CJ, Valenti JK, Jacobson S & Pevear DC (1982) Cytotoxic T Cells Are Induced in Mice Infected with Lymphocytic Choriomeningitis Virus Strains of Markedly Different Pathogenicities. *Infect. Immun.* **36:** 598–602 Available at: https://www-ncbi-nlm-nih-gov.ez.srv.meduniwien.ac.at/pmc/articles/PMC351270/pdf/iai00152-0166.pdf [Accessed June 13, 2018]

Pinschewer DD, Perez M & de la Torre JC (2005) Dual Role of the Lymphocytic Choriomeningitis Virus Intergenic Region in Transcription Termination and Virus Propagation. *J. Virol.* **79:** 4519–4526 Available at: http://jvi.asm.org/cgi/doi/10.1128/JVI.79.7.4519-4526.2005 [Accessed September 3, 2019]

Pitha PM & Kunzi MS (2007) Type I interferon: The ever unfolding story. *Curr. Top. Microbiol. Immunol.* **316:** 41–70 Available at: http://www.ncbi.nlm.nih.gov/pubmed/17969443 [Accessed July 26, 2019]

Price SR, Olivecrona T & Pekala PH (1986) Regulation of lipoprotein lipase synthesis by recombinant tumor necrosis factor-The primary regulatory role of the hormone in 3T3-L1 adipocytes. *Arch. Biochem. Biophys.* **251:** 738–746 Available at:

https://linkinghub.elsevier.com/retrieve/pii/000398618690384X [Accessed July 17, 2019]

Procaccini C, De Rosa V, Galgani M, Carbone F, Rocca C La, Formisano L & Matarese G (2013) Role of adipokines signaling in the modulation of T cells function. *Front. Immunol.* **4:** 1–12

Puppa MJ, White JP, Sato S, Cairns M, Baynes JW & Carson JA (2011) Gut barrier dysfunction in the Apc(Min/+) mouse model of colon cancer cachexia. *Biochim. Biophys. Acta* **1812:** 1601–6 Available at: https://linkinghub.elsevier.com/retrieve/pii/S092544391100192X [Accessed July 12, 2019]

Rambold AS, Cohen S & Lippincott-Schwartz J (2015) Fatty acid trafficking in starved cells: Regulation by lipid droplet lipolysis, autophagy, and mitochondrial fusion dynamics. *Dev. Cell* **32:** 678–692 Available at: http://dx.doi.org/10.1016/j.devcel.2015.01.029

Rao S, Schieber AMP, O'connor CP, Leblanc M, Michel D & Ayres Correspondence JS (2017) Pathogen-Mediated Inhibition of Anorexia Promotes Host Survival and Transmission. *Cell* **168:** 503–516 Available at: http://dx.doi.org/10.1016/j.cell.2017.01.006 [Accessed August 9, 2018]

Richter K & Oxenius A (2013) Non-neutralizing antibodies protect from chronic LCMV infection independently of activating FcγR or complement. *Eur. J. Immunol.* **43:** 2349–2360 Available at: http://doi.wiley.com/10.1002/eji.201343566 [Accessed September 4, 2019]

Rouse BT & Sehrawat S (2010) Immunity and immunopathology to viruses: What decides the outcome? *Nat. Rev. Immunol.* **10:** 514–526 Available at: http://dx.doi.org/10.1038/nri2802

Rydén M, Andersson DP, Bernard S, Spalding K & Arner P (2013) Adipocyte triglyceride turnover and lipolysis in lean and overweight subjects. *J. Lipid Res.* **54:** 2909–13 Available at: http://www.ncbi.nlm.nih.gov/pubmed/23899442 [Accessed July 30, 2019]

Sahar S & Sassone-Corsi P (2012) Regulation of metabolism: the circadian clock dictates the time. *Trends Endocrinol. Metab.* **23:** 1–8 Available at: http://www.ncbi.nlm.nih.gov/pubmed/22169754 [Accessed July 29, 2019]

Sandri M (2016) Protein breakdown in cancer cachexia. *Semin. Cell Dev. Biol.* **54:** 11–9 Available at: https://linkinghub.elsevier.com/retrieve/pii/S1084952115002487 [Accessed July 13, 2019]

Sassoon DA (2016) Fatty acid metabolism-the first trigger for cachexia? *Nat. Med.* **22:** 584–585 Available at: http://dx.doi.org/10.1038/nm.4121

Schmidt CS & Mescher MF (1999) Adjuvant effect of IL-12: conversion of peptide antigen administration from tolerizing to immunizing for CD8+ T cells in vivo. *J. Immunol.* **163:**

2561–7 Available at: http://www.ncbi.nlm.nih.gov/pubmed/10452994 [Accessed July 26, 2019]

Schweiger M, Schreiber R, Haemmerle G, Lass A, Fledelius C, Jacobsen P, Tornqvist H, Zechner R & Zimmermann R (2006) Adipose Triglyceride Lipase and Hormone-sensitive Lipase Are the Major Enzymes in Adipose Tissue Triacylglycerol Catabolism. *J. Biol. Chem.* **281:** 40236–40241 Available at: http://www.ncbi.nlm.nih.gov/pubmed/17074755 [Accessed July 30, 2019]

Sethi JK & Hotamisligil GS (1999) The role of TNFα in adipocyte metabolism. *Semin. Cell Dev. Biol.* **10:** 19–29 Available at: http://www.ncbi.nlm.nih.gov/pubmed/10355025 [Accessed July 17, 2019]

Sevilla N, McGavern DB, Teng C, Kunz S & Oldstone MBA (2004) Viral targeting of hematopoietic progenitors and inhibition of DC maturation as a dual strategy for immune subversion. *J. Clin. Invest.* **113:** 737–745 Available at: http://www.ncbi.nlm.nih.gov/pubmed/14991072 [Accessed July 26, 2019]

Shattuck EC & Muehlenbein MP (2015) Human sickness behavior: Ultimate and proximate explanations. *Am. J. Phys. Anthropol.* **157:** 1–18 Available at: http://doi.wiley.com/10.1002/ajpa.22698 [Accessed July 29, 2019]

Shi H & Bartness TJ (2005) White adipose tissue sensory nerve denervation mimics lipectomy-induced compensatory increases in adiposity. *Am J Physiol Regul Integr Comp Physiol* **289:** 514–520 Available at: www.ajpregu.org [Accessed September 6, 2018]

Shi LZ, Wang R, Huang G, Vogel P, Neale G, Green DR & Chi H (2011) HIF1alpha-dependent glycolytic pathway orchestrates a metabolic checkpoint for the differentiation of TH17 and Treg cells. *J. Exp. Med.* **208:** 1367–76 Available at: http://www.jem.org/lookup/doi/10.1084/jem.20110278 [Accessed July 29, 2019]

Shin E-C, Sung PS & Park S-H (2016) Immune responses and immunopathology in acute and chronic viral hepatitis. *Nat. Rev. Immunol.* **16:** 509–523 Available at: http://www.nature.com/doifinder/10.1038/nri.2016.69

Silvério R, Lira FS, Oyama LM, Oller do Nascimento CM, Otoch JP, Alcântara PSM, Batista ML & Seelaender M (2017) Lipases and lipid droplet-associated protein expression in subcutaneous white adipose tissue of cachectic patients with cancer. *Lipids Health Dis.* **16:** 159 Available at: http://www.ncbi.nlm.nih.gov/pubmed/28830524 [Accessed July 30, 2019]

Stene GB, Helbostad JL, Balstad TR, Riphagen II, Kaasa S & Oldervoll LM (2013) Effect of physical exercise on muscle mass and strength in cancer patients during treatment-A systematic review. *Crit. Rev. Oncol. Hematol.* **88:** 573–593 Available at: http://dx.doi.org/10.1016/j.critrevonc.2013.07.001

Sullivan BM, Teijaro JR, De La Torre JC & Oldstone MBA (2015) Early Virus-Host Interactions Dictate the Course of a Persistent Infection. *PLoS Pathog* **11:** 1004588 Available at: www.plospathogens.org [Accessed September 4, 2018]

Swiecki M & Colonna M (2015) The multifaceted biology of plasmacytoid dendritic cells. *Nat. Rev. Immunol.* **15:** 471–485 Available at: http://www.nature.com/articles/nri3865 [Accessed July 24, 2019]

Taylor KE & Mossman KL (2013) Recent advances in understanding viral evasion of type I interferon. *Immunology* **138:** 190–197 Available at: https://www.ncbi.nlm.nih.gov/pmc/articles/PMC3573272/pdf/imm0138-0190.pdf [Accessed July 24, 2019]

Teijaro JR, Ng C, Lee AM, Sullivan BM, Sheehan KCF, Welch M, Schreiber RD, de la Torre JC & Oldstone MBA (2013) Persistent LCMV infection is controlled by blockade of type I interferon signaling. *Science* **340:** 207–11 Available at: http://www.ncbi.nlm.nih.gov/pubmed/23580529 [Accessed July 15, 2019]

Teixeira MM, Gazzinelli RT & Silva JS (2002) Chemokines, inflammation and Trypanosoma cruzi infection. *Trends Parasitol.* **18:** 262–265 Available at: https://www.sciencedirect.com/science/article/abs/pii/S1471492202022833 [Accessed July 12, 2019]

Tisdale MJ (2002) Cachexia in cancer patients. *Nat. Rev. Cancer* **2:** 862–871 Available at: http://www.nature.com/articles/nrc927 [Accessed September 9, 2018]

Truyens C, Torrico F, Lucas R, De Baetselier † Patrick, Buurman WA & Carlier Y (1999) The Endogenous Balance of Soluble Tumor Necrosis Factor Receptors and Tumor Necrosis Factor Modulates Cachexia and Mortality in Mice Acutely Infected with Trypanosoma cruzi Available at: http://iai.asm.org/ [Accessed April 18, 2019]

Vegiopoulos A, Rohm M & Herzig S (2017) Adipose tissue: between the extremes. *EMBO J.* **36:** 1999–2017 Available at: http://emboj.embopress.org/lookup/doi/10.15252/embj.201696206

Vincent RP & le Roux CW (2008) The satiety hormone peptide YY as a regulator of appetite. *J. Clin. Pathol.* **61:** 548–552 Available at: http://jcp.bmj.com/cgi/doi/10.1136/jcp.2007.048488 [Accessed July 29, 2019]

Virgin HW, Wherry EJ & Ahmed R (2009) Redefining Chronic Viral Infection. *Cell* **138:** 30–50 Available at: https://www.cell.com/action/showPdf?pii=S0092-8674%2809%2900783-1 [Accessed August 29, 2018]

Walsh KB, Teijaro JR, Zuniga EI, Welch MJ, Fremgen DM, Blackburn SD, von Tiehl KF, Wherry EJ, Flavell RA & Oldstone MBA (2012) Toll-like Receptor 7 Is Required for Effective Adaptive Immune Responses that Prevent Persistent Virus Infection. *Cell Host Microbe* **11:** 643–653 Available at:

https://www.sciencedirect.com/science/article/pii/S1931312812001631?via%3Dihub [Accessed July 24, 2019]

Wang A, Huen SC, Luan HH, Yu S, Zhang C, Gallezot JD, Booth CJ & Medzhitov R (2016) Opposing Effects of Fasting Metabolism on Tissue Tolerance in Bacterial and Viral Inflammation. *Cell* **166:** 1512-1525.e12 Available at: http://dx.doi.org/10.1016/j.cell.2016.07.026

Wang A, Luan HH & Medzhitov R (2019) An evolutionary perspective on immunometaabolism. *Science* **363:** eaar3932 Available at: http://www.ncbi.nlm.nih.gov/pubmed/30630899 [Accessed January 17, 2019]

Wang A & Medzhitov R (2019) Not the usual suspect: type I interferon–responsive T cells drive infection-induced cachexia. *Nat. Immunol.* **20:** 666–667 Available at: https://doi.org/10.1038/s41590-019-0374-5 [Accessed May 20, 2019]

Wanke C (2004) Pathogenesis and Consequences of HIV-Associated Wasting. *JAIDS J. Acquir. Immune Defic. Syndr.* **37:** S277–S279 Available at: https://insights.ovid.com/crossref?an=00126334-200412015-00003 [Accessed August 28, 2018]

Wherry EJ (2011) T cell exhaustion. *Nat. Immunol.* **12:** 492–499 Available at: http://dx.doi.org/10.1038/ni.2035

Wherry EJ, Blattman JN, Murali-krishna K, Most R Van Der & Ahmed R (2003) Viral Persistence Alters CD8 T-Cell Immunodominance and Tissue Distribution and Results in Distinct Stages of Functional Impairment Viral Persistence Alters CD8 T-Cell Immunodominance and Tissue Distribution and Results in Distinct Stages of Functional Im. *J. Virol.* **77:** 4911–3927

Whitehead RH (1909) A NOTE ON THE ABSORPTION OF FAT. *Am. J. Physiol. Content* **24:** 294–296 Available at: http://www.physiology.org/doi/10.1152/ajplegacy.1909.24.2.294 [Accessed July 30, 2019]

Wing SS & Goldberg AL (1993) Glucocorticoids activate the ATP-ubiquitin-dependent proteolytic system in skeletal muscle during fasting. *Am. J. Physiol. Metab.* **264:** E668–E676 Available at: http://www.physiology.org/doi/10.1152/ajpendo.1993.264.4.E668 [Accessed July 17, 2019]

Wu D, Sanin DE, Everts B, Chen Q, Qiu J, Buck MD, Patterson A, Smith AM, Chang C-H, Liu Z, Artyomov MN, Pearce EL, Cella M & Pearce EJ (2016) Type 1 Interferons Induce Changes in Core Metabolism that Are Critical for Immune Function. *Immunity* **44:** 1325–1336 Available at: https://linkinghub.elsevier.com/retrieve/pii/S1074761316302096 [Accessed July 4, 2019]

Wu J, Boström P, Sparks LM, Ye L, Choi JH, Giang A-H, Khandekar M, Virtanen KA, Nuutila P, Schaart G, Huang K, Tu H, van Marken Lichtenbelt WD, Hoeks J, Enerbäck S, Schrauwen P & Spiegelman BM (2012) Beige Adipocytes Are a Distinct Type of Thermogenic Fat Cell in Mouse and Human. *Cell* **150:** 366–376 Available at: http://www.ncbi.nlm.nih.gov/pubmed/22796012 [Accessed July 29, 2019]

Xu C, He J, Jiang H, Zu L, Zhai W, Pu S & Xu G (2009) Direct Effect of Glucocorticoids on Lipolysis in Adipocytes. *Mol. Endocrinol.* **23:** 1161–1170 Available at: https://academic.oup.com/mend/article-abstract/23/8/1161/2684001 [Accessed August 22, 2018]

Yang X, Zhang X, Heckmann BL, Lu X & Liu J (2011) Relative contribution of adipose triglyceride lipase and hormone-sensitive lipase to tumor necrosis factor-α (TNF-α)-induced lipolysis in adipocytes. *J. Biol. Chem.* **286:** 40477–85 Available at: http://www.ncbi.nlm.nih.gov/pubmed/21969372 [Accessed July 16, 2019]

Zechner R, Zimmermann R, Eichmann TO, Kohlwein SD, Haemmerle G, Lass A & Madeo F (2012) FAT SIGNALS - Lipases and lipolysis in lipid metabolism and signaling. *Cell Metab.* **15:** 279–291 Available at: http://dx.doi.org/10.1016/j.cmet.2011.12.018

Zeng W, Pirzgalska RM, Pereira MMA, Kubasova N, Barateiro A, Seixas E, Lu YH, Kozlova A, Voss H, Martins GG, Friedman JM & Domingos AI (2015) Sympathetic Neuro-adipose Connections Mediate Leptin-Driven Lipolysis. *Cell* **163:** 84–94 Available at: http://dx.doi.org/10.1016/j.cell.2015.08.055

Zhou S, Ou R, Huang L & Moskophidis D (2002) Critical role for perforin-, Fas/FasL-, and TNFR1-mediated cytotoxic pathways in down-regulation of antigen-specific T cells during persistent viral infection. *J. Virol.* **76:** 829–40 Available at: http://www.ncbi.nlm.nih.gov/pubmed/11752172 [Accessed July 31, 2019]

Zhou X, Ramachandran S, Mann M & Popkin DL (2012) Role of lymphocytic choriomeningitis virus (LCMV) in understanding viral immunology: Past, present and future. *Viruses* **4:** 2650–2669 Available at: www.mdpi.com/journal/viruses [Accessed December 3, 2018]

Zhou X, Wang JL, Lu J, Song Y, Kwak KS, Jiao Q, Rosenfeld R, Chen Q, Boone T, Simonet WS, Lacey DL, Goldberg AL & Han HQ (2010) Reversal of Cancer Cachexia and Muscle Wasting by ActRIIB Antagonism Leads to Prolonged Survival. *Cell* **142:** 531–543 Available at: https://www.cell.com/cell/pdfExtended/S0092-8674(10)00780-4 [Accessed June 24, 2019]

Zinkernagel RM & Doherty PC (1979) MHC-Restricted Cytotoxic T Cells: Studies on the Biological Role of Polymorphic Major Transplantation Antigens Determining T-Cell Restriction-Specificity, Function, and Responsiveness. *Adv. Immunol.* **27:** 51–177 Available at: https://www.sciencedirect.com/science/article/pii/S006527760860262X

[Accessed July 31, 2019]

Zinkernagel RM, Haenseler E, Leist T, Cerny A, Hengartner H & Althage A (1986) T cell-mediated hepatitis in mice infected with lymphocytic choriomeningitis virus. Liver cell destruction by H-2 class I-restricted virus-specific cytotoxic T cells as a physiological correlate of the 51Cr-release assay? *J Exp Med* **164:** 1075–1092 Available at: http://www.ncbi.nlm.nih.gov/entrez/query.fcgi?cmd=Retrieve&db=PubMed&dopt=Citation&list_uids=3489805%5Cnhttp://pubmedcentralcanada.ca/picrender.cgi?artid=1343445&blobtype=pdf [Accessed June 13, 2018]

Hatoon Baazim

Education:

2014 – present **CeMM Research Center of Molecular Medicine of the Austrian Academy of Sciences. Vienna, Austria.**
- PhD fellow, Andreas Bergthaler Lab.

2012 – 2014 **King Abdullah University of Science and Technology. Thuwal, Saudi Arabia.**
- MSc degree in Bioscience department, genome engineering group.
- GPA: 3.75 (out of 4)

2009 – 2012 **King Saud University. Riyadh, Saudi Arabia.**
- Obtained a Second Degree with Honors BSc in Biochemistry.
- GPA 4.22 (out of 5)

2007 – 2009 **Riyadh Najd School:** 96%

Publications:

- **CD8⁺ T cells induce cachexia during chronic viral infection.** H. Baazim*, M. Schweiger, M. Moschinger, H. Xu, T. Scherer, A. Popa, S. Gallage, S. A. Ali, K. Khamina, L. Kosack, B. Vilagos, M. Smyth, A. Lercher, J. Friske, D. Merkler, T. H. Helbich, M. Heikenwälder, P. A. Lang, R. Zechner, A. Bergthaler**. Nature Immunology 2019. DOI: 10.1038/s41590-019-0397-y.
- **Hepatocyte-intrinsic Ifnar1 signaling modulates hepatic metabolism and adaptive immunity.** A. Lercher*, A. Bhattacharya*, A. M. Popa, M. Caldera, M. F. Schlapansky, H. Baazim, P. Majek, J. S. Brunner, L. J. Kosack, D. Vitko, T. Pinter, B. Gürtl, D. Reil, U. Kalinke, K. L. Bennett, J. Menche, G. Schabbauer, M. Trauner, K. Klavins, A. Bergthaler**. (In review).
- **Immunomodulatory mechanisms of the novel therapeutic bile acid 24-nor-ursodeoxycholicacid.** C. Zhu*, N. Boucheron, C. D. Fuchs, H. Baazim, A. Lercher, E. Halilbasic, M. Tardelli, A. Bergthaler, W. Ellmeier, M. Trauner**. (In review).
- **The ERBB-STAT3 Axis Drives Tasmanian Devil Facial Tumor Disease.** L. Kosack*, B. Wingelhofer*, A. Popa*, A. Orlova, B. Agerer, B. Vilagos, P. Majek, K. Parapatics, A. Lercher, A. Ringler, J. Klughammer, M. Smyth, K. Khamina, H. Baazim, E. D. de Araujo, D. A. Rosa, J. Park, G. Tin, S. Ahmar, P. T. Gunning, C. Bock, H. V. Siddle, G. M. Woods, S. Kubicek, E. P. Murchison, K. L. Bennett, R. Moriggl, A. Bergthaler**. Cancer Cell, 2019. DOI: 10.1016/j.ccell.2018.11.018.
- **Superoxide Dismutase 1 protects hepatocytes from type I interferon-driven oxidative damage.** A. Bhattacharya*, A. N. Hegazy*, N. Deigendesch, L. Kosack, J. Cupovic, R. K. Kandasamy, A. Hildebrandt, D. Merkler, A. A. Kühl, B. Vilagos, C. Schliehe, I. Panse, K. Khamina, H. Baazim, I. Arnold, L. Flatz, H. C. Xu, P. A. Lang, A.

Aderem, A. Takaoka, G. Superti-Furga, J. Colinge, B. Ludewig, M. Löhning, and A. Bergthaler**. Immunity 2015. DOI: 10.1016/j.immuni.2015.10.013.

- **RNA-guided transcriptional regulation in planta via synthetic dCas9-based transcription factors**. A. Piatek*, Z. Ali, H. Baazim, L. Li, A. Abulfaraj, S. Al-Shareef, M. Aouida and M. M. Mahfouz**. Plant Biotechnology Journal, 2015. DOI: 10.1111/pbi.12284.

Training and Conferences

28thMay – 2nd June 2019	**International Conference on Immunometabolism: Molecular and Celluar Immunology of Metabolism.** • Oral presentation. • Awarded the Aegean Conference Travel Award for an excellent research contribution.
19th – 20th October 2018	**Annual Meeting of the Austrian Obesity Association (ÖAG). Vienna, Austria.** • Invited speaker.
21st – 25th January 2018	**Keystone Symposium: Organ Crosstalk in Obesity and NAFLD. Keystone, Colorado, US.** • Poster presentation.
29th May – 2nd June 2017	**Keystone Symposium: Integrating Metabolism and Immunity. Dublin, Ireland.** • Awarded the Keystone Symposia Future of Science Fund Scholarship. • Poster presentation.
30th May – 2nd June 2016	**CEMIR: Conference on Molecular Mechanisms of Inflammation. Trondheim, Norway.** • Poster presentation.
12th – 19th September 2015	**FEBS Immunology Summer School. Rabac, Croatia.**
6th – 9th September 2015	**European Congress of Immunology (ECI). Vienna, Austria.**
6th – 7th November 2014	**Vienna Biocenter Symposium: Complexity of Life. Vienna, Austria.**
30 June – 25 July, 2012	**Internship: Human Cancer Genome Research in King Faisal Specialist hospital & Research Center. Experimental Molecular Pathology Lab. Riyadh, Saudi Arabia.**
26 June – 20 July, 2011	**Internship: Obesity Research Center, College of Medicine, King Saud University. Riyadh, Saudi Arabia.**

Conference and Symposium Organization.

2015 – 2018	**Annual Young Scientist Association PhD Symposium. Vienna, Austria.** • Board member and organizing committee for four consecutive years.
6 – 8 March, 2012	**International Conference of the Saudi Osteoporosis Society. Riyadh Saudi Arabia.** • Organization committee.

Relevant Skills

- Mouse handling, dissection of various organ types, gavage feeding, intravenous, intraperitoneal, and intranasal injections as well as whole-body and liver perfusion.
- Experience with experimental diets and pharmacological perturbations.
- Immune cell isolation, FACS and ICS analysis from blood and various tissue types.
- Immune adoptive transfer.
- RNA and protein extraction and analysis from various tissue including liver, adipose tissue and muscles.
- Adipose tissue CVF and cell line (3T3-L1) differentiation, culture, and staining.
- Bone marrow isolation.
- Experience with various virus-infection models (injections, analysis, and virus stock propagation).
- Seahorse metabolic flux analysis.
- Proficient use of molecular biology techniques.
- Histological image analysis of H/E and co-immunofluorescent staining.
- Basic-level understanding of MRI imaging and analysis.
- Scientific illustration and design.

Experience

- **Proficient and independent project management and design.**
- **Initiated and/or maintained multiple international collaborations.**
- **Supervised a junior PhD student, a Master student and a short-term diploma student.**
- **Vice-president and board member of the Young Scientist Association (YSA), at the Medical University Vienna (MUV) from 2015 to 2018.** https://ysa.meduniwien.ac.at/phd-symposium/

Started as a volunteer, then moved to be the director of public relations, then vice-president, and finally acting president for half a year in the absence of the president at the time. In this capacity I organized both scientific and social workshops, in addition to the annual YSA PhD symposium. For this symposium I was heavily involved in organizing tasks within the board, coordinating with the Medical University and selecting, inviting and hosting international keynote speakers.

- **Founder and coordinator of the Science | Art competition, in the Medical University Vienna. 2016-2018.** https://ysa.meduniwien.ac.at/phd-symposium/scienceart/
  This required securing support from the Medical University Vienna (MUW), initiating collaborations with local artists, and both local and international professors in Applied and Conceptual Art, philosophy and culture, as well as local scientists with artistic inclinations and interest in science communication.
- **PhD-student representative of the year 2015 at the Center for Molecular Medicine (CeMM).**
- **Convocation student speaker in King Abdullah University KAUST for the year 2013.**
  http://vimeo.com/73851983
- **Selected delegate from King Saud University to represent Saudi women to the United nation agencies in Geneva, Switzerland.**
  The delegation included a visit to the United Nation, World Health Organization, World Food Program, United Nations Environment Program, International Organization for Migration, International Committee of the Red Cross, in addition to the European Organization for Nuclear Research (CERN), and a visit to the University of Lausanne.
- Graduate life Committee member, in the fourth student council in KAUST.
- Founder of the Biochemistry Club in King Saud University.
- Vice President of the Health Committee in “Mojtam3e Club”.
- Supervised the organization and sales for a fundraiser exhibition.
- Represented the students of the Science College in the student council of King Saud University.
- **Published author of two science fiction novels**. The novels were published in Arabic and have earned great interest from the media, it was featured in two newspaper articles and won a prestigious sponsorship from a Dubai-based foundation Mohammed bin Rashid Al Maktoum Foundation.

Languages:

Arabic: Native. **English:** Fluent.